Tetra Tech, Inc.

FINAL REPORT NASW 1872

DECLINATION RATE AND RELATED INTERFEROMETRIC SCHEMES FOR PRECISE SATELLITE TRACKING

TC-161 November 1969

FINAL REPORT

DECLINATION RATE AND RELATED INTERFEROMETRIC SCHEMES FOR PRECISE SATELLITE TRACKING

Prepared for:

National Aeronautics and Space Administration
Headquarters, Code SAG
Washington, D. C. 20546

Prepared by:

W. Wells
M. Milder
H. Hodara

Contract No. NASW 1872

Tetra Tech No. TC-161

November, 1969

Tetra Tech, Incorporated
630 North Rosemead Boulevard
Pasadena, California 91107

DECLINATION RATE
and Related Interferometric Schemes for
PRECISE SATELLITE TRACKING

Abstract

A study of optical and microwave interferometers and related systems for precision satellite tracking was motivated by the high angular resolutions reported with interferometric systems. Five novel tracking schemes are analyzed and compared. Systems 3 and 4 (paragraphs 3 and 4 below) are strictly interferometric; Systems 2 and 5 resemble interferometers, measuring angles relative to a baseline joining two stations, and System 1, while not interferometric, is included for comparison.

1. In principle a star occultation system can locate a satellite relative to a star and a point on the ground with an accuracy of 10 cm. However, the positions of most stars are not well enough known for precise comparisons, so the system would have to be transported to random (usually undesirable) places to observe occultations of a few standard stars. Moreover, a special satellite is required since, except for balloons, existing satellites are too small, and balloons are perturbed by unpredictable forces. A possible but improbable satellite design is given.

2. The second system would measure angles by triangulation, using the differential range between the satellite and two lidar (optical radar) stations at the ends of the baseline. This differential lidar system is based on picosecond pulses from the neodymium-glass laser. System development is premature, because some components, though laboratory demonstrated, are not fully developed. The accuracy is limited by atmospherics and pulse length. With a 1,500 meter baseline (enclosed in a pipe that is straight at least in segments),

the ultimate precision should exceed 10^{-7} radian = 0.02 arc sec, or 10 cm at a range of 2 Mm. Differential lidar is an advanced system for long-range planning. There are logical steps to the advanced status with beneficial results along the way.

3. An interferometer based on the carbon dioxide laser has properties which probably restrict its use to synchronous (24-hour) or near-geostationary orbits, for which the measurement of dec-rate (rate of change of the satellites declination angle) is especially important. The 10-micron dec-rate system with a nearly polar baseline of 300 meters will give accuracy of 0.3×10^{-8} rad = 0.01 arc sec. At the geostationary orbit range of 40 Mm, this error is 10 meters. The system is especially simple to build for the ATS-F mission which will carry a carbon dioxide laser transmitter on the satellite. We strongly recommend building the interferometer for this mission, a rare opportunity to test the concept at reduced cost and the first of the logical steps toward System 2.

4. The microwave systems are large and complicated, requiring two sites at the ends of a very long baseline plus active participation of the satellite. The impressive angles (e. g., 1/1000 arc sec) for very-long-baseline interferometers (VLBI) refer to resolution, not absolute angular position. Nevertheless, much microwave equipment and active satellite systems already exist and may be useful in special cases. In particular, we suggest testing a differential VLBI system which uses the signal from a satellite as a local oscillator for measuring the position of a celestial radio source. When the source is nearly behind the satellite, the differential angle can be measured accurately, comparable to VLBI astronomical resolution.

5. Another version of microwave VLBI is a differential range rate system. The concept is instructive, but the system requires two active transponders on the satellite.

In conclusion, we recommend building the 10-micron dec-rate system for the ATS-F mission to evaluate optical interferometry followed, if successful, by steps toward the differential lidar system.

TABLE OF CONTENTS

DECLINATION RATE
and Related Interferometric Schemes for
PRECISE SATELLITE TRACKING

The work reported here is partly experimental but mostly a systems analysis of candidate angular tracking systems in comparison to one another and to existing tracking systems. In the experimental task we measured the temperature fluctuations on Mt. Palomar to gain a rough measure of the atmospheric limitations on interferometric satellite tracking systems. The results of the experimental task which are reported in Appendix B were then applied to the comparisons of the candidate tracking systems. This report is divided into three parts of which the first is entitled "Background". It gives the motivation for this study and establishes the need for interferometric tracking in Sec. 1.1. In Sec. 1.2 a special form of angular tracking called star occultation is described. Unlike the rest of the report it has nothing to do with interferometric systems, but represents a possible means of obtaining precision angles that may be used as a basis of comparison in deciding whether interferometry is worthwhile. Section 1.3 in Part 1 begins the transition to the main topic of interferometric systems. This section describes the triangulation properties of interferometers and other systems which are based on the concept of two stations connected by a baseline.

Part 2 entitled "Candidate Tracking Systems" describes the bulk of the study in which the angular accuracy and other properties of the principal candidate systems are derived. These candidates are

* A differential lidar system based on picosecond pulses obtained from the neodymium:glass laser (Nd:glass) at 1.06 micron,
* A dec-rate system based on the carbon dioxide laser at 10.6 microns
* A very-long-baseline interferometer (VLBI) system based on measurements of differential angle from a a satellite to a celestial radio source
* A microwave differential range rate system.

Part 3 of the report contains the comparisons, recommendations and conclusions. Here we find that in general laser systems have more growth potential for the following reasons:

* Like the laser satellite ranging systems, the laser interferometers do not require the active participation of the satellite. A passive laser retroreflector will suffice.
* The laser interferometer or related laser angular tracking system will use a relatively short baseline that will fit on a single parcel of land where both stations may be manned by a single crew.
* Microwave VLBI systems require elaborate techniques to replace the direct link between the two stations along the baseline.

Our principal recommendation is that the 10-micron dec-rate system should be built for the ATS-F satellite mission, since the satellite's active laser provides a rare opportunity to test the optical interferometric concept at greatly reduced cost. After this if the tracking system proves sufficiently valuable, steps should be taken to transform the technique into the differential lidar system based on the Nd:glass picosecond pulse lasers. The latter system is much more versatile, measures absolute angles instead of only angle rates, and is usable with the type of retroreflector which is already attached to six satellites now in orbit.

Throughout this study we adhere to certain ground rules. We assume that the satellite can carry the retroreflector for any infrared wavelength out to 10 microns, or simple active microwave systems such as transmitters or transponders. We do not assume that the satellite will carry systems that are more complicated than these, except for the special case of the ATS-F satellite for which the carbon dioxide laser beacon is already planned. Next, we regard the light second as a valid measure of distance even at accuracies beyond that to which the velocity of light (c) is known. The light second is constant and provides a self-consistent set of measurements whether or not it can be related to the standard meter with the same

accuracy. Finally, we omit discussions of various corrections that would have to be included in an operational orbit determination program, simply because these corrections have no bearing on the comparison and tradeoff of the various systems. Corrections such as relativity, solar pressure, atmospheric refraction, high harmonics of the gravitational potential either effect all systems similarly or may be entered as precise corrections which do not effect the final accuracy of the system in question. Similarly, the bootstrapping techniques which remove the uncertainties in the location of tracking stations by repeated tracking of many satellites will also apply to all systems equally. Finally, the effects of timing errors, i.e., clock synchronization amongst the tracking stations, are severe, but common to all types of tracking. Therefore, timing is not discussed here.

PART I

BACKGROUND

1.1 MOTIVATION FOR INTERFEROMETRIC STUDIES

A good summary of the current status of satellite tracking and the needs for more precise tracking may be found in Ref. 1 entitled "Geodesy - Cartography", Part 13 of "Useful Applications of Earth Oriented Satellites". The authors of this report use the term dynamic geodesy to refer to the determinations of various positions on the earth and gravity harmonics that result from the precise tracking of satellites. Regarding dynamic geodesy they say in part:

> "There is apparently no limit to the accuracy with which satellite position in orbit must be determined. For most applications, an accuracy of sensor positioning to a few tens of meters seems adequate; for others, such as measuring geoid profiles a few meters is required; for ultimate objectives, such as dynamic oceanography, a few centimeters is necessary. The conclusion is that whatever accuracy can be obtained will eventually be exploited."

The same reference summarizes the accuracy with which satellite positions may be determined:

> "Spacecraft positions can be established within an error ellipsoid whose principal axes are ±100 m along track, ±10 m across track, and ±30 m in elevation."

This accuracy should not be confused with the accuracies of predictions for acquiring a satellite track. Between a fix and a prediction, uncertain forces will act to decay the accuracy to about 1000 m along track and 200 meters across track.

By prolonged tracking of a number of satellites with the same set of stations, one can employ bootstrapping techniques to establish better coordinates of the tracking stations themselves. On this topic the Geodesy - Cartography panel states:

> "The geocentric coordinates of approximately 25 tracking stations have been established with an error of about ±15 meters."

This number differs only slightly from the estimated error of 10 meters given by Lehr [Ref. 2] for Baker-Nunn camera stations. The fix accuracies in the range from 10 to 100 meters may readily be converted to an equivalent angular accuracy be dividing by a typical range to a geodetic satellite, say 2 megameters. The resulting angles fall in the range 5 to 50 μ radians or 1 to 10 arc sec*. The systems we compare in detail all have potential for improved accuracy, i.e., errors $\ll$ 1 arc second.

Systems currently in use for satellite tracking are based on the measurement of range, range rate or angle. The angular systems are the Baker-Nunn cameras and the minitrack interferometers. The Baker-Nunn systems are the more accurate of the two; they routinely produce satellite position measurements with an accuracy of 2 to 3 arc sec [Ref. 2].

The motivation for this study derives from the comparison of the Baker-Nunn accuracies with angular resolutions that have been obtained with interferometry. Microwave VLBI has realized angular resolutions on the order of 10^{-3} arc sec [Ref. 3]. Moreover, in a classic optical experiment Michelson [Ref. 4] succeeded in measuring star diameters as small as 0.02 seconds of arc = 10^{-7} rad with his celebrated stellar interferometer, despite the difficulties of working with white light interference. A comparison of 0.02 and 0.001 arc sec suggests using VLBI for the ultimate angular accuracy, but these numbers apply to angular resolution rather than absolute accuracy. In other words, these are angles that define the structure of a very small but extended source and do not give the absolute angular directions of the source in geocentric coordinates. When the interferometric concepts are modified and studied for the latter application the balance tilts in favor of the optical techniques.

---

*For the most part in this report we shall deal with angles expressed as radians or microradians, but for comparison with other data it is often necessary to have the conversion factor:

1 arc sec = 4.85 μ rad

The novel systems described in this report will be capable of exceeding the Baker-Nunn accuracy, providing they are developed to the fullest extent allowed by the theory described herein. However, practical limitations and compromises for cost reduction may degrade the performance of an actual system below that estimated herein. Therefore, it is desirable to describe certain significant benefits of interferometric and related systems that cannot be summarized merely as absolute accuracy in the typical tracking situation. This is done in the following subsections, the first of which describes benefits of mixing data types, and the second describes equatorial orbits, especially geosynchronous (24 hour) ones for which existing tracking systems are inadequate.

1.1.1 Mixture of Data Types

Suppose that the typical tracking errors of two tracking systems are about equal for orbits of typical geodetic satellites, and further suppose that the two systems differ drastically in their physics or kinematics. Then it is advantageous to build a tracking net that consists of both types of systems instead of relying entirely on one or the other. The mix allows certain bootstrapping techniques to operate for removal of errors, since the two react to various perturbing influences in different ways. Lundquist [Ref. 5] has remarked on this type of improvement as follows:

> "Satellite geodesy has matured to the state where it is a recognized branch of geodetic science with its own established procedures. The conventional cycle of analysis begins at a tracking station, which measures some quantity depending on satellite position or velocity. Each observation yields an equation of condition relating orbital elements and geodetic parameters. Very many such equations are used to refine orbital elements and geodetic parameters, either simultaneously or cyclically. In these solutions the equations need not all arise from measurement of the same function of satellite position or velocity. Rather, a blend of data from various tracking systems can strengthen the solution." (emphasis ours)

In this sense precision interferometry can make valuable contributions to tracking, because its angular reference is entirely different from that of other techniques. In range and range-rate tracking the angular reference is in part the geographic location of the tracking station (note that the range rate vanishes at the closest point of approach to the station) and in part the known angular positions of gravitating bodies (especially the sun and moon) which influence range rate by perturbing the orbit. For tracking with the Baker-Nunn cameras the angular reference is the star field against which the satellite is photographed. By contrast to these systems the angular reference for the interferometer is one or more baselines which are fixed in the earth's crust. Each measurement with a pair of stations fixes the satellite on a cone for which the baseline joining the two stations is the axis.

Moreover, the accuracy of the three forms of tracking is limited by different factors. Unfortunately timing of the tracking events is an important source of error in all forms of tracking in the direction along the satellites track. However, in the cross track direction range and range-rate is limited by uncertainty in the troposphere and ionosphere, the Baker-Nunn systems are limited by the accuracy of image measurements in a photographic emulsion, while the interferometric schemes are limited by the gradient of the refractive index of air projected along the baseline. These factors refer to the physical barriers that limit further improvement once the system has been fully optimized. In specific systems certain technical difficulties limit the current accuracies to values that fall short of the limit. For example, electronic and operational considerations limit the accuracy of lidar (optical radar) range determinations to 1 or 2 meters instead of the atmospheric limit of about 10 cm. From these considerations it is clear that the use of interferometric angular data will strengthen the mix of data that is used in the overall orbit determination problem.

1.1.2 Equatorial and Especially Geosynchronous Orbits

This subsection considers the value of data mixtures from the point of view of kinematic leverage. By kinematic leverage we mean the angle of intersection between two curves that determine a satellite fix. That is, suppose one datum locates a satellite on a surface with a certain accuracy, a second datum locates it on another surface which intersects the first in a curve, and a third datum locates the satellite on a third surface which intersects the curve in a point, this point being the fix. If the angles of intersection of the various surfaces are small then the errors are amplified and the leverage is said to be poor. Conversely large angle intersections give good kinematic leverage. Alternatively one may be using a known satellite orbit as a coordinate reference with which to locate the tracking station. In this inverse problem (or geodetic experiment) the same principles apply in reverse except that the surfaces or curves intersect to locate the tracking station at a geographic position and elevation on the ground. The concern of this subsection is the special orbits in which the kinematic leverage from existing tracking systems is especially poor.

Regarding the overall problem of dynamic geodesy, the geodesy - cartography panel has stated:

> "The lack of data on satellites with lower inclination is a significant deficiency in the data base." [Ref. 1]

An equatorial orbit is a degenerate case for range-rate tracking, because all passes over the tracking station are in an east-west direction. In these cases it would be particularly desirable to have a declination or dec-rate tracking system to measure directly the small movements in the north-south direction.

The degeneracy of range-rate tracking worsens if the orbit is geosynchronous, especially if it is nearly geostationary. An analysis in Appendix A describes a severely degenerate kinematic condition that gives special importance

Abbreviations and Satellite Orbit Nomenclature

HA	=	hour angle, i.e., east-west or longitudinal position of the satellite
dec	=	δ or declination = latitude or north-south position of satellite
dec rate	=	$d\delta/dt$
μ rad	=	10^{-6} radian = 1 arc sec/4.85
Mm	=	10^{6} meters = 1000 km.
R	=	range to the satellite from earth's center or any tracking station in question
RR	=	range rate = $dR/dt = \dot{R}$
e	=	eccentricity of elliptical satellite orbit
i	=	inclination of the orbit (see below)
RA	=	right ascention of satellite or other point (see below)
Ω	=	RA of ascending node (see below)
ω	=	argument of perigee (see below)
v	=	true anomaly (see below)
VLB	-	very long baseline
ODP	-	orbit determination program
$GM_{\oplus}$	-	gravitational const times mass of the earth
n	=	mean (anomalistic) motion, revolutions per day

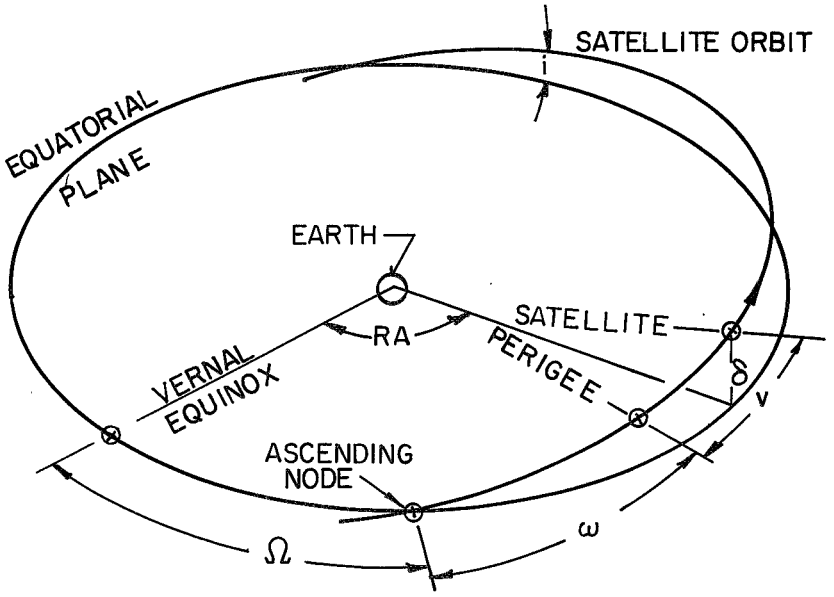

to declination or dec-rate measurements for precise determination of geostationary orbits. When an orbit is determined solely from range or range-rate data, the degeneracy causes excessive error in the orbital elements that describe residual movement in declination, namely inclination and right ascention of the ascending node. These and other orbital elements and abbreviations used in the following discussion are defined in the list and Fig. p. 10. Two results of the analysis in Appendix A are noteworthy:

* Without dec or dec-rate tracking, i and Ω are not determined as well as e and $\Omega + \omega$.
* A bonus from dec-rate tracking is greater sensitivity to tidal perturbations, which relate the orbit to the known angular positions of the sun and moon.

By "tidal" we mean the differential acceleration between satellite and earth as caused by the moon and sun, not the change in earth gravity that results from ocean tides. A more detailed diagram of the logic and results of Appendix A is given on p. 12. Here the figure and equation numbers all refer to Appendix A, and the orbital elements and other abbreviations are defined on p. 10.

Having demonstrated the need for declination or dec-rate tracking of geostationary satellites, we should comment on the ability of Baker-Nunn photographs to provide the declination measurements. The threshold for detection of a geostationary satellite with this system is approximately 13th magnitude. Small satellites such as ATS-1 exceed this magnitude and cannot be photographed except with a large astronomical instrument. Large satellites including ATS-F will be bright enough for the Baker-Nunn, but the accuracy leaves much to be desired. At 40 Mm, the geostationary satellite distance, the usual error of 2 or 3 arc sec implies a 600 meter linear error.

The geostationary orbit has been emphasized here because it is an especially simple case to analyze, and because of the importance of

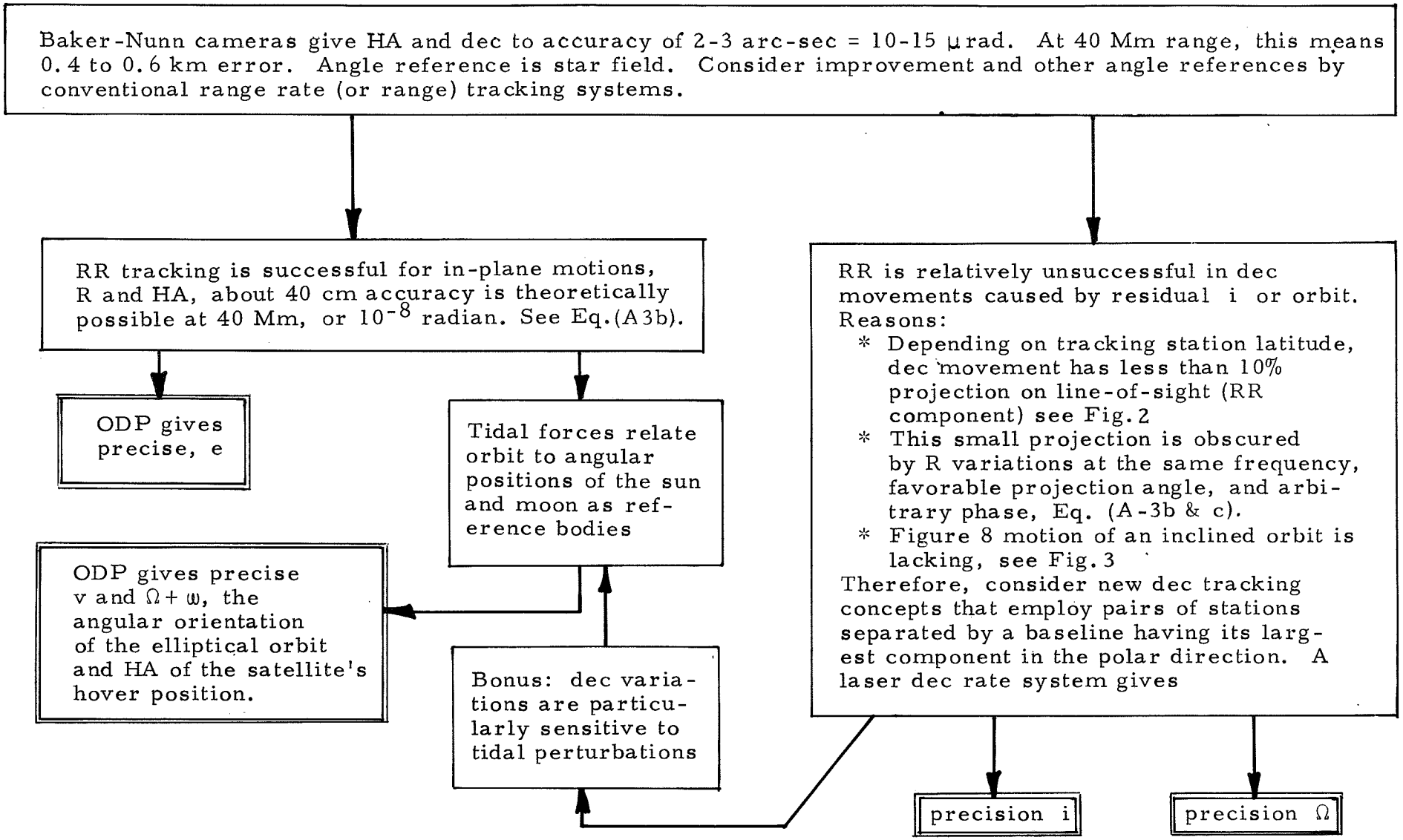
Baker-Nunn cameras give HA and dec to accuracy of 2-3 arc-sec = 10-15 μrad. At 40 Mm range, this means 0.4 to 0.6 km error. Angle reference is star field. Consider improvement and other angle references by conventional range rate (or range) tracking systems.
RR tracking is successful for in-plane motions, R and HA, about 40 cm accuracy is theoretically possible at 40 Mm, or 10^{-8} radian. See Eq.(A3b).
ODP gives precise, e
Tidal forces relate orbit to angular positions of the sun and moon as reference bodies
ODP gives precise v and Ω + ω, the angular orientation of the elliptical orbit and HA of the satellite's hover position.
Bonus: dec variations are particularly sensitive to tidal perturbations
RR is relatively unsuccessful in dec movements caused by residual i or orbit. Reasons:
* Depending on tracking station latitude, dec movement has less than 10% projection on line-of-sight (RR component) see Fig. 2
* This small projection is obscured by R variations at the same frequency, favorable projection angle, and arbitrary phase, Eq. (A-3b & c).
* Figure 8 motion of an inclined orbit is lacking, see Fig. 3
Therefore, consider new dec tracking concepts that employ pairs of stations separated by a baseline having its largest component in the polar direction. A laser dec rate system gives
precision i
precision Ω

the ATS-F to this study. For other orbits the part of our argument concerned with inclination measurement weakens if the orbit inclines significantly. The part concerned with tidal force to relate the orbit to sun and moon positions weakens if the orbit is not synchronous. The kinematic leverage on an equatorial orbit improves greatly if the satellite has a low orbit and is tracked from high latitude stations (see Appendix A, Fig. 2).

1.2 STAR OCCULTATION SYSTEM

To realistically evaluate interferometric satellite tracking and related systems that measure angles relative to a baseline, it is important to compare them to any other means of obtaining angular tracking data, even though these means are radically different. One such scheme has such intriguing possibilities that it is discussed here as background information which should influence any decision to build (or refrain from building) a major angular tracking facility that is intended for angular accuracies on the order of 0.01 arc sec. The system is portable and consists of a number of small star tracking telescopes and an accurate clock. The telescopes are set up in advance in a position where a satellite may be observed to occult a star. When the occultation is observed on two or more of the telescopes, and the time is noted, the data provide a precise relationship between the satellite, the star and a point on the ground at a known time. We assume a low-orbit satellite within the earth's shadow.

The star occultation technique was originally studied by Gordon [Ref. 6] and Kolaczek [Ref. 7]. Its advantages and disadvantages are both formidable. The most important advantages are that the basic accuracy of measurement on the ground is about 10 cm, and the system is simple and portable so that it could be moved to many continents and islands for geodetic measurements around the world. The main disadvantages are that a special satellite would be required, and there are few stars whose relative positions are known well enough to maintain the basic precision of 10 cm when occultations of various stars are compared.

The basic advantage of the system derives from two considerations. To understand the first, think of a particular star as though it were the only light in the sky, and the satellite as a body that casts a shadow on the earth as it moves across in its orbit. The satellite and its shadow are both large (tens of meters) to provide a good chance of finding the shadow with a reasonable number of telescopes. Note that the sharpness of the

shadow, i.e., the distance in passing from dark to light, is determined by the large aperture of the satellite cross-section and has nothing to do with the small aperture of the telescope or with its pointing accuracy. The telescope need only be large enough to see the star with a short photoelectric time constant so that the time and duration of occultation can be accurately recorded. Optically the occultation is observed in the near field of the satellite aperture. Here the dimension over which the shadow changes from light to dark is approximately $\sqrt{R\lambda}$, where R is the range to the satellite and λ is the wavelength of 0.5μ for visible light. If we choose a rather typical range of 2 Mm (1000 km) then the shadow sharpness is one meter, of which one can judge the center to an accuracy of at least 10 cm with a reasonable signal-to-noise ratio.

The second consideration which permits particularly high accuracy by star occultation derives from the errors caused by image dancing, that is the bending of light rays in turbulent layers of the atmosphere. The Fig. p. 16 shows a bend occuring in the air at a height h above the ground and a distance $r-h$ from the satellite. When the angle reference is a baseline fixed on the ground, the linear error is caused by the angle of bend operating on the long lever arm $r-h$. By contrast, when the angle reference is a star, the error angle operates on the short lever arm of length h. If the light ray bends through an angle of 1 arc sec at a height $h = 10$ km, then the linear error is

$$h\Delta\theta = 10 \text{ km} \times 5 \times 10^{-6} = 5 \text{ cm} \quad .$$

Now let us consider the kind of satellite that is required to observe the occultation. Suppose that the satellite ephemeris in the cross track direction is somewhat more accurate than the garden variety of prediction; e.g., let us suppose that we know where to look with an accuracy of $\frac{1}{2} \times 10^{-4}$ rad. Again imagine that the star in question is the only light in the sky. If the range to the satellite is 2 Mm, this means that there is an uncertainty of 100 meters in our knowledge of where the

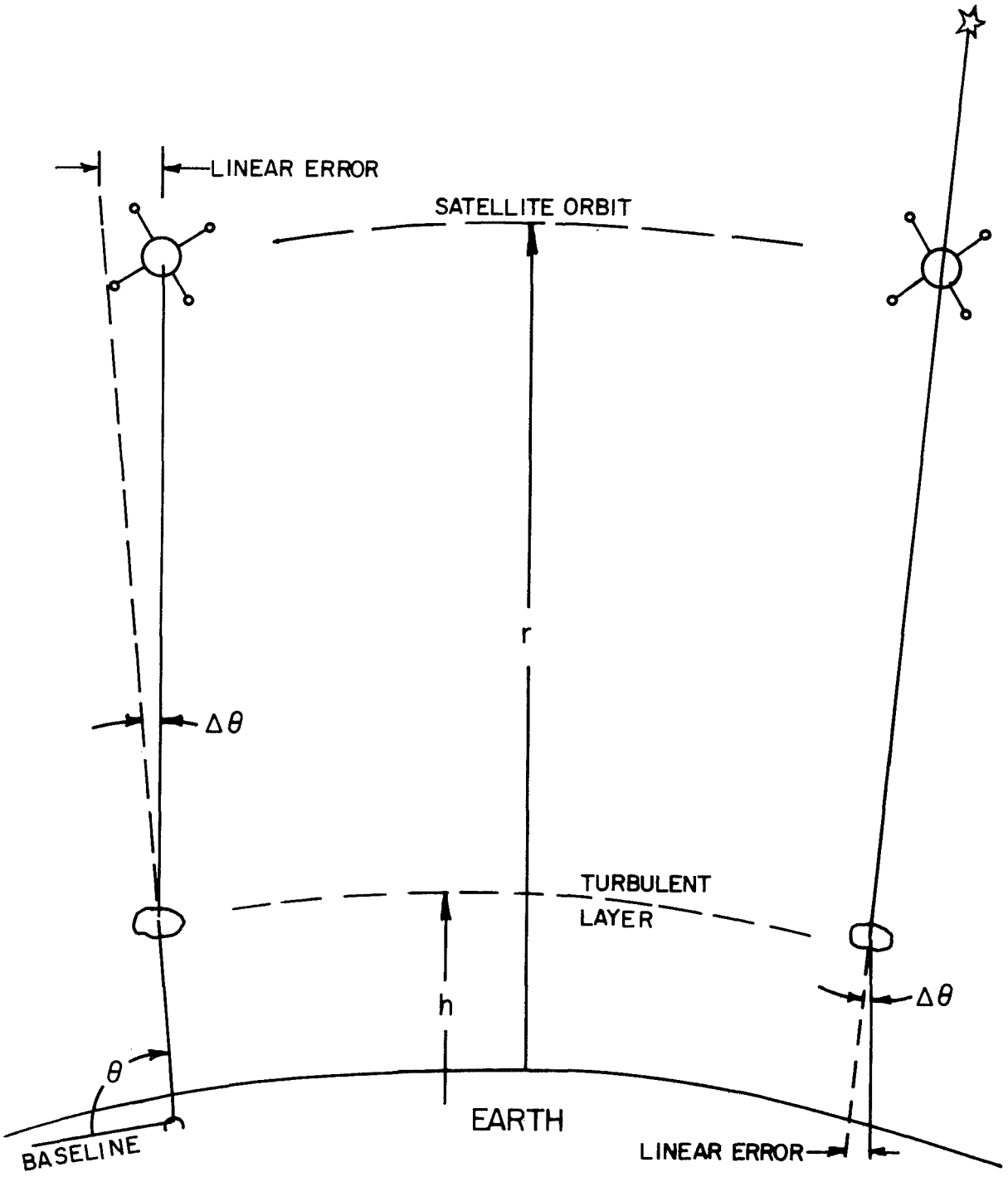

Angular error $\Delta\theta$ acts on a long lever arm (r-h) when a baseline is the angular reference.

Angular error $\Delta\theta$ acts on a short lever arm h when a star is the angular reference.

shadow will pass along the ground. We have already noted that the satellite diameter should be tens of meters so that the distance of 100 meters can be covered with a reasonable number of telescopes to intercept the shadow on at least two of them. The only existing satellites of this size are the balloon satellites, which unfortunately are so lightweight that their orbits are perturbed unduly by random forces. In other words, the history of the satellite's movement is not known sufficiently well to use the satellite as a geodetic reference or fiducial mark.

One such small random force is the radiation pressure from earth albedo. The effects of this force have recently been identified by Prior in satellite tracking data [Ref. 8]. While Prior used estimates of average albedo [Ref. 9]., we have considered the effects of albedo noise, on the assumption that the average albedo will be accurately known from weather satellites. By albedo noise we mean such things as variations in the amount of ocean covered by clouds. Ocean and clouds are an appropriate example since ocean has a very low albedo and looks dark from above while clouds have high albedo and look white. Of course there are also uncertainties in other forces that act upon a large balloon, for example the atmospheric density at high altitude [Ref. 10]. However, we chose to emphasize earth albedo forces because of its obvious dependence on cloud cover, an extremely variable quantity. In Appendix F of this report we show that an extremely small perturbation in the albedo suffices to spoil the orbit of the balloon such as Pageos in so far as geodetic accuracy on the order of 1 meter is concerned.

Now consider the requirements of a special satellite that would avoid the random forces from the earth's albedo and from random variations in the solar radiation pressure. The satellite must have both a large cross-sectional area and a small interaction with radiation. These requirements are incompatible unless the satellite cooperates by changing its radiation cross-section on command when the satellite moves into the earth's shadow. The Fig. p. 18 shows a possible futuristic design for a special geodetic

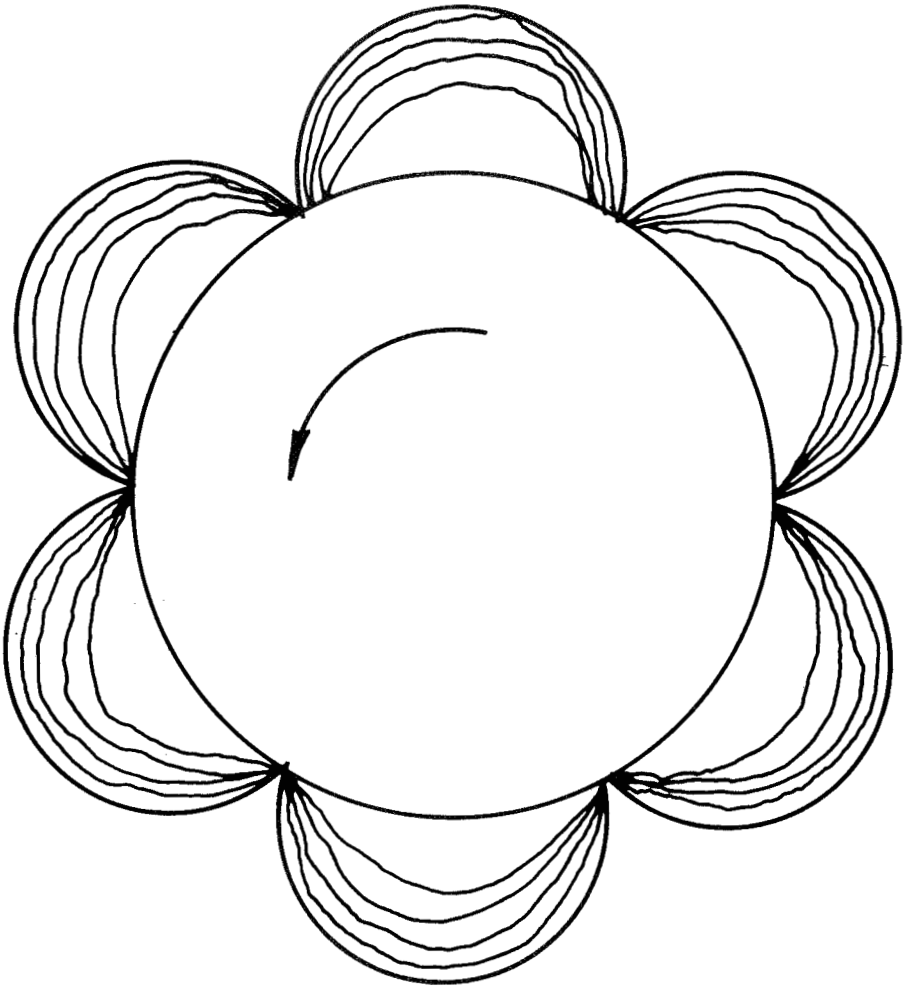

Conceivable Star Occultation Satellite

satellite that would combine the required properties. The satellite is spin stabilized with its axis pointed at the sun. The material around the periphery is a large plastic disk that has been gathered together with a pull-cord rather like a curtain. Whenever the satellite passes into the earth's shadow, the pull-cords may be released on command. Centrifugal force then extends the disk into an effective star occulting area. With the aid of vanes that act as solar sails (not shown), one can build a passive attitude control system that keeps the spin axis pointed at the sun [Ref. 11].

A more fundamental limitation on the star occultation system is the accuracy with which the absolute or relative positions of the stars are catalogued. Gordon [Ref. 6] has tabulated the average accuracy as a function of magnitude of the star. The frequency with which stars of various magnitudes may be found in various parts of the sky have been tabulated by Allen [Ref. 12]. If we were to first choose an area say an island like Hawaii with the idea of observing the occultation of any convenient star that comes along, then the odds are that the star would have to be of magnitude 7 or 8. But the angular positions of such stars are not known to the accuracy comensurate with the required accuracy of geodetic measurement on the order of a meter. Rather one should choose a very small number of bright stars as reference points in the celestial sphere and then let the satellite shadow with respect to these stars pass wherever they will around the earth. Only large continental areas are certain to fall in the path of the shadows, and the experiment would have to be set up in a wide variety of places around the world that are less than ideal sites.

1.3 TRIANGULATION CONCEPT AND INTERFEROMETRY

The remainder of this report deals with precision angle measurements by the triangulation concept illustrated in the Fig. p. 21. The reference for measuring angles is the baseline, and the angle θ is the complement of the angle which the baseline makes with the line-of-sight to the target. The figure shows a signal wavefront above the atmosphere, and two rays from the wavefront that follow different paths to arrive at the same detector. If the incoming signal is a continuous wave, this detector will see interference between the two rays and will count the interference fringes. However, if the incoming signal is a pulse of light, the detector will receive one pulse via each ray, and the receiver will time the delay between the two. In either case the basic triangulation applies. Also microwave components may replace the optical ones attached.

In the Fig. p. 21 the baseline is not necessarily horizontal. Instead, horizontal is the average direction of the wavy line that indicates the approximate upper boundary of the troublesome part of the troposphere, i. e., the air in which refractive index variations are a significant source of error. The northern station is elevated so that the baseline is more nearly parallel to the polar axis, i. e., the earth's spin axis. If the direction of the baseline is exactly north and south, and if the upward slope is equal to the (northern) latitude, then θ is equal to δ, the declination. However, there is a good chance that this much baseline slope will be impractical to build, so we treat the general case in which θ is the angle to the target measured from a plane perpendicular to the baseline.

1.3.1 Propagation Path Analysis

The triangulation measurement depends upon the difference in effective path length between the two rays as they pass from the wavefront to the

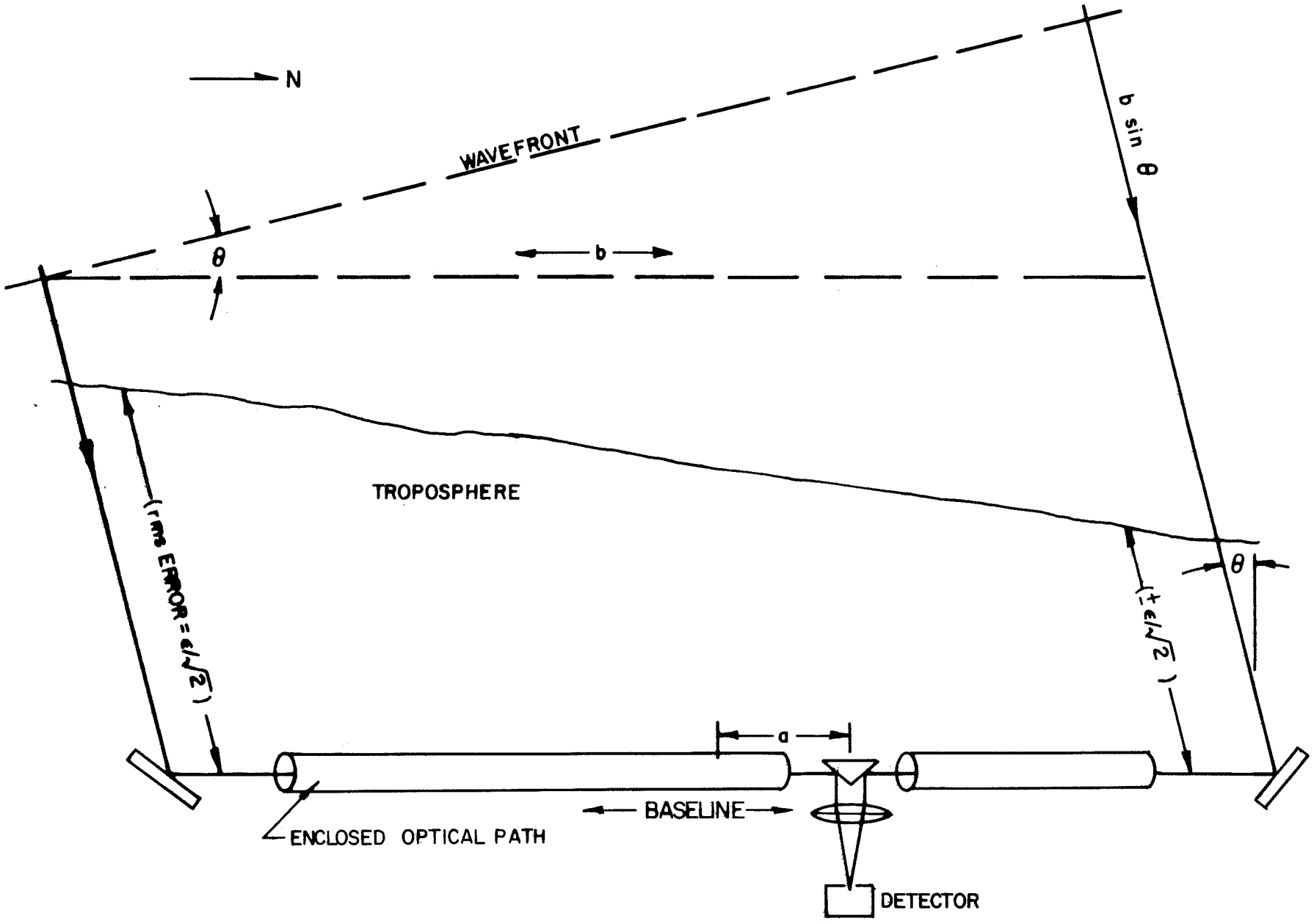

Geometry of the Interference Condition and Its Errors

detector. Effective path p is the pulse or phase propagation time multiplied by c (velocity of light); it is given by

$$p = \int_{1\text{-o-s}} n_a(s)ds \ , \qquad (1)$$

where 1-o-s indicates integration along the line-of-sight, and n_a is the refractive index of air, c/v, where v is the group or phase velocity in air depending on whether triangulation is by pulse or interferometry, respectively. The figure shows the basic triangle drawn in dash lines above the atmosphere to avoid any confusion between the part of the northern path that equals $b \sin \theta$ and the part of both paths caused by the refractive index of air. The distance a is a detector offset from the center of the baseline, a quantity that will be adjusted to achieve certain advantages as discussed later. The equations below express p in terms of the geometry of this figure. Here the parts of the phase path that are the same for both the north and south rays (note the subscripts n and s) are lumped into "const":

$$p_n = \text{const} + b \sin \theta - a$$

$$p_s = \text{const} + \Delta p(\text{air}) + a$$

The correction $\Delta p(\text{air})$ accounts for the extra amount of air above the southern interferometer station, since it is at lower elevation. The extra path length in air at the southern station equals $bg(\theta, \varphi)$, where g is a function of the pointing angles θ and φ, and of the orientation and slope of the baseline. It follows that

$$\Delta p(\text{air}) = (n_{ao} - 1)bg(\theta, \varphi) \ ,$$

where n_{ao} is the average refractive index of air over a distance of bg next to the ground at the southern station.

The path difference between the two rays is the measured quantity

$$q \equiv p_n - p_s$$

for which the above equations give

$$q = b \sin\theta - 2a - (n_{ao}-1)bg(\theta,\varphi) \quad .$$

To solve this equation for θ we do not have to treat $g(\theta)$ as unknown, since this is a small correction term and the nominal value of θ, i.e. θ_{nom} (from ephemeris or telescope shaft angles) suffices here, so finally,

$$\sin\theta = (q + 2a)/b + (n_{ao}-1)g(\theta_{nom},\varphi_{nom}) \quad . \tag{2}$$

Equation (2) is the fundamental equation for the angular measurements.

For various estimates we need an approximate version of Eq. (2) which neglects the small atmospheric correction, namely

$$\sin\theta \approx (q + 2a)/b \tag{3}$$

In the systems discussed in Part 2 of this report, it is advantageous to place the detector (Fig. p. 21) at the point along the baseline where $q = 0$, i.e., the two propagation paths are nearly equal. To locate this point we set $q = 0$ in Eq. (2) and solve for the detector offset a:

$$a = \tfrac{1}{2} b \sin\theta \quad . \tag{4}$$

Note that $a < b/2$, so the required position always exists.

1.3.2 Error Analysis

The basic equation for tracking error $\Delta\theta$ is

$$\cos\theta\Delta\theta = (\Delta q + \epsilon)/b + g\Delta n_{ao} \qquad (5)$$

Several features of this require explanation. Two of the terms come from differentiating Eq. (2), but an additional error ϵ in the effective path is inserted to allow for random air temperature differences between the two lines-of-sight. This error is indicated in the Fig. p. 21 by the quantity $\epsilon/\sqrt{2}$. The two stations are far enough apart so that the air temperature fluctuations are statistically independent, which means that the rms total error is the root-sum-squares that equals ϵ.

Equation (5) contains no terms in Δa or Δb, because we are assuming that these two distances are rigidly fixed in the ground so that their only changes are the very small ones that result from microseismic and tidal phenomena.* Of course, even if these quantities are precisely constant there can be a systematic error from imperfect precision in measuring them. However, we shall assume that constant systematic errors will be removed by the usual bootstrapping techniques used in orbit determination programs. That is, many quantities are treated as unknowns and adjusted to obtain a best fit to all the tracking data. In a similar manner the precise location of various tracking stations has been determined by treating these locations as an unknown during the orbit determination process.

Part II of this report follows immediately and describes candidate tracking systems based on the principles described here. All except one of the systems is interferometric, i.e., q is measured as $N\lambda$, counted wavelengths or interference fringes. The error term Δq [Eq. (5)] for interferometric systems becomes

$$\Delta q = \Delta N\lambda + N\Delta\lambda \quad .$$

---

*order of 10^{-8} radian

If the signal-to-noise ratio is large enough, the first term is minimized by accurately determining the phase of the beat between the signals from the 2 apertures, or in optical parlance, accurately finding the center of each interference fringe.

The second term is error from uncertainty in the wavelength. In various cases it will be minimized by stabilizing λ against an atomic clock standard, or by keeping N small. Small N implies that the detector is situated near the $q = 0$ (or $N = 0$) position, for which the criterion is given by Eq. (4). For this case we need an expression for the tolerance in a; i.e., how accurately must the detector be situated at the $q = 0$ position to maintain $N\Delta\lambda$ less than some acceptable level ϵ_λ (< other errors)? We find

$$N\Delta\lambda = N\lambda(\Delta\lambda/\lambda) = q\Delta\lambda/\lambda < \epsilon_\lambda \quad .$$

But since q is supposed to be zero, $q = \Delta q = 2\Delta a$; also $\Delta\lambda/\lambda = \Delta f/f$, the frequency stability of the oscillator, and so

$$\Delta a = \frac{q}{2} < \frac{\epsilon_\lambda}{2}\frac{\lambda}{\Delta\lambda} = \frac{\epsilon_\lambda}{2}\frac{f}{\Delta f} \quad .$$

However, the particular case in which we use the above expression will have its pulse separation doubled since the two-aperture optical system is used as transmitter as well as receiver. Then

$$\Delta a = \Delta q = \epsilon_\lambda \lambda/\Delta\lambda = \epsilon_\lambda f/\Delta f \qquad (6)$$

To complete a set of equations especially for the interferometers, we substitute $N\lambda$ and its increment into Eqs. (2) and (5) which become

$$\sin\theta = (N\lambda + 2a)/b + (n_{ao}-1)g(\theta_{nom}, \varphi_{nom}) \qquad (7)$$

and

$$\cos\theta\Delta\theta = (\lambda\Delta N + N\Delta\lambda + \epsilon)/b + g\,\Delta n_{ao} \qquad (8)$$

1.3.3 Interferometers versus Differential Lidar

The interferometers have the disadvantage that the absolute value of N can never be determined. Only increments $N_2 - N_1$ can be counted to give increments in $\sin\theta$, i.e. $\sin\theta_1 - \sin\theta_2$. The trouble with these systems is that there is no way to tag any inteference fringe including the N = 0 one. However, it is convenient to use equations with N instead of $N_2 - N_1$ with the understanding that ultimately a subtraction is necessary to obtain the difference form.

While the interferometers have the disadvantage of measuring only increments, this is offset by the fact that the required technology is fully developed. By contrast the system described in the next section (Sec. 2.1) measures an absolute q by differential lidar (optical radar: light detection and ranging). However, it involves very new components and techniques, and the problems of combining them into an operational system are not entirely obvious at present, but the prospects for development seem excellent. The interferometer-type optics are unaltered, and in fact the lidar system can be regarded as a special case of an intensity interferometer in which the pulse modulation waveform is the special intensity signal to be correlated.

PART II

CANDIDATE TRACKING SYSTEMS

2.1 DIFFERENTIAL LIDAR SYSTEM WITH PICOSECOND PULSES AT 1.06μ

Including the moon, there are now seven satellites in orbit which are equipped with panels of quartz retroreflectors for lidar ranging. Since the quartz panels are the only type of optical retroreflector that has been space qualified, it is important to consider any form of angular tracking that is compatible with them. The system described in this section was selected primarily for its compatibility with these retroreflectors. Unfortunately the quartz panels are not usable with wavelengths longer than about 3.5μ, because the cube corners reflect from their back surfaces, and quartz of this thickness is not transparent to longer wavelengths.

A light beam reflected from any of the six panels currently in orbit is so narrow that the spot it illuminates on the ground is not large enough for a significant baseline to fit inside the spot. At first thought, this may appear to preclude the use of any of these orbiting panels in interferometry. However, it is relatively simple to circumvent this difficulty by using the two interferometric telescopes as transmitters as well as receivers, each telescope receiving the return from its own transmission but not intercepting any of the return from the other telescope. When the two-aperture optics are used in this manner for two-way propagation, the measured difference in propagation paths is $2q$ instead of q in the notation of Sec. 1.3. In the case of the retroreflector on the moon a separate transmitter may be used, because the return will illuminate a spot on the ground approximately 13 km in diameter, which is certainly adequate for any optical baseline considered in this report. Instead, the problem in the moon case is that of receiving sufficient power.

In Sec. 1.3 the basic triangulation was discussed and Eq. (2) was derived to find the angle θ (Fig. p. 21) from the measured difference q in the (phase or group) path distance to the two stations. In principle, q can

be measured by timing the difference in arrival time of 2 pulses, or by counting interference fringes, i.e., $q = N\lambda$. However, in practice it does not appear advisable to attempt to form optical interference fringes using wavelengths shorter that 3.5μ when the two light beams are received in separate telescopes. Such a system would place requirements that are too stringent upon the dimensional stability of the telescopes and upon the equipment used to track out the atmospheric jitter in the interference fringes. Therefore, for use with the quartz reflector panels, the appropriate system is a form of intensity interferometry in which the light beam serves only as a carrier while measurements are made on the modulation envelope.

The modulation wave form must have wavelengths much shorter than a centimeter so that the carrier is tagged at short intervals to attain the desired angular resolution. There is only one high-power short-wavelength laser which has a sufficiently wide bandwidth as well as means for modulating at the desired rate. This is the neodymium-glass laser (Nd:glass) with emission at 1.06μ. [Refs. 13, 14] These lasers have a natural tendency to emit pulses with widths on the order of 1 picosecond, i.e. 10^{-12} sec or a length of 0.3 mm in a vacuum. Thus the appropriate waveform is a single pulse, or perhaps pulse train, and the intensity interferometry degenerates to the simple concept of timing the interval between the arrival of 2 pulses.

The technology of controlling and measuring such extraordinarily short pulses is quite new. At the detector of Fig. p. 21 we have the problem of sensing the difference in arrival time of 2 pulses with picosecond accuracy. This is done by replacing the beam combining optics and detector with the system in Fig. p. 30. The fluorescent cell is filled with Rhodamine 6G dye in ethanol [Ref. 15], which exhibits a non-linear fluorescence that is strongest where the 2 pulses collide. Hence the delay between pulses is timed by photographing the exact point at which they collide. To observe non-linear fluorescence, the pulses must be

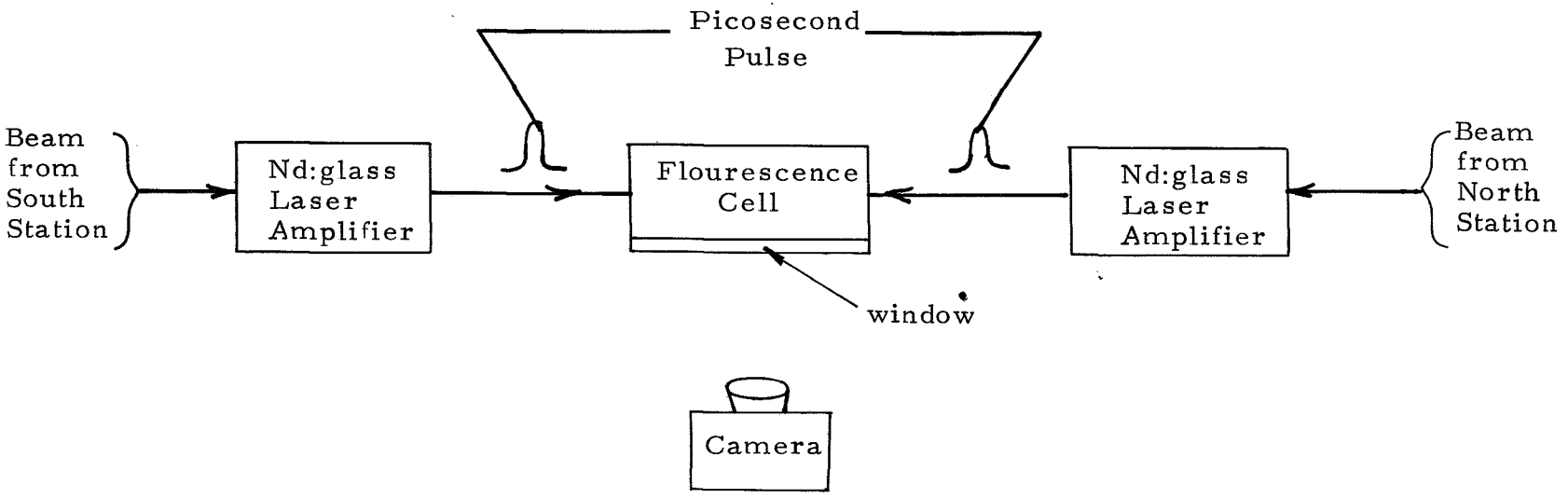

Detector for Picosecond Pulses

preamplified as shown in the figure. This technology needs further development before it is ready for construction of the tracking system.

The fluorescence cell must be situated at the point along the baseline where $q = 0$; otherwise, the pulse collision would occur outside the small cell. This is the point where the two propagation paths are equal, and where white light interference could be observed if the system were operated as a stellar interferometer. Such an interferometer with a 1 km baseline was once proposed by Miller [Ref. 16] to observe white light fringes. The construction of Miller's interferometer would certainly be a formidable undertaking since white light fringes are visible for distances of only a few microns and therefore difficult to find. However, the psec pulses discussed here will collide over a range of about 150μ. It is quite practical to maintain the dimensional stability of optical telescopes and their associated apparatus within this limit. Miller mentioned two kinds of apparatus to find and follow the $q = 0$ point. One is a precision trolley that would ride on a track and the other an optical delay line in a form resembling a trombone slide. A detector (cell) on a trolley car corresponds to a continuous adjustment of the parameter a (Fig. p. 21) to the value $\frac{1}{2}b \sin\theta$ given by Eq. (4).

The trolley system implies that the receiver system would have to ride a precision railroad of some form which must have a length less than but comprable to b, if the overall system is to be usable for a wide variety of angles θ. There are several undesirable features of this straightforward technique. First, the receiver system is likely to be rather large, requiring that the precision track be the outdoor type, a quality that is hardly compatible with its precision nature. Second, the system is likely to be situated on mountainous terrain for seeing conditions of astronomical quality. The terrain may require corners in the baseline path with mirrors to turn the light beam. The corners would obviously interfer with a trolley continuously tracking the $q = 0$ point as θ varies. Finally, the optical path along the baseline must be either evacuated or filled with helium (low refractive index) to reduce disturbances from

refraction in air. This means that any trolley would have to connect to air-tight telescoping tubing.

2.1.1 Optical Delay Line

A more complicated but much preferable system for finding the zero order fringe or pulse collision point is shown in Fig. p. 33. Here the receiver system is stationary, but an optical delay line is inserted in the propagation path from either or both of the two telescopes so the shorter of the two paths is lengthened until both paths are approximately equal. The length adjustments in the various delay lines cause the two optical pulses to collide in the fixed fluorescent cell shown at the top of the figure. This delay line system does not require a long track for moving parts; instead, the delays are adjusted by movements of small parts which switch the beam in or out of the various delay lines and determine the number of passes of the folded optical path within each delay line. The figure shows schematically some of the parts for gross adjustment of the length of the optical delay. These are cross-hatched mirrors that determine which delay goes into which beam.

As an example of distances that might be involved, the figure includes some plausible dimensions. The reasonable maximum for the propagation distance in the longest cell might be 800 m . This path can be folded about 40 times so that the cell need be only 20 m long. The delay is adjustable in discrete steps of 40 m which correspond to two passes, one down the cell and one back. Note that the shorter delay lines have adjustment increments of 4 m and 40 cm, respectively; in other words, each differs from the other by a factor of 10. Various mirrors and prisms are movable so that the beams from either telescope may be passed through one or more of the delay lines or the beams from both telescopes may be passed through as shown in the figure. This allows an adjustment in either beam that varies in steps of 40 cm anywhere from 0 to 888 m . Regarding 40 cm as the unit of distance, the delay is adjustable in

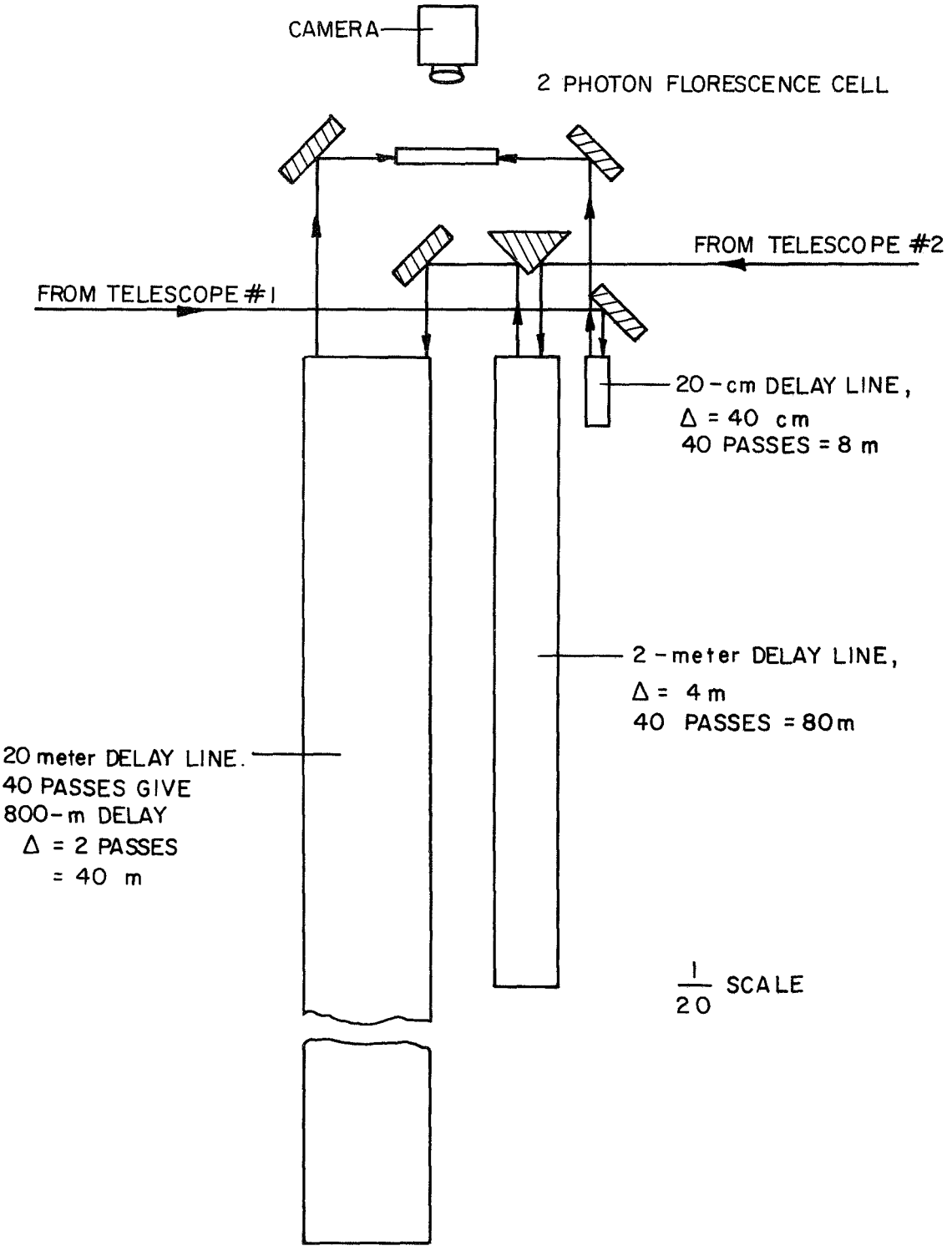

DIGITAL OPTICAL DELAY LINE

increments of one unit from 1 to 2220 units, or rather -2220 to +2220 considering a switch to the other beam as a sign change. To achieve any integer in this range of ±2220 one could set the shortest delay line so that the number of passes is twice the units digit of the integer, the middle-sized delay line for twice the tens digit, and the longest line for twice the hundreds digit (+10 × thousands digit). To achieve each integer exactly one way, we need a range of only 10 increments in each of the 2 smaller lines. As shown in Fig. p. 33 20 increments are actually provided, or rather 40 considering the possibility of switching the line into either beam. This redundancy is desirable for tracking with the minimum amount of frantic switching.

For tracking the lunar retroreflector or a near synchronous satellite, the 20 cm delay line could be replaced with a movable roof-top reflector (prism) on a 4 meter track. This permits smooth continuous tracking with a lead screw. However, for tracking low-orbit satellites, such as the six that are equipped with retroreflectors, the lead screw would have to track at rates in excess of a meter/sec unless the satellite's track is nearly perpendicular to the baseline. Only a few seconds of continuous track are possible at this rate. In these cases it seems advisable to abandon continuous tracking in favor of intermittant (digital) tracking. The operator can photograph a single pulse collision in the fluorescence cell, then quickly readjust the various mirrors and delay lines to catch the satellite in a new position that it will occupy after a brief pause. For intermittant tracking, the fine adjustment of 40 cm in Fig. p. 33 clearly suffices.

The intermittant tracking mode raises a problem of satellite acquisition. To catch the first satellite echo the fluorescence cell length must be $L \approx 2b\Delta\theta$, where $\Delta\theta$ is the ephemeris error. Assuming $b = 1500$ m and $\Delta\theta = 1/2$ mrad gives $L = 1.5$ meter, which is excessively long. Several solutions to this problem are possible, such as multiple cells, or a multiple-pulse first transmission with some tens of m sec spacing.

However, the most attractive solution is an accurate visual fix early in the satellite pass over the station so that its position is known to $< 10^{-4}$ rad (20 arc sec) when the fluorescence cell is used later in the same pass.

As shown in Fig. p. 36 the optical delay line may have the form of the White absorption cell. This is a classical optical arrangement for lengthening the path of light in a gas in which the experimenter desires to measure optical absorption. Each delay line has three mirrors. Two are shown on the left and one on the right. These are curved confocal mirrors meaning that the focal planes of the three mirrors coinside near the center of the delay line. The input and output of the White cell are on the right end where the beam for each pass is focused down to a defraction-limited spot on the mirror's reflecting surface. On the left of the cell, the beams are defocused to fill the areas of the mirrors. Only eight passes in the cell are shown to avoid cluttering the figure; however, 40 passes is a number that is commonly used to fill the volume to good advantage. On the right mirror, where the beams are focused, the passes terminate in 19 spots arrayed in two rows, nine spots in one and 10 in the other. Each spot represents two passes, one where the beam approaches the spot, and one where it is heading back toward the left. This gives 38 passes, and the input and output passes make the other two. Making small tilt adjustments in the mirrors at the left, accompanied by small movements of the prisms that produce and extract the input and output beams, the operator can adjust the total number of passes in the delay line and thereby perform the digital adjustment of the optical path length.

The White absoption cell is not the only configuration of mirrors that is suitable for folding a very long optical path into a relatively small volume. Another form of optical delay line that has gained acceptance was invented by Herriott [Ref. 17]. Like the White cell, Herriott's

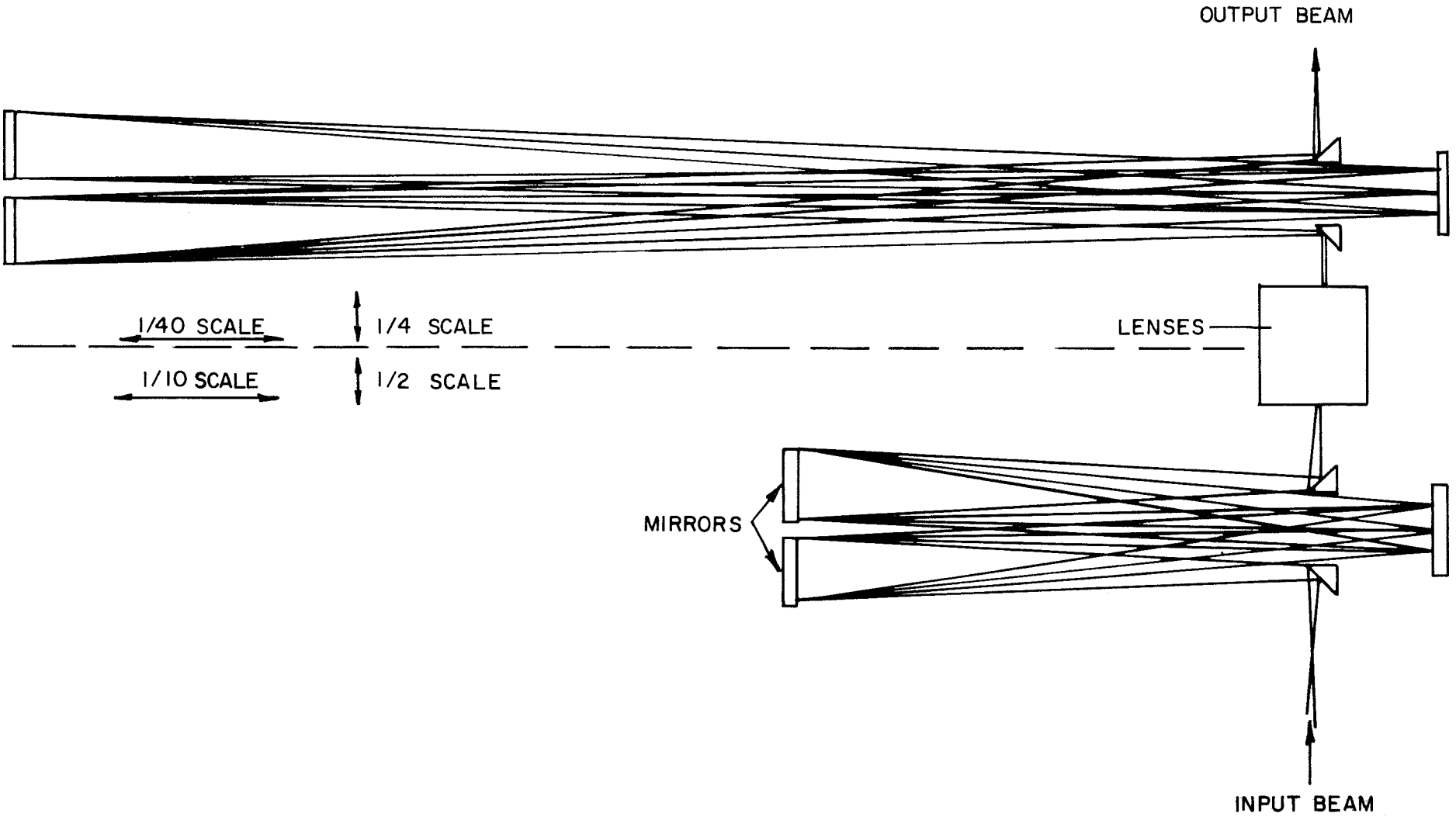

White Cell Configuration of an Optical Delay Line

delay line has focal spots, one for each pair of passes, on one of the end mirrors. However, in his configuration the spots form a circle instead of two straight lines. If a slight asymmetry is introduced to Herriott's optics, the focal spots line up in more than one approximate circle, slightly displaced from one another rather like a spring viewed from the side.

To conclude this subsection, let us point out certain components that were omitted from Fig. p. 33 to avoid clutter. The delay lines of different lengths will require input and output beams having different diameters and f numbers. Various lenses will be required to make these adjustments. Finally the numerous reflections from the mirrors in the delay line will absorb most of the power in the pulse, say 0.1 db attenuation (2%) per reflection for 100 reflections gives 10db total attenuation. A Nd:glass amplifier with about 20 cm gain length (propagation distance in the glass) will compensate this loss if necessary, since Nd:glass exhibits as much as 60 db gain per meter. [Ref. 18] This amplifier is in addition to a preamp situated as close as possible to the collecting optics. Amplifiers should be distributed so that the signal is always stronger than the quantum limit, but never intense enough to damage a component.

2.1.2 Picosecond Pulse and Nd:glass Laser Technology

2.1.2.1 Pulse Generator

The Nd:glass laser consists of a glass rod, some cm long and mm in diameter, that is doped with a neodymium compound to give Nd^{3+} ions.* A nearby flashlamp excites the Nd ions with incoherent light, and the rod exhibits gain at 1.06μ for the duration of the flash. Mirrors near the ends of the rod provide the feedback to convert the amplifying medium into an oscillator. Usually a so-called Q-switch is situated in the light path between the rod and the mirror. It is a device or non-linear material that enhances the laser's tendency to oscillate in brief powerful bursts.

*Also a doped fibre microns in diameter is often clad with undoped glass.

The table on p. 39 summarizes recent advances in the generation of psec pulses. Note that the shortest pulse is 0.25 psec (<100μ long!), the greatest pulse energy 0.3J, and the shortest overall emission was a single pulse that Kachen et al [Ref. 19] extracted from a pulse train using an electro-optic switch. However, not all these superlatives were achieved in the same apparatus, and there may be some practical problem of incompatibility.

As shown in the subsection 2.1.3 the tracking accuracy of the differential lidar system is proportional to the pulse duration under most seeing conditions. Therefore an estimate of the shortest practical pulse length is pertinent. For a most conservative pulse length, let us consider 3 mm. This corresponds to 10 psec, a length which Kachen et al [Ref. 19] have extracted as a single pulse and amplified to as much as 300 millijoules (mJ), enough for a lidar echo from a retroreflector in synchronous orbit at 40 megameters (Mm). The shortest pulse that is theoretically possible from the Nd:glass laser is about 0.2 psec, a limit that is set by the gain bandwidth of the material, which is about 100 cm^{-1}.* This pulse duration converts to 60μ of pulse length. Somewhere between the conservative and liberal figures lies a figure which we can reasonably expect to attain after the technology develops. The value $\frac{1}{2}$ psec is reasonable because pulses somewhat shorter than this have already been observed but have not yet been amplified to high energy levels. Since there is no apparent fundamental limit to amplification of pulses this short, we expect that, in the near future, high energy pulses of $\frac{1}{2}$ psec duration will be available. This duration converts to 150μ of pulse length.

2.1.2.2 Preamplifier

A traveling wave (TW) laser amplifier should be situated as close as possible to the light collecting system so that the signal is amplified

---

* $\tau = (2B)^{-1} = (2 * 100\ cm^{-1} \times 3 \times 10^{10}\ cm/sec)^{-1} = 1/6$ psec .

Authors	Reference	Shortest Pulse Duration,[a] psec.	Energy of Shortest Pulse, mJ.	Pulse Rep. Period, psec. and sync.[b]	Q-Switch	Remarks
A. J. Alcock & M. Richardson	Phys. Rev. Ltrs. 21, 667 (2 Sept 68)	10	100	8000 resonator	Saturable dye	Intracavity polarizer dumps energy in one pulse. Air spark.
A. J. Alcock, et. al.	Appl. Phys. Ltrs. 14, 145 (1 Mar 69)	5	20			Self focusing output
E. B. Treacy	Appl. Phys. Ltrs. 14, 112 (1 Feb 69)	0.44 (compressed from 8)	small	~7000 resonator	Saturable dye	Grating pairs were dispersive element for pulse compression like chirp radar. 4.5 ps/100 Å
M. A. Duguay, S. L. Shapiro, P. M. Rentzepis	Phys. Rev. Ltrs. 19, 1014 (30 Oct 67)	< 1.0	0.5	67 output flat	Rotating mirror	Ripple period = 3.3 nsec = 2 L/c
G. Kachen, L. Steinmetz, J. Kysilka	Appl. Phys. Ltrs. 13, 229 (1 Oct 68)	10	300	8000 resonator	Saturable dye	Extracted single pulse with external optics
S. L. Shapiro, M. A. Duguay, L. B. Kreuzer	Appl. Phys. Ltrs. 12, 36 (15 Jan 68)	3	0.06	38 output flat	None	600-900μ sec output 200 n sec spikes Ripple or pulse at c/2L rate
M. A. Duguay and S. L. Shapiro	Bull. Am. Phys. Soc., meeting 11 May 69, abs. HC1	0.25				

a. Theoretical limit is about 0.2 psec, set by the 100 cm^{-1} gain bandwidth in Nd: glass.

b. Pulses synchronize at the round trip propagation time of light either within the optical resonator or between the two faces of an uncoated flat used as the output reflector.

before losses in the optics reduce the signal to the photon* limit; i.e., there should be several photons in each pulse at the point in the system where the signal is weakest. The amplifier should have enough gain to raise a signal of 2 photons $\approx 10^{-17}$ J (or -170 dbJ) to about 1 mJ (or -30 dbJ), i.e., a gain of 140 db. At 60 db per meter, this requires a path length of 2.4 meters in Nd:glass. A likely configuration is a glass rod 30 cm long inserted in a White cell that provides 8 (or more) passes through the rod. Fig. p. 41 shows amplifying glass rods at the unfocused end of the White absorption cells. This is done so that the pulse will sweep out the whole volume of the Nd:glass during its passage and extract power with maximum efficiency. During the time the pulse takes to bounce to the focused end of the cell and back, the rod has recovered some lost gain, and so more energy is available during the pulse's next pass through the rod.

A significant problem in using a White cell or similar folded optical path for high-gain traveling-wave amplification is the possibility of accidental positive feedback within the cell. Minute scratches or flecks of dust tend to reflect some of the output back into the input, causing the amplifier to be noisy or to break into spurious oscillations, much like the problems of the super-regenerative radio receiver. Fortunately Nd:glass has good optical quality. One precaution to lessen the chance of this is a series of masks that will absorb scattered light on the focused end of the cell. Also it is advisable to preceed the multipass amplifier by a single-pass preamp if the input signal is close to the photon limit.

To our knowledge** the Nd:glass laser has never been tested for its noise properties as a small signal preamplifier. In laser communications

---

* Strictly speaking a linear amplifier does not exhibit the same statistical behavior as a photon (energy) counter, but to the accuracy required of this report, the results are the same.

** Also to the knowledge of Dr. Heinz P. Weber of Bell Telephone Labs.

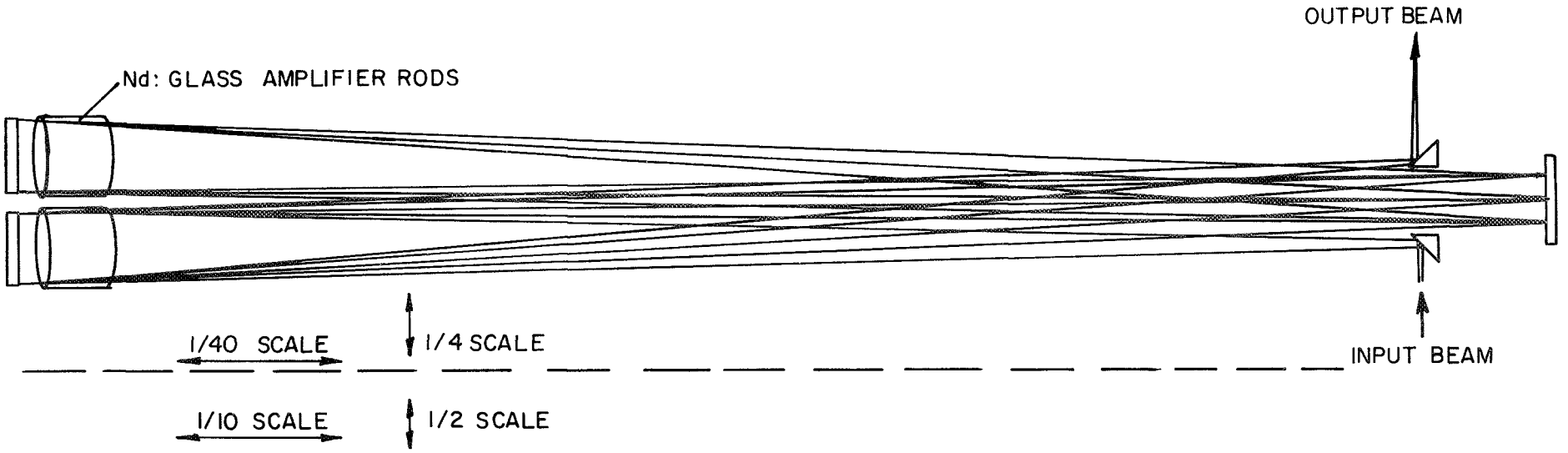

SIDE VIEW OF END, FULL SCALE

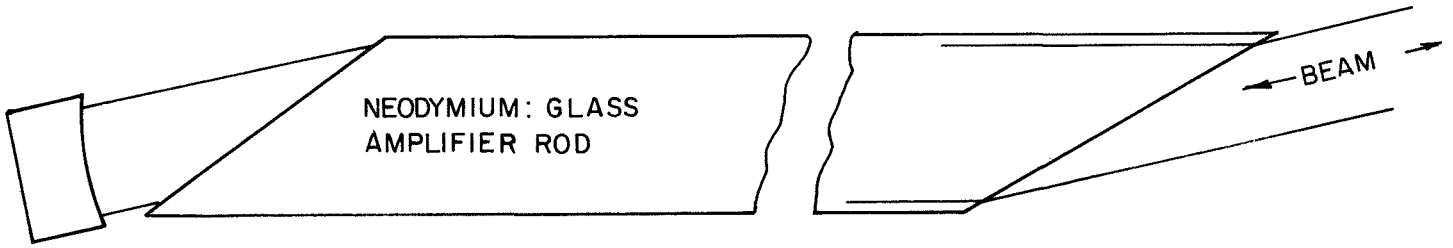

Nd:glass TW Amp in White Cell

studies, one does not normally consider the use of a laser preamplifier especially one with a bandwidth as wide as the Nd:glass. This is because the noise which limits the performance of such an amplifier is the spontaneous emission from the Nd ions within the material. This emission fills the whole bandwidth of 100 cm^{-1}, which in frequency units is 3000 GHz (3 THz), much broader than the bandwidth of any known communications system. The trouble is that no known optical filter has a sufficiently narrow pass band to remove the noise in this excess bandwidth and limit the noise to the unavoidable part in the information bandwidth of the communications system. However, in our application a picosecond or sub-picosecond pulse will nearly fill the gain bandwidth of the crystal, and the discrimination against noise will take place in time instead of frequency. That is, the lidar echoes are so short that their peak power is exceedingly high, high enough to be discernable despite the noise level if there are at least several photons in each pulse. In Sec. 2.1.4 we discuss the radar range of this system as though the Nd:glass preamplifier has the noise properties of an ideal laser amplifier, i.e., only a few photons/pulse are required, since to our knowledge there are no theoretical reasons to suspect otherwise.

2.1.2.3 Duplex Operation

As mentioned previously a special problem arises when the 1.06μ differential lidar system is used with retroreflectors on artificial satellites; viz., the echo from any one transmitter does not illuminate enough area on the ground to cover a reasonable baseline. The solution is to transmit through both apertures and let each receive its own echo. This requires the duplex arrangement shown in Fig. p. 43, which is largely self explanatory. The duplexer can be any one of a number of electro-optic switches [Refs. 20, 21, 22], which switch in 3 msec or less. This interval is less than the round trip propagation time to the lowest satellite orbits.

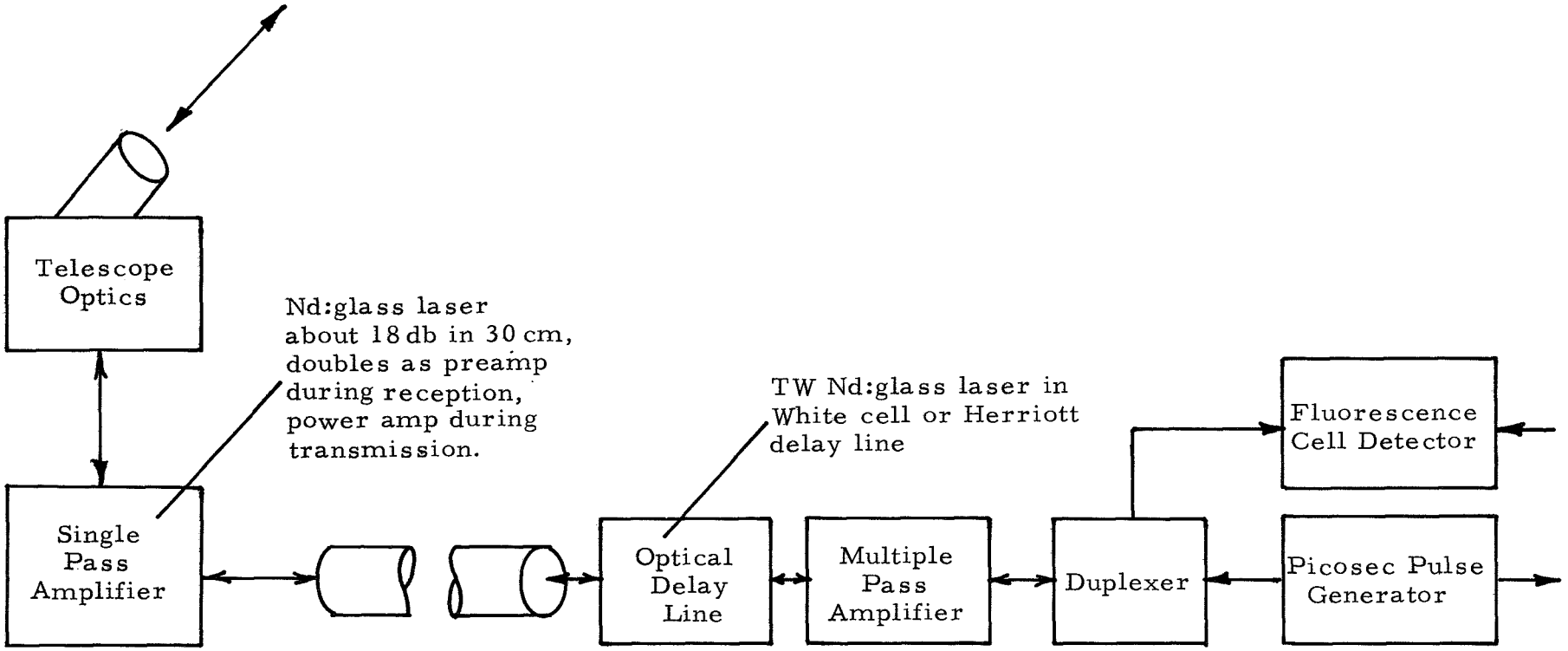

One side of the two-aperture differential lidar system showing duplex operation required for artificial satellites. Switch must have 2 ms response time. Power amplifier has only one pass to avoid damaging components with high intensity at a focal point.

One suitable duplexer would employ frustrated total internal reflection at a small gap between two prism faces as shown in Fig. p. 45 . A very small piezoelectric movement at the gap will open or close it enough to allow or frustrate the internal reflection. Fig. p. 46 defines some optical component notation, and Fig. p. 47 uses this notation to illustrate part of the duplexing arrangement in a less abstract way than the block diagram of Fig. p. 43.

2.1.2.4 Fluorescence Cell Detector

As already noted the preferred detector for timing picosecond pulses is the pulse collision technique in a fluorescence cell. Giordmaine et al [Ref. 23] first described the method in a paper which caused quite a flurry of activity in this area recently. They reported experiments in which fluorescence was observed in a dye excited by two photon absorption of the light from a Nd:glass laser. The fluorescence was enhanced at points where two pulses collided as a result of the extra light intensity during the collision. Since this original demonstration, the technique has been improved with the use of Rhodamine 6G dye in ethanol [Ref. 15]. In their review of this topic [Ref. 15] DeMaria et al show excellent photographs [Fig. 23 p. 17] of pulse collisions in cells a few cm long. The fluorescent technique has a drawback for our application in that a relatively powerful laser pulse is required to observe two photon fluorescence. This means that the very weak signals coming through the receiving telescope need > 100 db amplification as was discussed in Sec. 2.1.2.2.

To our knowledge no one has attempted a two-photon fluorescence cell longer than a few cm, so there may be absorption difficulties in making a long enough cell to be certain the collision occurs inside it. A displacement of the collision by a distance x in the cell corresponds to a relative pulse delay of $2x/c_g$, where c_g is the group velocity of light in the cell. A cell of length L in the duplex system will contain

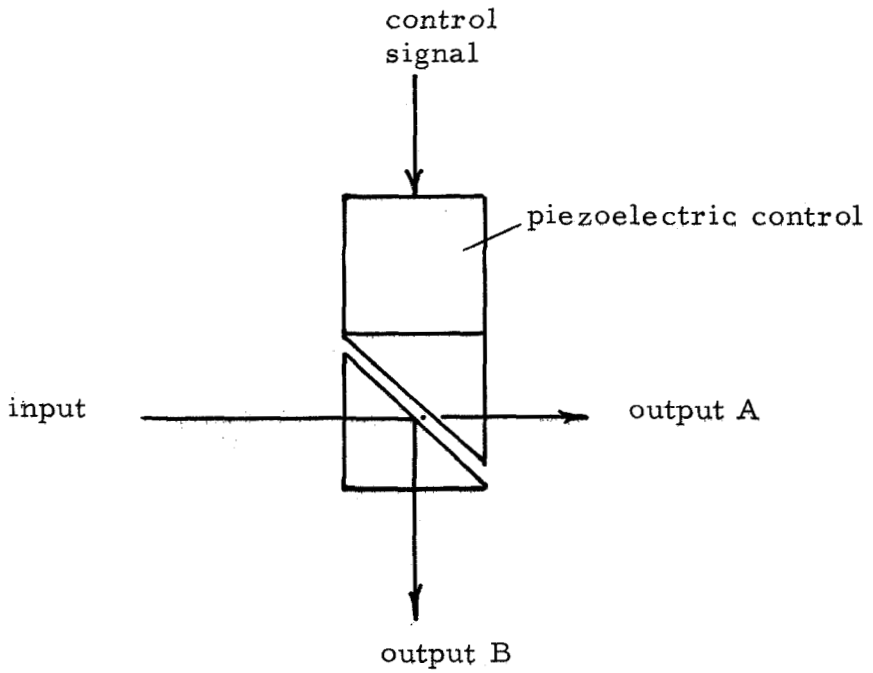

Electro-Optic Switch

Mirror:

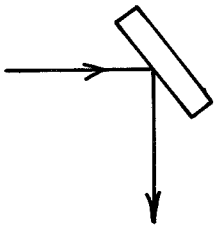

Beam Splitter:

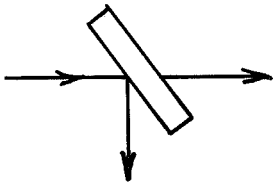

Optical Delay Line:

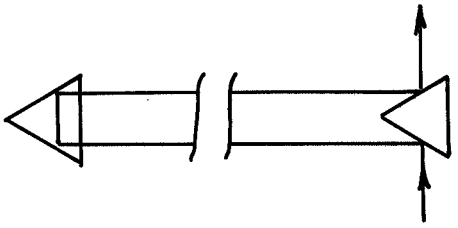

Fluorescence cell for pulse collision detection

Electro-optic switch

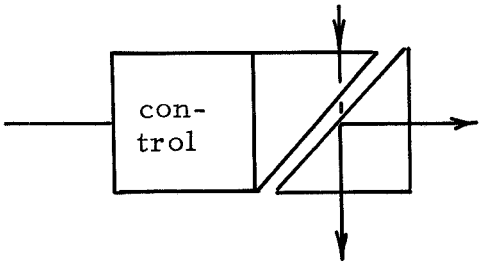

Traveling-wave amplifier

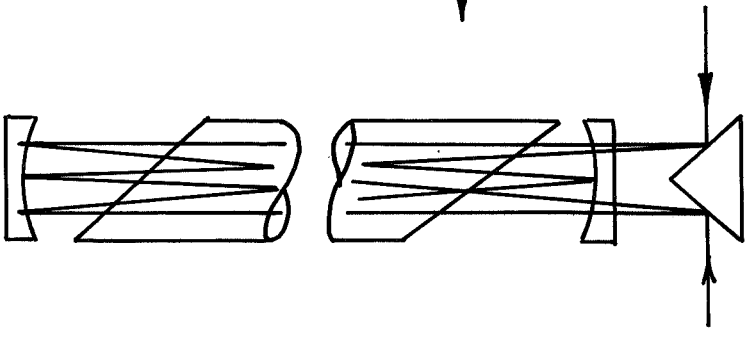

Optical Circuit Elements

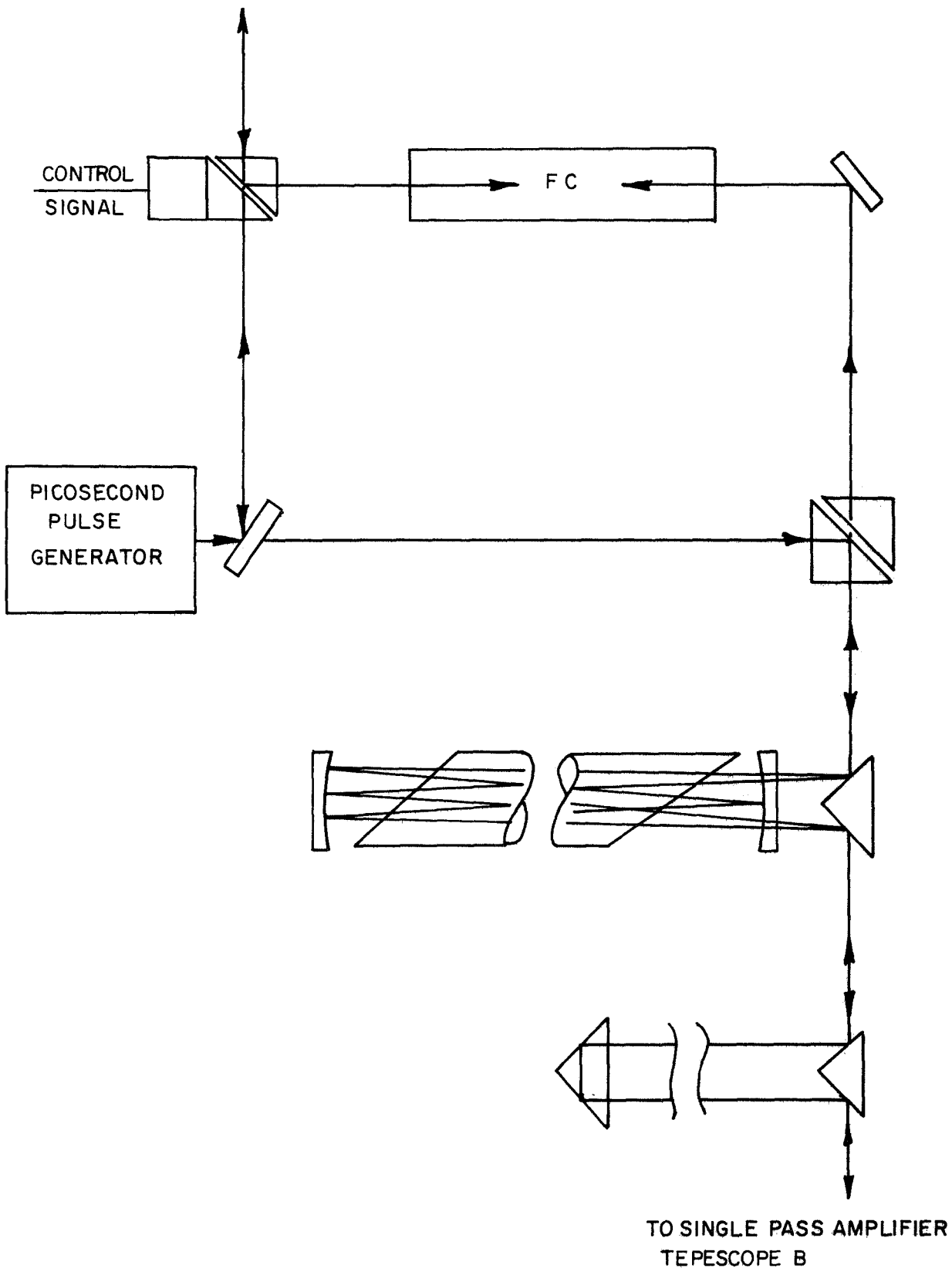

Optical Circuit with Duplexer, Delay Line, and Amplifier

the collision if the pointing of the telescope is accurate to an angle of $\Delta\theta = L/2b$. If $L = 10$ cm, $b = 1$ km, then $\Delta\theta = .5 \times 10^{-4}$ rad = 10 arc sec.

2.1.3 Tracking Error

The tracking error is determined by Eq. (5). Let us neglect $g\Delta n_{ao}$, since the refractive index of air near the ground can be monitored through its known dependence on temperature and pressure. Let us also take $\cos\theta \approx 1$ for rough estimation, and $\Delta a = \Delta q$ for the duplex system as in Eq. (6). Then

$$\Delta\theta \approx (\Delta q + \epsilon)/b \quad .$$

In Appendix B we show that ϵ is about 100μ for the worst case of air temperature differences during an experimental program on Mt. Palomar. The accuracy of finding the center of a collision between pulses 150μ long may be about 70μ. So a good conservative estimate for $\Delta q + \epsilon$ is about 150μ. If we assume that $b = 1.5$ km, then

$$\Delta\theta = 150\mu/1500\,\text{m} = 10^{-7}\,\text{rad} = 0.02\ \text{arc sec} \quad .$$

This would not be an impressive number for an angular increment, but it is very impressive for absolute angle. At a range of 2 Mm, typical for retroreflecting satellites, the linear error is

$$R\Delta\theta = 10^{-7} \times 2\ \text{Mm} = 20\ \text{cm} = 8\ \text{inches} \quad .$$

2.1.4 Range Equation

All range equations are derived in Appendix D. The pertinent one for the picosecond pulse system is Eq. (D-9), where Q_{sat} contains the range and reflecting properties of the satellite and is defined in

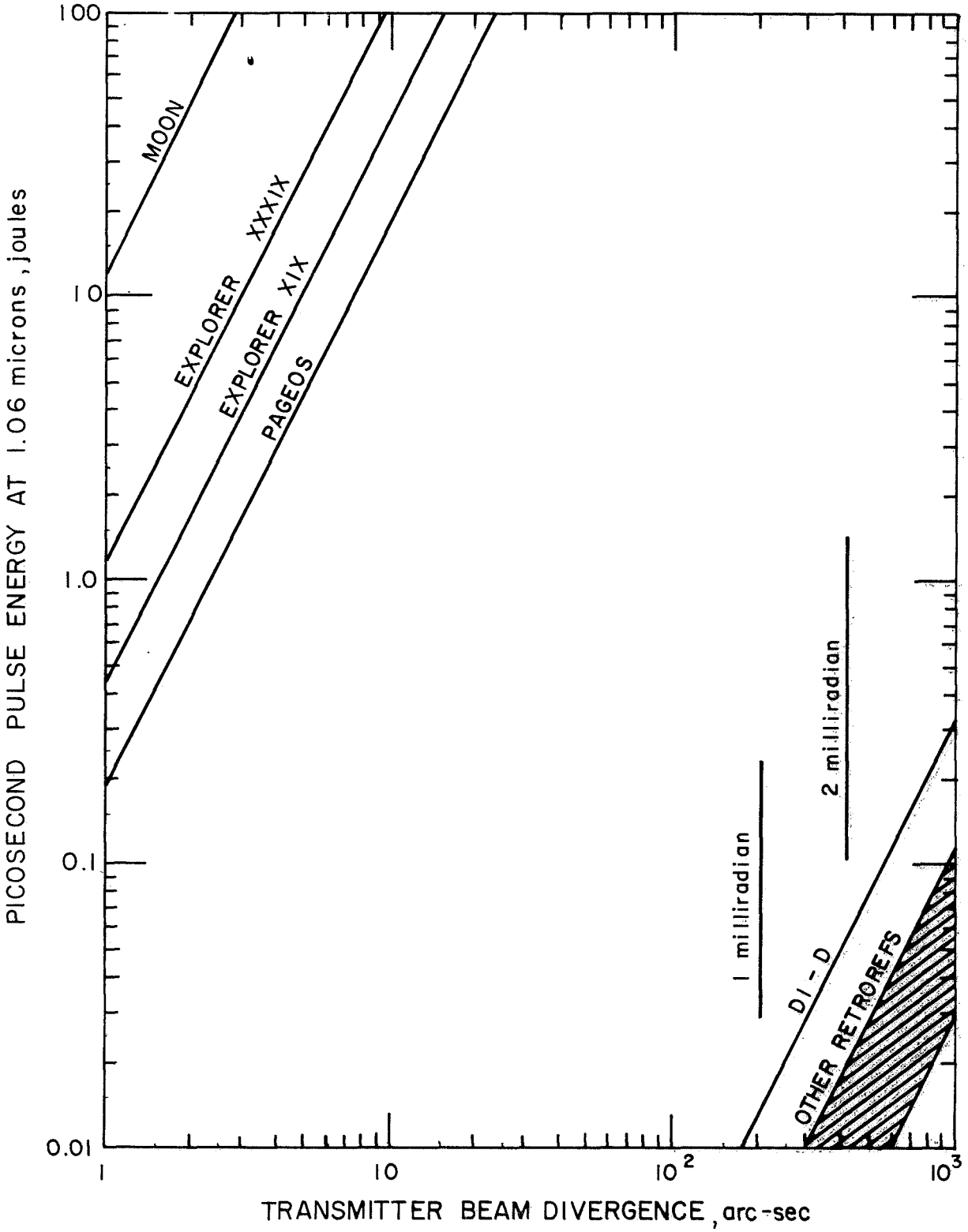

Energy required per pulse in a Nd:glass Picosecond Laser system.

Assumed: Seeing = 2 arc sec. Efficiency (telescope and atmosphere transparency) = 50%. Ten photons received at amplifier input.

Eqs. (D-1) and (D-7). In Equation (D-9), η is the efficiency or transparency of the telescopes and atmosphere, L is the energy loss E_R/E_T in two-way propagation, θ_{up} is the beam angle illuminating the satellite, and θ_{dn} is the seeing angle, i.e., angular diameter of the blur circle. Let us assume

η = 0.5 (astronomical quality),

θ_{dn} = 2 arc sec, E_R = 10 photons, and

Q_{sat} = values for various satellites in Appendix E.

This leaves two unspecified quantities, the required energy of transmission E_T, and the angle θ_{up} which may be greater than θ_{dn} to be sure of illuminating the satellite with imperfect ephemeris. These are plotted in Fig. p. 49.

As expected the satellites with quartz retroreflectors in low orbits require only moderate pulse energy, even with a broadened beam. The moon and balloon satellites require much more energy, near 100 J per pulse. However, the beam need not be broadened to intercept the target on the Moon.

2.1.5 Doppler, Velocity Aberration, and Conclusions

Two very simple estimates will complete the discussion of the differential lidar system and its feasibility. The first of these concerns the effect of doppler shift. Two-way doppler shift is the frequency

$$f_d = 2\dot{R}/\lambda ,$$

where $\dot{R}$ is the range rate. Using $\lambda = 1.06\mu$ and a large satellite $\dot{R}$ of 6 km/sec gives f_d = 11 GHz, which is small compared to the gain bandwidth of the Nd:glass, 100 cm^{-1} or 3,000 GHz. This means that the doppler will not interfere with reception and amplification of the signal; although, it may cause a small shift in the effective optical path,

i.e., a small change in refractive index of the Nd:glass that results from anamolous dispersion.

Velocity aberration occurs when a retroreflector has a significant component of tangential (i.e. not radial) velocity $\cdot v_t$. In earth fixed inertial coordinates the return is not exactly retro-directed*, but displaced by an angle $2v_t/c$ in the direction of satellite movement. This means that the cone angle φ_r of the return must be at least twice the angular displacement if the receiver is in the same telescope as the transmitter, i.e.

$$\varphi_r \geq 4v_t/c \ .$$

This can be expressed as a constraint on the coherent diameter of the retroreflector, i.e., the diameter d_c over which the cube corner surfaces are cubic to an accuracy of about $\lambda/2\pi$. Taking $\varphi_r = \lambda/d_c$ gives

$$d_c \leq \lambda c/4v_t \ . \tag{9}$$

This restriction implies a limit on the radar cross-section of a reflector, see Appendix D, Eqs. (D-1a) and (D-2c), where $A_e = \pi d_c^2/4$. The permissible coherent diameter is indeed small for low orbit satellites; for example $\lambda = 1.06\mu$, $v_t = 7.5$ km/sec gives $d_c = 1.1$ cm. However, note that any satellite that gives strong returns with a ruby laser (0.69μ) will also do so with a Nd:glass laser (1.06μ), since the wavelength change is in the favorable direction.

Even a geostationary satellite exhibits velocity aberration, since the coordinate system in which it is stationary is not an inertial one. In this case $v_t = 3.073$ km/sec and Eq. (9) gives $d_c \leq 2.59$ cm. Fig. p. 52 gives v_t for circular orbits as a function of orbit radius and of orbit height above the earth.

---

*It is exactly retro-directed in an inertial frame that is instantaneously at rest with respect to the satellite.

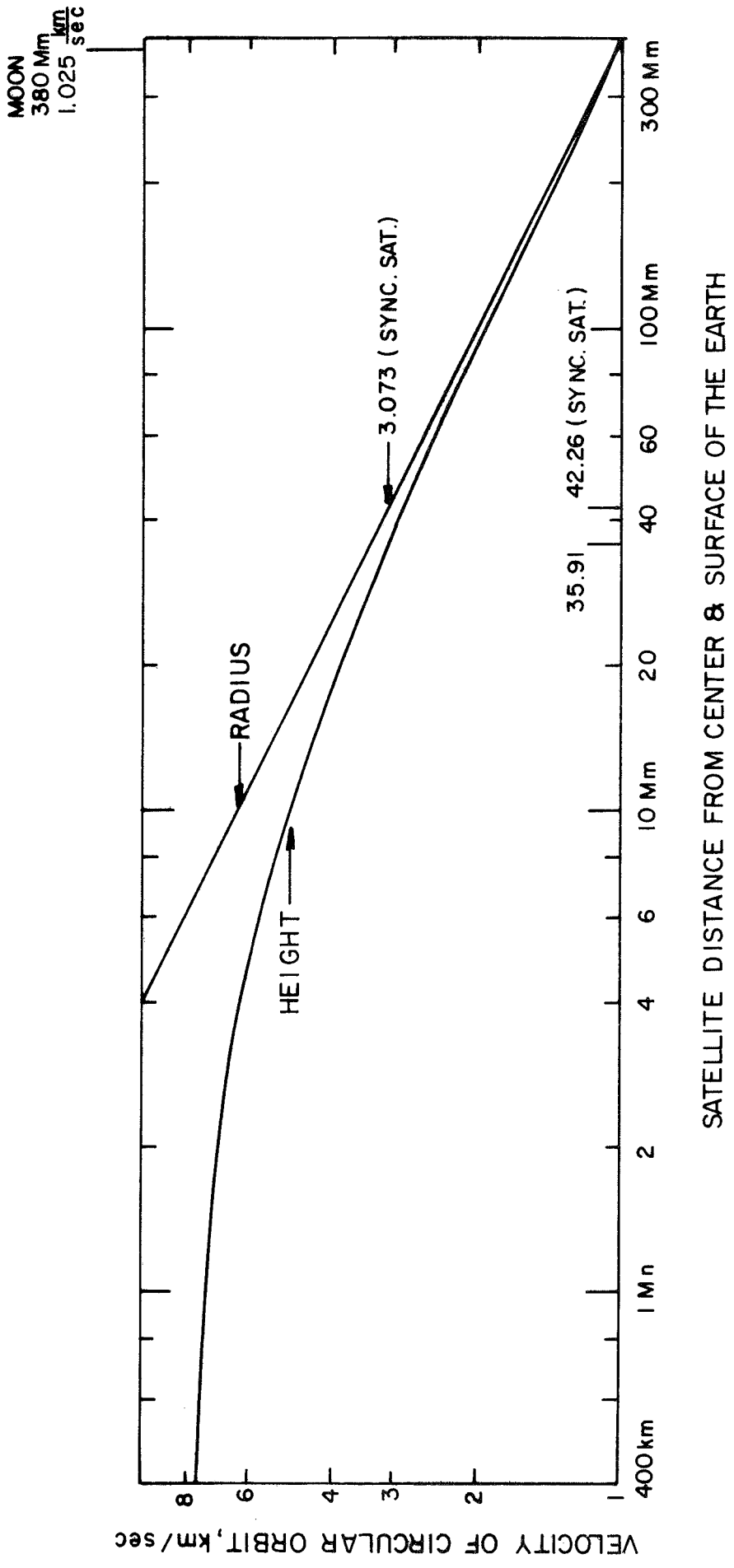
MOON
380 Mm
1.025 km/sec
VELOCITY OF CIRCULAR ORBIT, km/sec
8
6
4
3
2
1
400 km
1 Mn
2
4
6
10 Mm
20
35.91
42.26 (SYNC. SAT.)
40
60
100 Mm
300 Mm
SATELLITE DISTANCE FROM CENTER & SURFACE OF THE EARTH
RADIUS
HEIGHT
3.073 (SYNC. SAT.)

In conclusion we find that the Nd:glass differential-lidar system is in principle capable of remarkable satellite tracking to a precision of 0.02 arc sec in absolute angle relative to a baseline fixed in the earth's crust. However, the technology of picosecond pulses is not yet ready for development of big systems. The system is not simple, since it requires a long baseline for full accuracy, about 1.5 km, and rather elaborate optical delay lines and traveling wave amplifiers.

Some basic laboratory experiments to demonstrate feasibility of differential lidar should be performed merely because they are straightforward and inexpensive, and because the potential applications of differential lidar extend beyond the very specialized application that inspired the concept. In particular, the small signal behavior of the Nd:glass amplifier and the 2-photon fluorescence cell need investigation.

2.2 TEN MICRON DEC-RATE SYSTEM

As already noted in Sec. 1.1 the original motivation for studying the dec-rate system was the observation that Michelson [Ref. 4] succeeded in measuring star diameters as small as 10^{-7} radian with his celebrated stellar interferometer, despite the difficulties of working with white light interference. By using modern techniques and the strong intensity and coherence of laser light, it is only reasonable to expect a significant improvement over his precision, perhaps even an order of magnitude to measure angles as accurately as 10^{-8} radian. Even more attractive is the prospect of using the carbon dioxide laser at 10.6μ, a wavelength twenty times longer than the average wavelength of white light. The greater wavelength means that the phase of the light beam will be much less susceptible to scrambling by disturbances in the atmosphere.

In this report we discuss interferometric baselines on the order of hundreds of meters. Such a great length may seem unduly daring, because even at 10μ a wavefront cannot be expected to be coherent over so great a distance after passage through the atmosphere. However, full coherence is required only over the area of each of the small apertures at the ends of the baseline, not over full separation distance between them. We can turn to Michelson and Pease [Ref. 24] for experimental precedent. We quote their results as summarized by Born and Wolf: [Ref. 25]

> "Variations of refractive index above the small apertures of the interferometer cause the interference pattern to move as a whole, and providing this motion is slow the fringes remain observable, whereas under the same conditions the star image formed by the full aperture telescope would be much impaired." (emphasis ours)

The observation of interference fringes in coherent light is very different from that in white light. With white light one observes interference only when the phase path lengths of the two interfering rays are exactly equal, i.e., $q = 0$ or $N = 0$ in the notation of Sec. 1.3. By contrast the interference fringes in the light from a CO_2 laser may be observed

when the path differences are many kilometers. This completely eliminates the difficult task of finding the interference pattern, but it also eliminates any chance of observing absolute angles, and limits the system to an angular rate measurement. This is because there is no way to identify the zero order interference fringe where the two phase paths are equal; this fringe looks exactly the same as the others. This is one factor that contributes to a decision to limit the CO_2 laser interferometer to the measurement of the rate of change of the satellite's declination angle (dec-rate).

2.2.1 Restricted Applications

We have decided to limit our description and recommendations concerning the CO_2 laser interferometer to a special class of applications, namely the measurement of declination rate or integrated declination increments for satellites in geostationary orbit. This class may be extended somewhat to include objects in low inclination orbits which are not moving too rapidly in hour angle. In the case of synchronous satellites there is little or no loss from the fact that the system measures declination rate as opposed to absolute declination. This is because the rate may be integrated to give declination increments, which correspond to absolute declination except that the constant of that integration is not known. However, the constant of integration corresponds to knowing the average declination, which for a satellite is zero or near zero depending on the small perturbing forces acting on the satellite. With a geosynchronous orbit the tracking time is long enough to observe the full north-south excursion of the satellite and thereby relate the variation in the fringe count to the known average declination. In Appendix A, which is summarized in Sec. 1.1.2, we describe certain aspects of the kinematics and orbit determination problems for geosynchronous and related orbits and showed that the measurement of declination or declination-rate has particular importance in these cases.

For general applications the differential lidar system discussed in the last section is recommended instead of the 10μ system. However, for the special case of geostationary orbits important equipment simplifications make the 10μ dec-rate system very inexpensive and attractive. The simplifications result from the following properties:

a. Small doppler shifts simplify the laser receiver system.
b. A fixed line-of-sight permits air temperature corrections.
c. A fixed line-of-sight eliminates need for wavelength precision, i. e., long-term stability of the lasers is unnecessary.
d. A simplified acquisition and tracking system will suffice, since the satellite can always be located by photography.
e. Low angular rates minimize the mechanical requirements of the telescope.

Some of the above advantages are self-explanatory; others will be explained in the description to follow.

From the list above, first consider (a) the advantage of small doppler shift. This shift is given by the formula

$$f_d = \dot{R}/\lambda \tag{10}$$

where f_d is the doppler shift, $\dot{R}$ the satellite range rate, and λ the wavelength. Using this formula we find that low orbit satellites give shifts which range from about 300 MHz to 0 and back to 300 MHz as the satellite passes overhead. By contrast the residual movements of a geostationary satellite give doppler shifts that do not exceed 1 MHz at the most. Now a sensitive laser receiver system will use the optical heterodyne principle to give a beat frequency or IF (intermediate frequency) in the radio band. Normally one would tune the local oscillator laser to follow the doppler shifts and maintain a constant IF. However, the carbon dioxide laser is only tunable over a range of 30 MHz at the most, which means that a receiver system for a low orbit satellite would require a variable IF. In fact, it would have to be variable over a large dynamic

range which severely complicates the receiver. Moreover, large doppler would cause acquisition problems, since a search for the signal is required in frequency as well as in angular position of the satellite.

Next consider item (b), the advantage of air temperature corrections along a fixed line-of-sight. In Sec. 1.3.2 we showed that a given accuracy may be achieved by either reducing errors from air temperature changes, or by using a long baseline (ϵ/b in Eq. (5)). The latter would be very expensive. However, when the satellite is geostationary, the line-of-sight is in a fixed direction, which allows a shorter baseline, the required accuracy being achieved with air temperature corrections. This is done by employing towers and a long temperature sensor as shown in Fig. p. 58, which averages the air temperature along the bottom 200-300 feet of the line-of-sight. Above that height the air is better mixed and will have little effect on the interferometer because the air temperatures are about the same at the two ends of the baseline.

Item (c), the advantage of relaxed requirements for wavelength stability, will be explained in more detail in Sec. 2.2.2. In brief, the fixed line-of-sight to the satellite permits a receiver location at a point along the baseline where the two interfering rays have equal length. This is shown in the Fig. p. 59, where the receiver building is somewhat closer to the north end of the interferometer. This is the point where white light interference fringes could be observed, i.e., the zero order fringe. By counting relatively few fringes away from the zero order, very little error accumulates as a result of uncertainty in the wavelength, as was discussed in Sec. 1.3.2 in connection with Eq. (6).

Finally, item (d) above refers to the ease of photographing a geostationary satellite. Even with a small telescope aperture, this can be accomplished by taking a long exposure in the approximate direction of the fixed line-of-sight. This is not to be confused with the problem of photographing a synchronous satellite with the Baker-Nunn camera, since the latter tracks at the sidereal rate so that stars will appear as point images on the film.

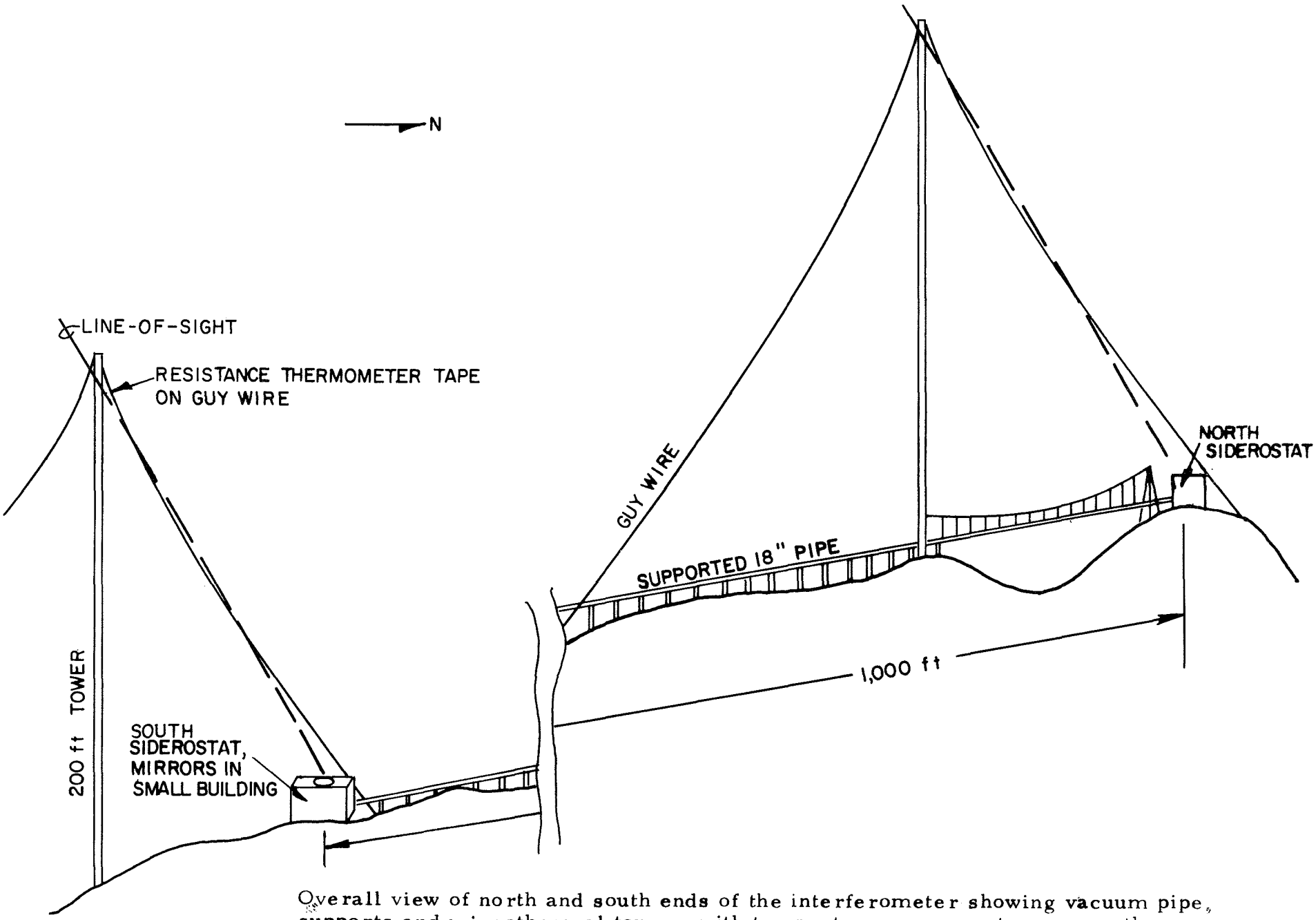

Overall view of north and south ends of the interferometer showing vacuum pipe, supports and microthermal towers with temperture sensors strung near the lines-of-sight.

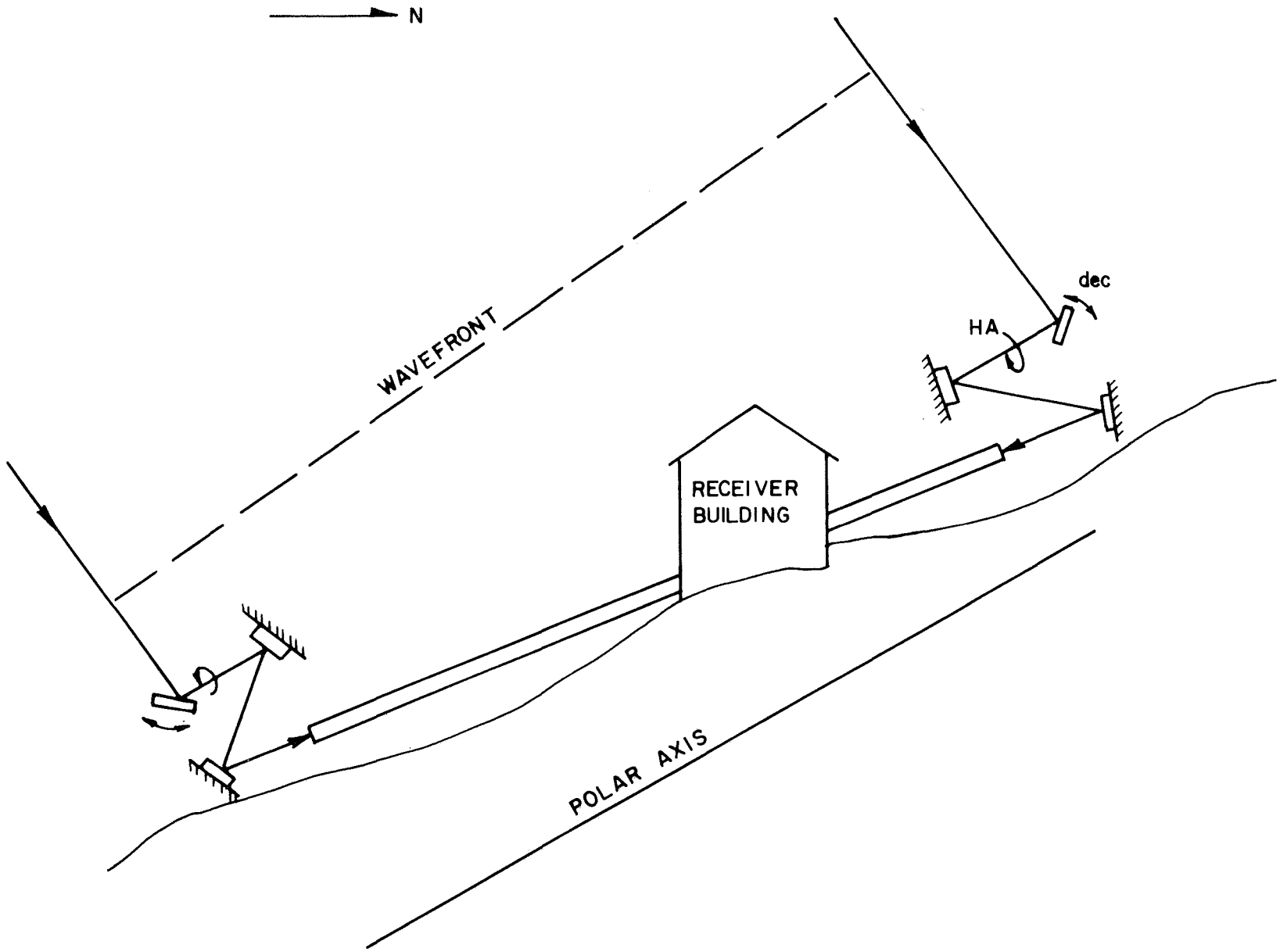

Overall view of the dec-rate interferometer showing siderostat hour angle-declination optics - not to scale. Optics will be installed in large concrete boxes, not shown. The baseline (vacuum pipe) slopes in a direction as nearly polar as terrain and access problems permit.

The Baker-Nunn would see a synchronous satellite as a streak rather than a point image. By contrast we are referring here to the ease of finding the satellite in terms of the shaft angles of the mechanical mount rather than the star field, and a geostationary satellite will make a point image when the pointing optics is stationary.

Many of the advantages described above will be explained in more detail in later sections, but for now we note that they make a formidable case for testing optical interferometry on a geostationary rather than a low orbit satellite. The ATS-F is the ideal opportunity since it will probably carry an active laser beacon, and since it will be large and easy to photograph.

2.2.2 Error Analysis

The basic equation for tracking error $\Delta\theta$ is Eq. (8) from Sec. 1.3.2, namely

$$\cos\theta\Delta\theta = (\lambda\Delta N + N\Delta\lambda + \epsilon)/b + g(\theta)\Delta n_{ao} \qquad (8)$$

Let us review the meaning of these terms and determine the principal sources of error by estimating each of the four terms that are proportional to ΔN, $\Delta\lambda$, ϵ and Δn_{ao}, respectively. First consider ΔN, the error that results from estimating fractional fringes. N may jitter by as much as one fringe as a result of atmospheric turbulence. However, the signal-to-noise ratio will be high (see Sec. 2.2.3) so it should be possible to use data smoothing and find a good average value of N down to an accuracy of about 1/5 or 1/6 of a fringe for ΔN, so

$$(\Delta\theta)_N \approx \frac{\lambda\Delta N}{b} \approx \frac{2\mu}{300\ \text{m}} \leq 10^{-8}\ \text{rad},$$

where we used $b = 300\ \text{m} \approx 1000$ ft., as will be discussed in Sec. 2.2.4 and we took $\cos\theta \approx 1$ for a rough estimate. Clearly $(\Delta\theta)_N$ is not a major source of error.

Next consider the ϵ term for air temperature difference between the two ends of the baseline We have experimentally measured temperature differences between simulated lines-of-sight atop Mt. Palomar. We shall use these numbers on the assumption that they are typical. The Palomar data are discussed in Appendix B where we show that a very conservative error estimate is $\epsilon \approx 100\mu$.

However, for the system discussed here we intend to monitor temperature fluctuations with air thermometer tapes strung along the lines-of-sight, to a height of 200 ft., or 3.3 times the scale height, as shown in Fig. p. 58. This procedure should reduce this error by a factor of 28, but we assume only 10 to be conservative. Therefore, until further microthermal data is available, probably from radiosonde equipment, we assume

$$\epsilon \approx 10\mu, \quad \text{and}$$

$$(\Delta\theta)_{temp} \approx \epsilon/b \approx 10\mu/300 \text{ m} = 3 \times 10^{-8} \text{rad}.$$

Next consider the term in Δn_{ao} in the error Eq. (8), which is error for the extra air path above the station at lower elevation. At a reasonable latitude, say 31 to 35 degrees, the trigonometric factor $g(\theta)$ will be about 0.5. If the temperature near the ground is measured with an accuracy of 0.02^{o}C then this term is

$$(\Delta\theta)_{g} \approx g(\theta)\Delta n_{ao} \approx 0.5 \times 0.02^{o} \times 10^{-6} \text{deg}^{-1} = 10^{-8} \text{rad},$$

which indicates that this is not a principal source of error.

Finally we consider the last of the error terms, $N\Delta\lambda/b$ for wavelength uncertainty. If N were large and if λ were uncertain as a result of an unstabilized laser, then this term could be the major source of error. So the strategy is to make N small enough so that the error is insignificant for any reasonable value of $\Delta\lambda$ as was discussed in Sec. 1.3.2. To review briefly, an adjustable parameter is available, namely the distance a shown

in Fig. p. 21, which will be determined to give the smallest possible values of N. In other words, the main interferometer station will be situated at a point along the baseline that is close to the point at which white light interference fringes could be observed. For the present discussion it suffices to estimate Δa, the permissible error in locating this point, which is given by Eq. (6):

$$\Delta a = \epsilon_\lambda (\Delta\lambda/\lambda)^{-1} , \tag{6}$$

where ϵ_λ is the largest permissible value of $N\Delta\lambda$, and $\Delta\lambda/\lambda$ is the wavelength stability of the laser that can be obtained with a moderate but not excessive amount of effort to stabilize the laser.

We can readily estimate an upper limit for $\Delta\lambda$ by using the known tuning range of the CO_2 laser, about 50 MHz. With rudimentary stabilization the transmitter will operate within 5 or 6 percent of the center of this band which gives $\Delta f = 3$ MHz, and

$$\frac{\Delta\lambda}{\lambda} = \frac{\Delta f}{f} \approx \frac{3}{30}\,\frac{\text{MHz}}{\text{THz}} = 10^{-7} .$$

For ϵ_λ let us take a value of 2μ so that it is small compared to the thermal path error $\epsilon \approx 10\mu$. Now Eq. (6) gives

$$\Delta a \approx 2\mu \times 10^{7} = 20 \text{ m} .$$

This distance, 20 m $\approx$ 66 ft., is the accuracy to which the distance a in Fig. p. 21 must be adjusted to insure that laser stability will not be a significant source of error. This is not a difficult constraint so long as θ is constant. The Δa tolerance will be maintained while the angular position of the satellite changes somewhat, namely $\Delta\theta$ given by

$$\Delta\theta \approx \Delta a/b \approx 20\,\text{m}/300\,\text{m} = .07 \text{ rad} = 4^{\circ} , \tag{11}$$

which is not a difficult constraint if the orbit is geostationary, but will require some corrective measures if the spacecraft varies in declination as much as the ecliptic plane does.

In summary, the uncertainty in the difference between the air temperature at the two lines-of-sight is the principal source of error. A conservative estimate for it is

$$\Delta\theta \approx \cos\theta(\Delta\theta)_{temp} \approx \epsilon/b \approx 3 \times 10^{-8}\,\text{rad.} \tag{12}$$

We have experimentally found that ϵ is independent of the baseline b whenever $b \geq 100$ meters. Hence the limiting error is inversely proportional to the baseline, and for this reason it is advantageous to increase the baseline up to a distance of about 1 km, where other errors become appreciable. However, a baseline this long proves to be costly.

2.2.3 Range Equation

This subsection treats only the case of a ground transmitter and satellite retroreflector. In the ATS-F case (satellite transmitter) the signal is so strong that details are superfluous.

The appropriate range equation is derived in Appendix D, see Eqs. (D-11) and (D-7). It may be expressed in the form

$$\eta P_T Q = 3.21 \times 10^{-31}\ \frac{m^2\text{-watt}}{Hz - \mu}\ \lambda r \left(\frac{R}{d}\right)^4 . \tag{13}$$

Here P_T is the power transmitted,

R is range to the satellite,

d is the aperture diameter of the ground telescopes

η is the product of all efficiency factors that pertain to the ground station (aperture efficiency of the two telescopes, transparency of the air squared for two way propagation, etc.),

Q is the figure-of-merit of the retroreflector

$$Q \equiv \frac{\sigma}{4\pi} \equiv \frac{\text{power return/steradian}}{\text{power flux/area at moon}} = \eta_r \left(\frac{A}{\lambda}\right)^2 , \tag{14}$$

r is related to the information content in the return signal, i.e., $r \equiv$ bandwidth $\times$ power signal-to-noise ratio,

σ is the radar cross-section of the retroreflector,

A is its area, and

η_r is its efficiency.

In deriving Eq. (13) from the more basic radar range equation, we have assumed that the receiver is the optical heterodyne variety originally described by Oliver [Ref. 26]. It has a spectral density of noise equivalent to

$$hc/\lambda\eta_q$$

at the receiver input. Here h is Planck's constant, c the velocity of light, and η_q the detector quantum efficiency, included in Eq. (13) as a factor in η.

Let us assume the following values

$r = 2\text{kHz}$	$d = 25\ \text{cm} \approx 10\ \text{in.}$
$\lambda = 10.6\mu$	$\eta_r = 0.6$
$\eta = 0.05$	$A_e = 100\ \text{cm}^2$

Some of these assumptions require explanation. First turbulence in the atmosphere may cause the bandwidth of the incoming signal to be as great as 100 Hz. We have increased this to 200 Hz (to be conservative) since some effort is required to achieve a local oscillator bandwidth as narrow as 100 Hz [Ref. 27]. So assuming a signal-to-noise ratio of 10 gives $r = 2\text{kHz}$. The ground telescope apertures of 10 inches were chosen for both the transmitter and each of the two interferometer apertures because this is an approximate break-point in cost, a diameter above which the cost of optical components is significant. The parameters for the retro-reflector, η_r and A, are reasonable for a small spaceborne cube-corner,

metal plated on the cube faces, and trimmed to the usual hexagonal shape with the hexagon about five or six inches across. The other assumptions require no special comment. Substituting the assumed values in Eq. (13) gives

$$P_T = 0.65 \times 10^{-4} \text{ watts/Mm}^4 \times R^4 \quad .$$

At the geostationary orbit range of 40 Mm, this gives $P_T = 170$ watts, which is readily attainable with a CO_2 power laser on the ground.

2.2.4 Interferometer Design

The gross structure of the proposed interferometer is shown in the Figs. pp. 58 and 59. The first of these two figures is drawn to scale. It shows structures only at the two ends of the baseline, since the laboratory building and central part of the baseline were cut out of the figure to fit it on the page. A tower approximately 200 feet in height is located near each of the two interferometric stations. The line-of-sight to the satellite (which is fixed in direction) runs quite close to one of the guy wires to the top of each tower. A loop of wire that serves as a resistance thermometer for air temperature runs up and back down each of these two guy wires. These loops will be made of any wire having fairly high resistance and a high temperature coefficient of resistance, for example tungsten, which we used in the experimental task of our study program. The resistance thermometer loop will be insulated and covered with aluminum foil so that it reflects sunlight and gives a reasonably true measure of air temperature. During our study program we observed the effects of sunlight on a resistance thermometer of this type, since we were fortunate enought to have intermittant clouds on one of the days, which intermittantly shaded the thermometer. The effect of sunlight was small but discernible and correctable. The effect of a long wire is to average the temperature fluctuations over its length,

and fortunately this type of average gives the same results as the average that we need to correct the phase path, as noted by Hall [Ref. 28], also referred to in Appendix B. In practice we will probably use more than one temperature sensor for each tower, since breaking the temperature average into increments will be an aid in extrapolating to greater height. Moreover, we particularly need temperature near the ground for the southern tower (which is at a lower elevation) in order to apply the temperature correction for the elevation difference Δn_{ao}, in Eq. (8), Sec. 1.3.2.

The Fig. p. 59 is a schematic diagram which is not to scale. The baseline is shortened and the collecting optics are enlarged to show their layout. Pointing at a nearly geostationary satellite that moves only a fraction of a degree could obviously be accomplished with fewer light reflections than those indicated in the figure. However, we consider the hour angle-declination movement as shown to be advantageous because it allows the mechanical movement to be calibrated by tracking stars at the sidereal rate, and because it constitutes a siderostat which may be useful in other applications. The cost of the multiple reflections is small, both in dollars and in light absorption. In the 10μ band the percent reflectivity of a good metallic surface is in the high nineties. The reflecting optics will of course be enclosed in the small building with an open viewing port. Inside the air is free from the turbulent heat waves of sunlit ground. This means that there is some advantage to the multiple siderostat reflections, since they lift the pivot point of the beam off the ground somewhat and help protect the beam from thermal disturbances. Alternatively, the siderostats can be elevated on a heavy pedestal.

We recommend a beam aperture ten inches in diameter, which means that mirrors for slant reflection may have to be elongated up to 13 or 14 inches. Any aperture larger than about 6 inches suffices to eliminate spreading of the beam by diffraction during passage along the baseline, i.e., the distance between stations is well within the near field. A 10 inch aperture is larger than needed to collect enough power to satisfy the range equation (Sec. 2.2.3); however, the increased collecting area is so inexpensive that it seems unwise to refuse it. The cost of the six flats and their

mountings is only about $1800. As shown in Sec. 2.2.3, this aperture is sufficient to operate with a passive geostationary satellite that carries a 5 or 6 inch retroreflector that is suitable for the 10μ band. The diffraction limited beam width from a 10 inch aperture will be about $1.22\lambda/d = 1.22 \times 10.6\mu/25.4$ cm = 51μrad = 10.5 arc sec. There should be no significant acquisition problem with this much pointing tolerance.*

The light propagation paths from the two siderostats to the receiver station must be enclosed in a pipe that is either isothermal and filled with helium, or else evacuated to about 0.5 torr. Either precaution eliminates refractive index fluctuations. We recommend evacuation merely because it is the sure brute-force solution that has been proven feasible and inexpensive in other applications. We suggest 18 inch aluminum pipe for this purpose so that there will be about 4 inches of clearance around the light beam. This mitigates the problem of supporting the pipe rigidly enough to remain clear of the beam under varying wind loads. One suitable type of low cost pipe is 18 inch aluminum irrigation tubing. The sections of tubing can be joined in the normal manner with occasional thermal expansion joints, and then all joints may be covered with RTV rubber cement, which forms a seal that is more than adequate for about 0.5 torr.

If the baseline were much larger, say 1 km or more, and if the baseline turned a number of corners to follow the terrain, then it would be advisable to employ two receivers, one in each siderostat station. In such a system the beam passing through the baseline pipe would be the beam from a local oscillator laser. The common local oscillator would provide the same optical phase reference to each of the optical receivers, and the actual interference between two signals would be performed at radio frequency (IF). This system would have the advantage that the signal which suffers multiple reflections in passage from one station to another is the strong local signal rather than the weak signal from deep space. However, for the

* If defocussing to a beam angle θ_{up} is needed to acquire the satellite, then Eq. (D-10) is the appropriate range equation.

relatively short baseline of a first experiment, say 1000 feet as we recommend here, it is possible to find terrain that permits the baseline to be quite straight, and so the few reflections required cause a negligible absorption of the signal from deep space. Moreover, at the current state-of-the-art a suitable optical heterodyne receiver cannot be purchased "off the shelf". Thus a significant cost saving results from using a single optical receiver in the central building instead of two optical receivers, one at each end.

When a CO_2 laser dec-rate system operates with a passive satellite, the question arises whether the transmitter can employ one (or both) of the same telescopes used for reception. Fortunately only one transmitter is necessary because, unlike the short wavelength laser systems, the CO_2 laser will illuminate a spot on the ground that is large enough to contain any reasonable size of baseline in all cases considered. However, unfortunately we have been unable to devise a suitable technique for an optical duplexer or isolator that would allow the receiver and transmitter to share a telescope. The trouble is that the dec-rate system is basically a CW instead of pulse system and more than a hundred db of isolation of the receiver from the transmitter would be required. The basic scheme then requires three telescopes, one transmitter and two interferometric receivers for use with passive satellites. An active satellite experiment such as the ATS-F will of course require only two telescopes.

2.2.4.1 Carbon Dioxide Laser Technology

The basic techniques for employing CO_2 lasers in communications and tracking applications are described in a very wide variety of literature. The ones most pertinent here are those employed in optical heterodyne communication systems with the CO_2 laser [Refs. 29, 30]. The carbon dioxide laser will oscillate in either of two bands centered at 10.4μ and 9.4μ. The usual frequency is the 10.6μ line in the P branch of the 10.4μ band. The strongest oscillations in the laser are given along with the other descriptions of the system in a classic paper by Patel [Ref. 31].

An important consideration in employing the CO_2 laser in space applications is that the carbon dioxide of the atmosphere will absorb the signal on precisely the same molecular transitions that the laser uses in emission. This absorption may amount to 3db each way [Ref. 32]. The best way to eliminate the atmospheric absorption is to use a rare isotope of carbon dioxide which has negligible abundance in the atmosphere. The oscillation wavelengths of isotopic carbon dioxide are given by McCurdy and Wieder [Ref. 33]. Only recently has the CO_2 laser been operated satisfactorily for long periods of time in a sealed off condition. That is, formerly the gases were replaced continuously in the laser tube in order to wash away molecular species that resulted from atomic rearrangements in the gas discharge. Carbone [Ref. 34] reports single frequency operation in a sealed off laser giving gain of 4.8 db/m in an unsaturated small signal amplifier, or 1.2 db/m with 95 watts output in a power saturated oscillator.

2.2.4.2 Detector Subsystem

The Fig. p. 70 shows the optics at the middle station where the focusing, beam combining, the detection apparatus are located. This figure shows one end of the vacuum pipe terminated by a lens which focuses a beam onto the detector. Alternatively the pipe can be terminated with a plane window followed by a Cassegrain focusing system that employs two reflectors instead of a lens. The beam combining prism can be made of KCl or NaCl. The detector will probably be a photoconductor of mercury doped germanium cooled to about $20^{\circ}K$ with liquid hydrogen. Liquid hydrogen is quite safe in an observatory environment where the vapors quickly pass through a hole in the ceiling. Liquid hydrogen has high heat of vaporization, is inexpensive, and is commonly used at the Mt. Palomar observatory.

Note the prism in the Fig. p. 70 which superimposes the two interfering beams on a common focal point. The V-shaped surface should be about 90% reflecting (more or less) so that very little of the signal from space is lost by transmission through the surface. This means that the V

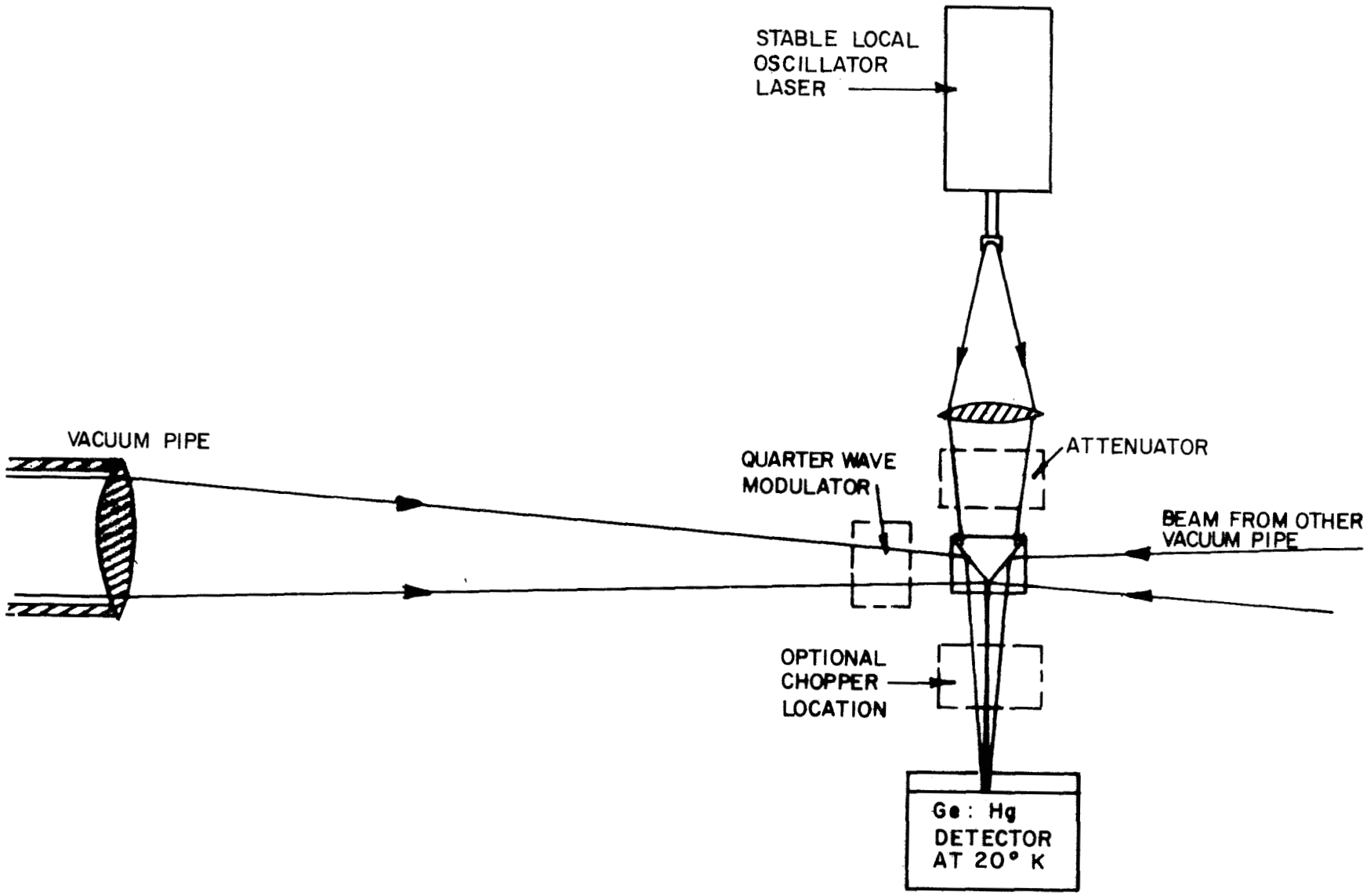

Optics in the Middle or Main Interferometer Station

surface passes only about 10% of the local oscillator power, but this inefficiency is of no concern since an ordinary CO_2 laser emits far more power than necessary for the local oscillator function. In fact, it is advisable to sacrifice even more local oscillator power with an attenuator situated as indicated. To understand the purpose of this attenuator note that the V surface acts as a corner reflector to return most of the LO's power to the laser. The attenuator damps out spurious standing wave modes that would form between the corner reflector and the output mirror inside the laser. Alternatively the V surface in the prism could serve as the output mirror of the laser per se, but the use of one component in such a dual capacity is often poor practice at the prototype stage of development.

2.2.4.3 Fringe Count Incrementing Logic

Each time the detector sees one cycle of minimum and maximum light intensity the logic in the receiver must change the interference fringe count by one unit. It is essential to derive an algebraic sign so that the fringe counting logic knows whether to increment or decrement the fringe count. This sign may be derived in any one of at least three ways, namely

1. classical optics technique,
2. radio frequency technique, or
3. quarter-wave phase modulation,

of which we recommend the last. The classical optics technique consists of tilting one of the two interfering beams slightly with respect to the other. Then the detector field contains a set of parallel light and dark interference fringes. When any one point in this field completes a cycle from light to dark and back, the fringe count is incremented or decremented according as the overall fringe pattern appeared to move to the right or to the left. The dec-rate system could employ this technique, but it requires at least one extra detector [Ref. 35] and amplifier and therefore is probably not cost effective.

The second technique for increment sign logic also requires two detectors. The left signal falls on the left detector and the right signal on the right detector. Both signals mix with the local oscillator beam but not with one another. In this case the final superposition of signals and the determination of the sign are performed at radio frequency where the techniques have been standardized.* However, the disadvantage of this technique is that the local oscillator illumination is absolutely required. We recommend having a receiver mode of operation in which the local oscillator is turned off and the system functions as a conventional infrared detector instead of an optical heterodyne receiver. While this mode is much less sensitive, it has the advantage of being able to operate with a signal from the laser experiment on the ATS-F. This signal will often carry wide band modulation from the GSFC laser communications experiment. Such modulation may confuse the optical heterodyne receiver unless it is especially designed to accept many megacycles of modulation.

For determining increment signs we recommend the third technique which requires only one infrared detector. As shown in the Fig. p. 70 it requires a quarter-wave phase modulator in one of the two interfering beams but not the other. This can be an electro-optic modulator or a rotating phase plate driven at about 1 kHz to be sure that its modulation is more rapid than the random atmospheric modulation. When the interference fringe on the detector is changing from light to dark (or vice versa) the detector will transform the phase dither (imposed by the modulator) into amplitude modulation. The fringe increment sign is positive or negative according to the positive or negative correlation between the intensity fluctuations at the detector and the sign of the phase shift.

2.2.4.4 Laser Stability

Section 2.2.2 described a scheme that eliminates the necessity for a precisely known laser wavelength. In the parlance of laser technology

---

* Hewlett Packard manufactures an electronic counter which comes already wired for increment sign logic.

the scheme eliminates the need for long-term stability. However, the scheme breaks down if the satellite moves more than a few degrees in declination as we noted in Sec. 2.2.2. In such cases the laser wavelength will have to be refered to a length standard, or else the laser frequency will have to be slaved to some characteristic frequency of the carbon dioxide molecule, or an appropriate transition in some other molecular species. Many schemes for stabilizing lasers in the laboratory have been proposed and attempted, but with the CO_2 laser none has been nearly as effective as the atomic clock techniques used in the microwave part of the spectrum, at least not for a reasonable cost. Therefore in the decrate system we recommend using the baseline itself as a standard of length instead of the laser wavelength.

A baseline length standard is established by situating the laser transmitter at one end of the baseline, splitting off a part of the beam which propagates down the baseline to a mirror at the other end and back. This beam is used interferometrically to monitor the number of wavelengths in the baseline. This monitor beam, which travels down and back the baseline, may be enclosed in a pipe that runs parallel to the main interferometer pipe. Unfortunately, one or more shorter interferometric length standards are required to resolve cycle ambiguities. When the baseline length is expressed as N_b wavelengths, then $N\lambda/b$ in Eq. (7) becomes N/N_b and the wavelength has dropped out of the tracking problem. Even if the wavelength is changing appreciably during the length of time that the signal propagates to the satellite and back, it is still possible to make the correction because the fringe counter of the baseline monitor has maintained a complete time history of the variations in the wavelength. However, the complexity of this extra equipment and data may limit the application of the ten-micron system to orbits that are accurately geostationary (such as ATS-F) in which case rudimentary stabilization suffices.

In the event that it becomes necessary to reset a laser to an accurate wavelength reference, we give a capsule review of stabilization techniques that have been proposed and attempted. Siegman [Ref. 36] has proposed

stabilizing the laser to the center frequency of the gain bandwidth in a laser amplifier. To our knowledge this has not yet performed as well as his original predictions. Mocker [Ref. 29] has discussed stabilizing the CO_2 laser at a cross over point where the CO_2 molecule wants to oscillate on two of the spectral lines in its rotational fine structure. Some other discussions of CO_2 laser stabilization are given in Refs. 37 and 38. Mocker [Ref. 39] has given the effects of various parameters which tend to alter the frequency of the laser, especially the dependence on electric current and pressure of the gas. Fein et al. [Ref. 40] described a technique that removes the electrical factors which perturb the wavelengths. They succeeded in pumping a CO_2 laser thermally so that there were no electrical phenomena in the laser tube.

The most precise frequency references are the atomic clocks, but to use these one must span the gap between microwave and optical frequencies. This has been done in the laboratory, but it can hardly be regarded as an operational technique to use in the field. Hocker et al. [Ref. 41] detected the beat between a laser at .337 μ and the 13th harmonic of a klystron at 75 GHz. Frenkel et al. [Ref. 42] beat 118.6 μ with the 17th harmonic of a klystron at 148 GHz. To our knowledge, no one has extended these harmonic methods to 10μ.

Besides long-term stability, there is another problem of laser stabilization commonly known as short-term stability. In the ordinary laboratory environment the vibration and acoustic noise shake the resonator mirrors of the laser and cause a random frequency modulation that broadens the spectrum of the laser to a bandwidth on the order of a MHz. This is undesirable because the receiver must not only be built to handle the greater bandwidth, but must also accept the noise contained in the broadened bandwidth. The topic of short-term laser stability was studied experimentally by Freed [Ref. 27]. He succeeded in achieving a stability of 5 parts in 10^{12}, which corresponds to 150 Hz, for a time interval of 0.05 sec by using straightforward precautions such as a rigid resonator of superinvar, acoustic damping, magnetic shielding, and mounting on

a granite slab with vibration and acoustic isolation. A spectral analysis of his residual short-term instability indicated that the stability would have been 5 parts in 10^{13} or 15 Hz had the system been free from 60 Hz modulation in the power supply. Anywhere in this range from 15 to 150 Hz is adequate stability for the interferometer system recommended here. In the remote environment of a tracking station it is easier to achieve short-term stability than in the noisy laboratory environment. For conservative estimates in the range equation (Sec. 2.2.3) we assumed a bandwidth of 200 Hz from residual short-term instability.

2.2.5 Site Selection

Selection of the best site for the most uniform distribution of air temperature depends on the patterns of air flow in the area under consideration. The best sites for night seeing are on mountain tops, because the ground cools the air at night and the air flows down the sides of the mountain leaving the observatory in undisturbed air which has come from above to displace the air flowing down. For good day seeing opposite considerations apply and the mountain top is likely to be a poor choice. Instruments for daytime seeing have been situated on an island surrounded by a large lake, or even in the middle of a depressed terrain. For the best average seeing day and night, which is probably the appropriate criterion for the dec-rate system, it is probably impossible to find good air drainage all of the time or even most of the time. In this case the best compromise is probably to situate the station at the highest possible altitude consistent with the cost of building facilities in remote locations.

In describing the original concept as a declination-rate system we have assumed that the baseline can be aligned parallel to the earth's axis or nearly so. The southwestern United States lies between latitudes 31° to about 37°, and one interesting site, the Smithsonian observatory on Mt. Hopkins is at latitude 32°. This means that the ground from the southern to the northern siderostat station would slope upward at 30° or more in a truly polar system. This is a steep slope indeed, but several areas

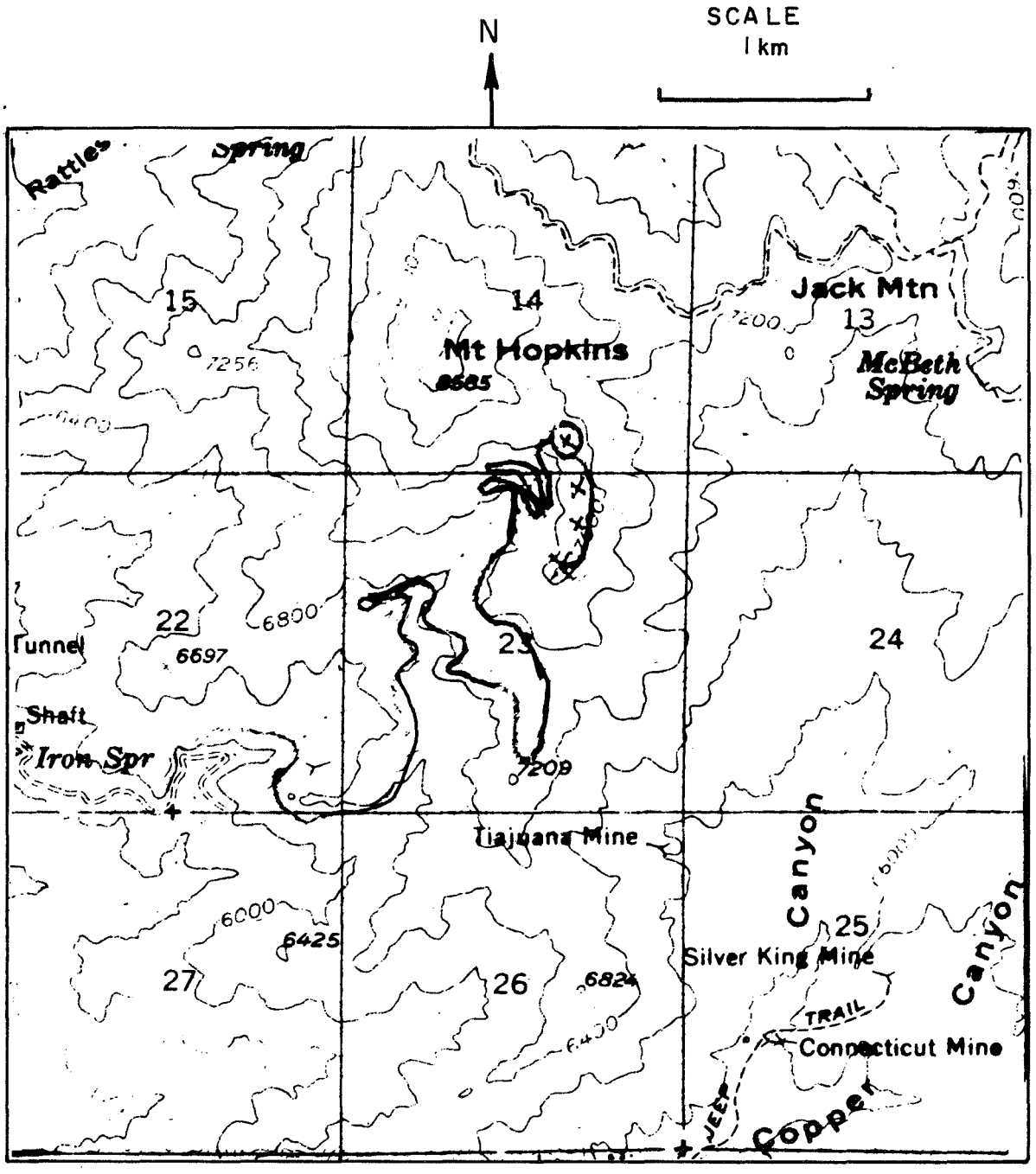
N
SCALE
1 km
Rattle
Spring
15
14
Mt Hopkins
8685
Jack Mtn
13
McBeth
Spring
7200
7256
6800
22
6697
Tunnel
Shaft
Iron Spr
23
24
7209
Tiajuana Mine
Canyon
25
Silver King Mine
6000
6425
27
26
6824
6400
TRAIL
Connecticut Mine
Canyon
JEEP
Copper

adjacent to the Mt. Hopkins road have a north-south slope equal to the latitude as the contour map on page 32 shows. On this map the polar slope corresponds to this distance between adjacent heavy contour lines:

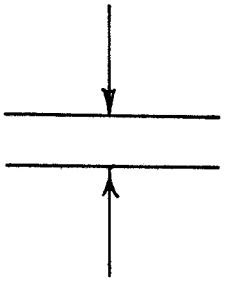

The only serious difficulty with a non-polar north-south baseline occurs if and only if <u>both</u> of the following conditions apply:

* The system tracks a geostationary satellite with an unstabilized laser, and so the interferometer detector is situated near the zero order interference fringe as discussed in Sec. 2.2.2.
* The dec-rate system tracks one or more satellites that hover in two or more different geostationary positions that differ significantly in hour angle (longitude).

The problem is that the zero fringe position where the detector should be located is not the same for the two hover positions unless the baseline is polar.

These site selection factors are only the beginning of a complicated trade-off that is beyond the scope of this report. Recall that the tracking error is $\Delta\theta \approx \epsilon/b$, so that there is a cost effectiveness factor in determining whether to make ϵ as small as possible or b as large as possible. Small ϵ raises cost by putting the station in a remote site at very high altitude. Large b raises cost in two ways; first is the length of pipe for the enclosed baseline, and second is cost associated with the fact that large b precludes the use of a polar basline and may require a

stabilized laser. A preliminary cost estimate for installed baseline pipe is $10 per foot on Mt. Hopkins or $6 per foot in a rather level area with good paved access. The tradeoff suggested here probably will not be resolved fully until after a preliminary dec-rate system has been built and used. Our inclination for a first experiment is to use a short polar baseline in a high altitude site, because the complications in this case (access and construction on an incline) are not so highly technical.

2.3 VERY-LONG BASELINE MICROWAVE INTERFEROMETRY

Microwave interferometers that employ two stations situated at the same facility, e.g., 500 to 1500 meters apart, do not give accuracy that is adequate for the purposes of this report, since tracking errors in the range of one to several arc sec have been reported [Refs. 43, 44]. However, microwave stations separated by many thousands of miles have been used as interferometric pairs, without physically superimposing the two signals. This is possible if each station is equipped with an atomic clock of the most precise variety. Each station measures the signal frequency very accurately by counting the number of cycles in a known time interval. Then, the beat frequency between signals from each station is calculated by numerically subtracting the signal frequency at one station from that at the other without physically bringing the two signals together. [Refs. 3, 45, 46]

For radio astronomy the interferometer uses very wide bandwidth, and so (as in white light interferometry) the zero order interference fringe is readily identified to give absolute angles. However, with CW signals there are the usual cycle ambiguities, so only angle rate is available unless wideband modulation is used as in pseudo-random range codes. Moreover, we must emphasize that the astronomical technique applies only to relative angles within the structure of an extended source. Radio astronomers infer the angular extent of a radio source from the visibility of its interference fringes. They usually do not infer the angular position or angular rate of a radio source from an absolute fringe count. In fact, the data from two VLB stations are usually adjusted by trial and error in a manner that corresponds to searching for the radio source in angle.

The use of VLBI for the tracking of geodetic satellites is marginal for at least three reasons:

* An active transmitter on the satellite is required unless one can afford to irradiate the satellite with a very powerful transmitter that uses a separate antenna well removed from the receiver station. This is in contrast to the laser retroreflectors which achieve high gain owing to the very short wavelength of light.
* The stations are so far apart that they must be situated on separate parcels of land and manned by separate crews, a very important factor in costs unless the stations are existing ones that can spare the time for VLBI from other activities.
* Lengthy and expensive data reduction is required at the end of an experiment, which means that the tracking data are not available in real time. This disadvantage is shared by the Baker-Nunn camera systems.
* The baseline is comparable to the radius of the earth, which means that the curvature of the earth causes horizon difficulties as indicated in the Fig. p. 81 .

The Fig. p. 81 uses a 65° arc for the baseline, since this is the arc between a pair of existing stations in the NASA Deep Space Net which are almost on a N-S line (12th meridian E $\pm 15^{\circ}$). For the figure, we also assume that the effective horizon at each station is at 30° elevation, for below that elevation the air mass along the line-of-sight exceeds two (cosecant $30^{\circ} = 2$). The usable solid angle that a single station sees is contained in a cone that subtends 120° about the zenith. For an interferometric pair it is the intersection of two such cones that is usable tracking space. When the two cones are tilted apart by 65° (or even as little as 30°) the usable space is seriously decreased, especially since low altitude satellites are likely to pass beneath the volume of the cone intersection. However, for high altitude satellites, the horizon disadvantages are partially offset by the all-weather utility of the microwave bands.

SCALE : 1 cm – 500 miles

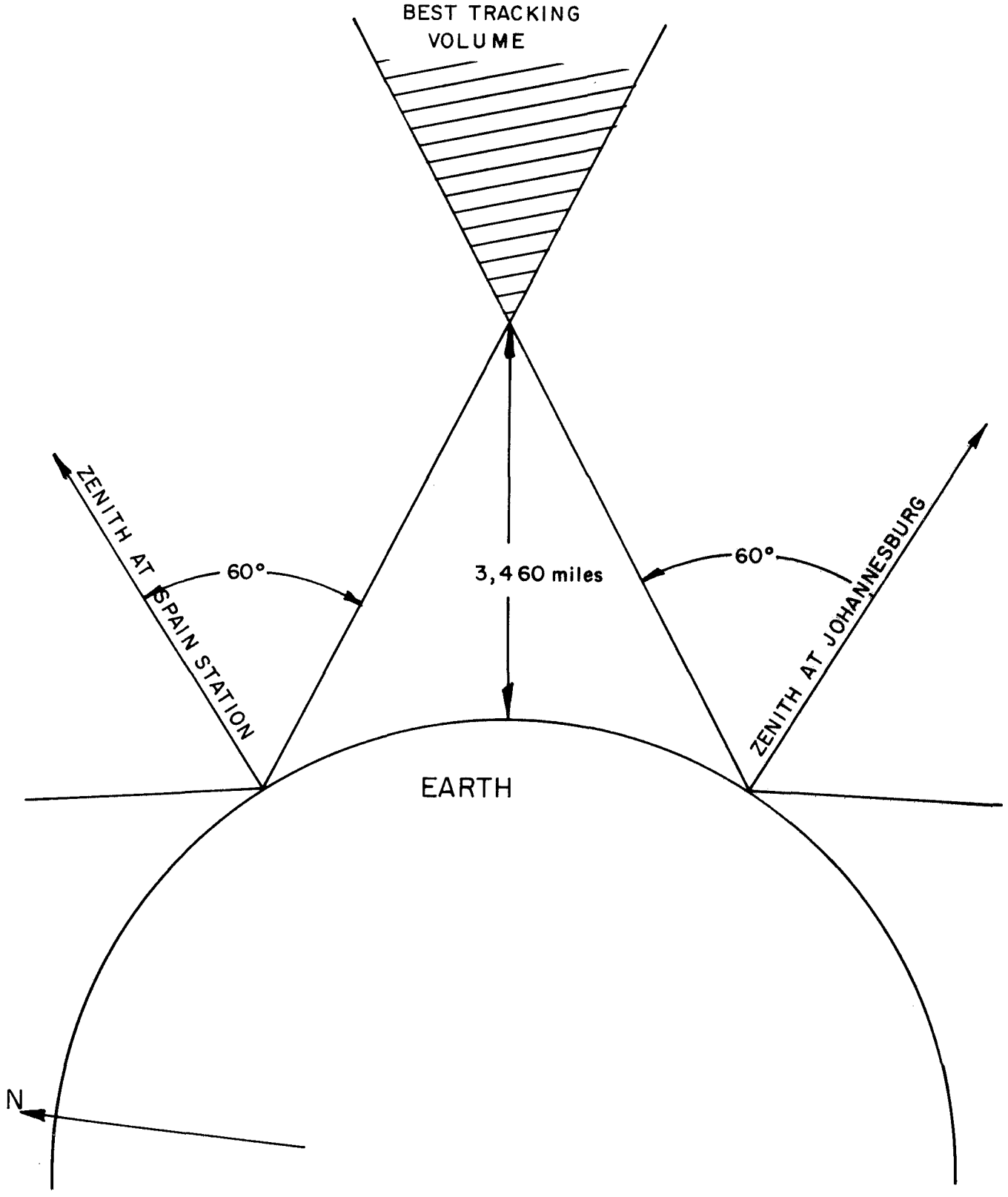

Despite all these difficulties the VLBI technique deserves consideration, since so much existing equipment could be used for this purpose. The optimum frequency for VLBI depends upon the weather and altitude at the sites in question, but they generally fall in the X-band part of the spectrum. Shorter wavelengths and especially millimeter waves suffer serious perturbations and absorption from the water vapor in the air. Longer wavelengths interact with the ionosphere and suffer similar phase disturbances. The basic accuracy of VLBI is about 20 cm in the difference in phase path between the two stations, a number derived from private communications with G. B. Thayer of ESSA, Boulder, Colorado. According to him one can use pressure and temperature readings to estimate the atmospheric phase delay to an accuracy having a standard deviation of about 5 cm. We have quadrupled this number to account for two stations and for the fact that one or both of the stations is likely to track to rather low elevation angles, either at the beginning or end of a satellite pass, as a result of the horizon difficulties discussed above. With optical interferometers we estimated tracking errors in angular units by dividing the phase path error by the baseline. However, for VLBI this is invalid in many cases because the baseline is longer than the range to the satellite. In these cases we can merely say that 20 cm is the ultimate accuracy with which increments in the satellite position can be measured parallel to the baseline. For satellites in high orbits such as geosynchronous orbit the old estimate $\Delta\theta \approx \epsilon/b$ is still valid and we find

$$\Delta\theta = 20 \text{ cm}/6 \text{ Mm} = 3 \times 10^{-8} \text{ rad},$$

a number that is comparable to the accuracies we have estimated with laser systems. In this estimate we chose a baseline of 1 radian of the earth's surface which slightly relieves the horizon problem illustrated in Fig. p. 81.

Having discussed the ultimate tracking accuracy, we now turn to the serious problem of the drift rate in the atomic clock as it relates to tracking accuracy with VLBI. Let us begin with the liberal assumption that the baseline is in a polar direction and has the optimum length, about 3 Mm or 1900 miles. In reality there is no assurance that two cooperative stations can be found with such a spacing, and one would probably have to chose two stations with a different spacing or else build a new one. If the baseline is much longer than the optimum value then there will be horizon difficulties; i. e., when the satellite is at high elevation as observed from one station it is likely to be too close to the horizon at the other. Conversely if the baseline is much shorter than 3 Mm then accuracy is sacrificed.

We extract the error term in Eq. (8) that is proportional to ΔN, and differentiate with respect to time (dot notation) to indicate a spurious fringe counting rate from the clock drift:

$$\Delta(\cos\theta\dot{\theta}) = (\lambda/b)\Delta\dot{N} = \epsilon\lambda/b ,$$

where $\Delta\dot{N} \equiv \epsilon$ (see Fig. p. 84) is the clock error frequency or drift rate. For the error in angular increment $\Delta\theta$ we integrate for an observation time T and find

$$\int_0^T \Delta(\cos\theta\dot{\theta})dt \approx \cos\theta \int_0^T \Delta\dot{\theta}\, dt = \cos\theta\Delta\theta = \epsilon T\lambda/b .$$

Let us also make the liberal assumption that the clock drift rate is 1 part in 10^{13}, a precision which can be achieved only with the hydrogen maser. Then the frequency error is

$$\epsilon = 10^{-13}f = 10^{-13}c/\lambda, \text{ and } \cos\theta\Delta\theta = 10^{-13}cT/b .$$

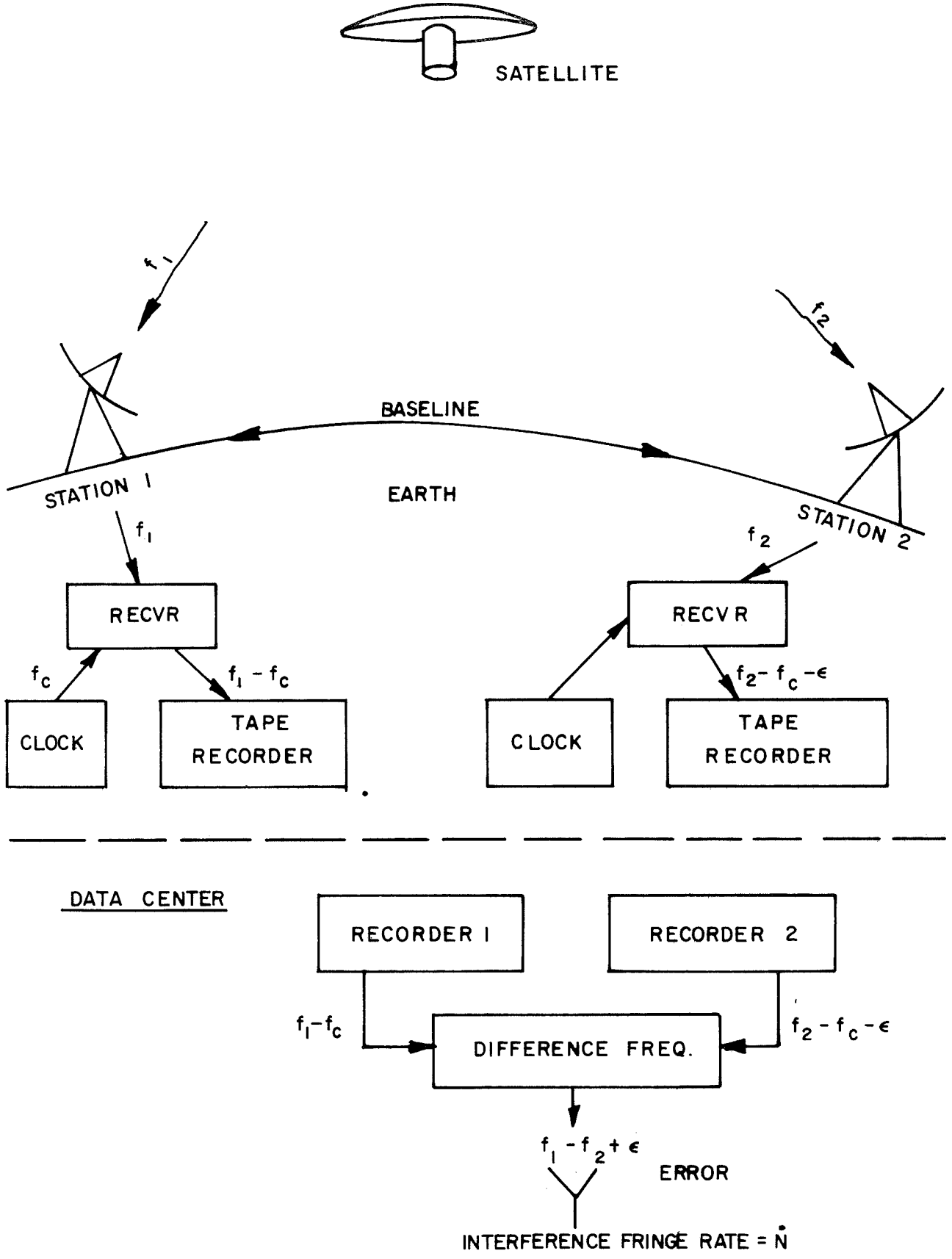

Clock error ϵ is preserved in VLB interferometer

Let us take $T = \frac{1}{2}$ day for the tracking time over which the error accumulates. The result is

$$\cos \theta \Delta\theta = 0.43 \times 10^{-6} \text{ radian} .$$

The above tracking accuracy represents a significant advance, but the error is much larger than that imposed by the atmosphere and the system requires the most sophisticated of all clocks. Moreover, the error is large compared to that of the two laser systems discussed in the last two sections. In two subsections to follow we describe ways to circumvent this difficulty and return to the accuracy estimated for the atmospheric limitation. However, the price in terms of hardware is severe. The first system requires several antennas just to measure one angular rate, and the second requires the participation of two satellite transponders each of which transmits a signal harmonically related to the received signal on two separate bands.

2.3.1 Celestial Radio Source as an Angle Reference

The feature which VLBI clearly needs for precision satellite tracking is a local oscillator in the sky which serves as a phase reference for both stations of the interferometric pair. A way to achieve this is to use the interferometer to examine a celestial radio source exactly as a radio astronomer would do, with one exception. The local oscillator in the receiver at each station does not supply a signal derived from an atomic clock, but rather the received signal from a satellite. In this way the celestial source serves as an angular reference for the satellite and the angular rate that is measured pertains to the difference between two cone angles. Both cones have the baseline as axis, one passes through the satellite and the other through the celestial source. Unfortunately this system may monopolize as many as five antennas. We add up five as follows, one transmitter sending a signal to the satellite that is derived from an atomic clock, the satellite transponder then generates a

harmonically related signal which it transmits back to earth. Two antennas one at each end of the baseline receive the satellite signal. Two antennas one at each end receive the broadband signal from the celestial radio source. The technique described here would make an extremely interesting experiment if existing facilities can be scheduled for a time when a satellite passes very close in angle to an appropriate celestial source. In this way the accuracy that has been achieved by radio astronomers looking at the structure of sources, i. e., 1/1000 arc sec, can be realized because the local oscillator is above the atmosphere and passes through the same disturbances on the way to the ground that the reference signal passes through. Thus the atmospheric tracking errors drop out in this case. However, because of the size and complexity of the experiment, we cannot recommend this technique as a new facility to be built for the primary purpose of tracking geodetic satellites.

2. 3. 2 Differential Range-Rate System

The system described here is not very practical, but its description is instructive in that it points out certain kinematic relations between different forms of tracking. In particular we begin by proving that declination rate is equivalent to differential range-rate between two stations on a north-south baseline. Alternatively hour angle rate is equivalent to differential range-rate between two stations on an east-west baseline. First consider the Fig. p. 87, viewing the diagram as an interferometer that gives the propagation path difference = $b \sin \theta = N\lambda$. Recall that the interference fringe count N is not measurable, only the counting rate $\dot{N}$ is observable, so we differentiate to obtain

$$b \cos \theta \dot{\theta} = \dot{N}\lambda . \tag{15}$$

The terminology "fringe counting rate" is that of optical interferometry. For rf systems it is more appropriate to call $\dot{N}$ the beat frequency between signals received at the two stations. Equation (15) is the fundamental equation of the angular rate interferometer.

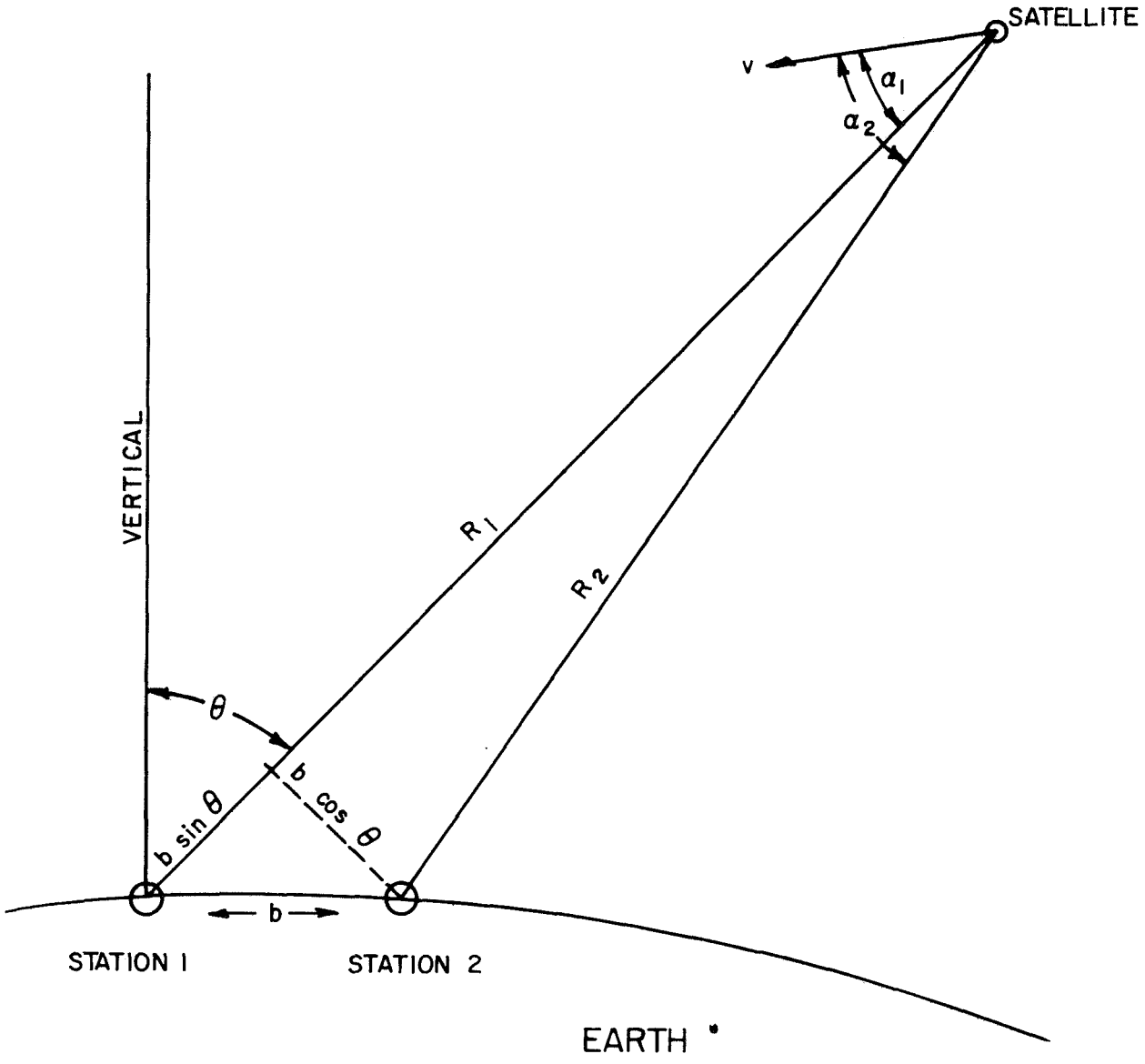

Geometry for proving the equivalence between interferometric angle (θ) rate and differential range rate.

Next we view the same diagram as a differential range rate system and accordingly calculate the range rate difference.

$$\Delta\dot{R} = \dot{R}_1 - \dot{R}_2 = v\cos\alpha_1 - v\cos\alpha_2$$

$$= 2v \sin \tfrac{1}{2}(\alpha_2 + \alpha_1) \sin \tfrac{1}{2}(\alpha_2 - \alpha_1)$$

$$= v \sin \bar{\alpha}\,(\alpha_2 - \alpha_1), \quad \text{since } \alpha_2 - \alpha_1 << 1 \ .$$

Here $\bar{\alpha}$ = average = $\frac{1}{2}(\alpha_2 + \alpha_1)$.

But $v \sin \bar{\alpha}$ = tangential velocity = $R\dot{\theta}$, so

$$\Delta \dot{R} = R\,\dot{\theta}(\alpha_2 - \alpha_1) = \dot{\theta}\, b \cos\theta \ .$$

In the last step we set $b \cos\theta = R_2(\alpha_2 - \alpha_1)$ or simply $R(\alpha_2 - \alpha_1)$, since $\alpha_2 - \alpha_1 << 1$ and $R_2 \approx R_1 = R$. Rewriting gives

$$b \cos\theta\,\dot{\theta} = \Delta\dot{R} \tag{16}$$

Equations (15) and (16) are the fundamental equations of the rate interferometer and the differential range-rate system respectively. To show the equivalence we need to prove that

$$\Delta\dot{R} = \dot{N}\lambda \ ,$$

which is readily demonstrated as follows:

$$\Delta\dot{R} = \frac{d}{dt}(R_1 - R_2)$$

$$= \frac{d}{dt}(N\lambda) = \lambda\dot{N} \ .$$

The last step tacitly assumes that λ is a constant, which it is not if the frequency drifts. Hence the equivalence applies only to the ideal system. The rate interferometer and differential range-rate systems respond differently to clock errors.

In the explanation of Fig. p. 87 and Eqs. (15) and (16) we have shown that a differential range-rate system is equivalent to the interferometer. The former also employs two microwave stations, one at each end of the baseline, but the two stations operate at different frequencies and independently measure range rate by transponding from the satellite.* A phase coherent transponder is required, which means that the spacecraft receives on one frequency, forms a fractional harmonic of the received signal at a second frequency that falls within the same band, and finally amplifies and transmits the harmonically related signal. When the seond signal is received on the ground the reciprocal harmonic is taken. The net result of the harmonic procedure is as though one frequency were transmitted round trip, except that the procedure prevents any interference between the transmitter and receiver at either station. Fig. p. 87 has already shown that the clock error ϵ is preserved in the interferometer output. We now show that it cancels to first order in the differential range-rate system.

The logic for one of the two microwave dec-rate stations is shown in Fig. p. 90. The factor A is approximately but not exactly one; it represents a multiplicative frequency (clock) error and corresponds to $(1+\epsilon)$ in the interferometer case (Fig. p. 84). Note that A drops out in the final raio. However, higher order clock errors will not cancel out, in particular the frequency drift that takes place during the round-trip

*Fortunately, the ATS-F mission will include phase coherent transponders at both L and S-band, and the experiment can be tried if desired.

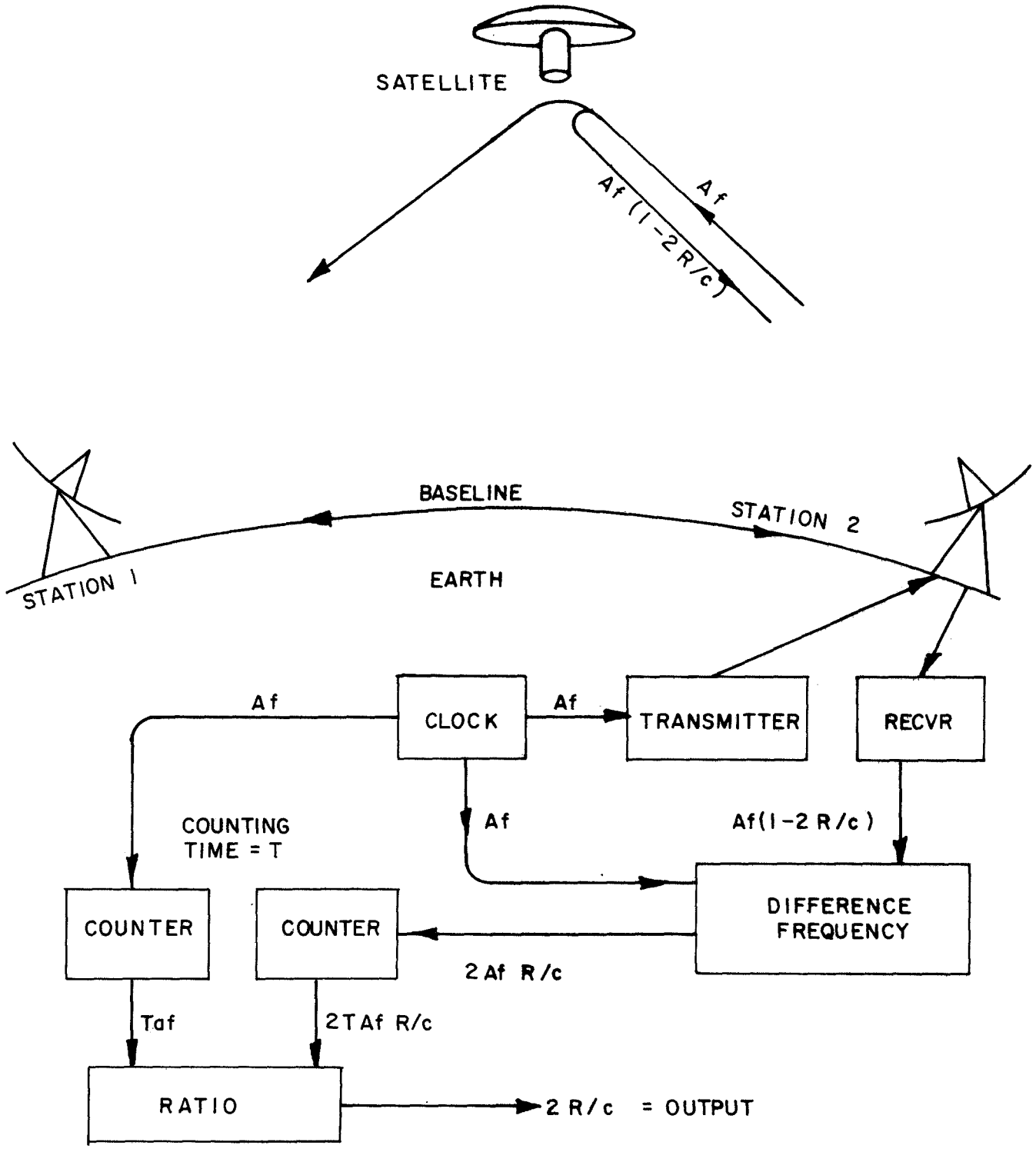

Microwave dec-rate system: block diagram for one station and one of two transponded frequencies. Note cancellation (in ratio block) of clock errors contained in factors A(≈1) and T. For simplicity diagram omits harmonic up and down conversions that prevent interference between transmitter and receiver.

signal propagation time. This can be made negligible in which case the limiting tracking error is the atmospheric one derived earlier, namely

$$\Delta\theta = 3 \times 10^{-8} \text{rad} \approx 0.01 \text{ arc sec},$$

or more, perhaps 0.02 arc sec, if the signals are not all at X-band, but include an L- or S-band link.

PART III

COMPARISONS, CONCLUSIONS, AND RECOMMENDATIONS

PART III

COMPARISONS, CONCLUSIONS, AND RECOMMENDATIONS

The summary table on the following page is largely self-explanatory. Five novel laser and microwave systems are compared to one another and to the Baker-Nunn camera system. The star occultation system was omitted from this table because it is hard to compare on the same basis. Recall that it requires a special satellite, but it could give 10 cm accuracies on the ground.

The microwave systems are too complex to consider except as special experiments using existing facilities at times when the scheduling of these facilities permits. The laser systems using passive retroreflectors on the satellites are candidates for new and permanent facilities for the tracking of geodetic satellites.

	Baker-Nunn	Candidate Laser Systems		Candidate Microwave Systems		
		One-Micron Differential Lidar	Ten-Micron Dec-Rate	VLBI with H_2 Maser	VLBI with Celestial Radio Source	Differential Range Rate
Tracking error, arc sec (a)	2-3	0.02	0.01	0.1	0.01 to 0.001 in special cases	0.01
Stations req'd (b)	1	1	1	2	2 + 4 or 5 antennas	2
Satellite Systems req'd	none	Passive retroreflector	Special passive retroreflector (or active CO_2 laser)	harmonic transponder	harmonic transponder	Two harmonic transponders on different bands
Absolute or Incremental Angles	absolute	absolute	incremental	incremental unless very wide band pseudo-random modulation	incremental	incremental
Restrictions and special problems	clouds	clouds	clouds, near geosynchronous orbits only	H_2 maser for freq stability of $1=10^{13}$	Many antennas req'd, need radio source near satellite in angle	Troposphere & ionosphere. Monopolizes satellite systems
Cost to NASA	operational	Guess \$1M + operation	Guess \$0.25-0.3M + operating cost	H_2 masers Stations very costly, but existing ones may be available		
Grown potential	hardly any	excellent	Step toward one-micron system	little	little	hardly any
Development risk	none	Wait, technology premature	Low cost test with ATS-F needs functioning satellite laser	hardly any	little	some
Output delay (c)	days	none	none	days	days or weeks	none
Recommendations	-	First see if ten-micron dec-rate successful	Test with ATS-F as first step toward laser interferometry	Test if maser installed for other uses	Test in special favorable cases	none

a) Order-of-magnitude estimate depending on many factors, see text.

b) Number of stations required means separate parcels of land and separate crews.

c) This refers to time spent transporting and reducing the data before it is available for use.

3.1 THE ATS-F OPPORTUNITY

Many features of the ATS-F mission make it the ideal opportunity to test optical interferometric tracking with minimum cost, development risk and difficulty. These features relate to the geostationary orbit and to the fact that the satellite will carry an active laser beacon. The advantages that derive from these properties are outlined below:

1. High intensity from the active satellite laser, i. e., square law propagation loss instead of the severe fourth power law of radar.
   a. Relieves requirements for aperture and receiver sensitivity.
   b. No high power ground transmitter requirement, however there must be an acquisition beacon within 2 or 3 miles of the interferometer.
2. Geostationary orbit advantages.
   a. Small doppler shifts simplify the laser receiver system.
   b. A fixed line-of-sight permits air temperature corrections.
   c. A fixed line-of-sight eliminates need for wavelength precision, i. e., long-term stability of the lasers is unnecessary.
   d. A simplified acquisition and tracking system will suffice, since the satellite can always be located by photography.
   e. Low angular rates minimize the mechanical requirements of the telescope.

Some of the above advantages are self-explanatory, 1b is explained below, and 2a through 2d are explained in detail in Sec. 2. 2. 1. The NASA plans for the series of applications technology satellites include a carbon dioxide laser experiment on board the ATS-F. If the mission is successful as

planned, a ground station will illuminate the satellite with a laser beacon, and the satellite will point its beacon back at the same ground station where the beam will irradiate a circle about 4 miles in diameter. This explains the remark in item 1b above. That is, a ground beacon is required, but it is only a beacon and not a transmitter with the very high power and directivity required to overcome the severe space propagation losses of echo ranging or lidar.

We strongly recommend that a laser interferometer experiment be included among the experiments associated with the ATS-F mission to experimentally prove the dec-rate tracking concept. The small interferometer that Bell Telephone Labs plans for this mission does not employ a long enough baseline for the purpose intended here. It is primarily a 10μ propagation experiment rather than a tracking feasibility experiment.

3.2 THE ULTIMATE LASER ANGLE TRACKER

The differential lidar system offers the greatest potential for the ultimate interferometric tracking system; although its development should wait for routine advances in the technology of picosecond pulses. Recall that two pulses only 150 microns long enter the two telescopes, propagate along the baseline, then collide at an accurately measured position. The recording of the collision event constitutes a sort of intensity interferometry using non-linear optics.

Unlike the ten-micron system, this laser system can

* operate with quartz (standard material) retroreflectors.
* measure absolute angle instead of increments only.
* track any satellite that laser ranging (lidar) systems track.
* operate in a duplex mode that eliminates the separate transmitting telescope.

Recall that its estimated accuracy is 0.02 arc sec = 10^{-7} radian with a baseline of 1500 meters. At a typical range of 2Mm, this gives linear accuracy of 20 cm. Moreover, picosecond pulses from the Nd:glass laser have been converted to second harmonic pulses at 0.53μ instead of 1.06μ. This opens the possibility of atmospheric correction by the technique of two color extrapolation.

Some basic questions, especially those regarding the small-signal amplifying and noise properties of the Nd:glass laser could be answered by straightforward laboratory experiments.

APPENDICES

APPENDIX A

A. THE PERTURBED MOTION OF A GEOSTATIONARY SATELLITE

Figure 1 shows three views of an orbit which is a small perturbation from the geostationary orbit. The scale is distorted to fit the figure to the page. The coordinates x, y, and z are geostationary coordinates having their origin at the position of a body in geostationary orbit. Thus non-zero values of x, y, and z represent perturbations, x in the tangential or hour angle direction, y in the radial direction, and z in the out-of-plane or declination direction. That is, if we let R stand for the radius of the geostationary orbit, then

$$\begin{aligned} &\text{(a)} \quad x/R = \text{hour angle (HA) change from the HA of the origin,} \\ &\text{(b)} \quad y+R = \text{geocentric range of the satellite,} \\ &\text{(c)} \quad z/R = \text{declination.} \end{aligned} \tag{A-1}$$

Let n denote the diurnal frequency, i.e., (1 sidereal day)$^{-1}$, and let $\vec{a}$ denote the instantaneous inertial perturbing acceleration from tidal forces, solar pressure, higher moments of the earth's gravity, etc. Then the linearized equations of motion for small displacements are

$$\begin{aligned} &\text{(a)} \quad \ddot{x} + 4\pi n \dot{y} = a_x \\ &\text{(b)} \quad \ddot{y} - 4\pi n \dot{x} - 3(2\pi n)^2 y = a_y \\ &\text{(c)} \quad \ddot{z} + (2\pi n)^2 z = a_z \end{aligned} \tag{A-2}$$

The general solution to these equations of satellite motion is

$$\begin{aligned} &\text{(a)} \quad x = A + Bt + 2C \sin(2\pi nt + D) + f(t, \vec{a}), \\ &\text{(b)} \quad y = -2B/(6\pi n) - C \cos(2\pi nt + D) + g(t, \vec{a}), \end{aligned} \tag{A-3}$$

(c) $z = E \sin (2\pi nt + F) + h(t, \vec{a})$.

In these equations f, g, and h represent functions that depend on $\vec{a}$, but A through F represent constants of integration which are independent of the perturbing forces.

The physical interpretation of the constants A - F becomes apparent by considering them one at a time; i.e., to understand any one of them assume that all of the others vanish and the perturbed solutions f, g, and h as well. A geostationary satellite can hover over any point on the earth's equator. A small displacement in the hovering point is given by the constant A. If the radius of the satellite orbit is a little too small or too large, then the satellite will drift slowly to the east or west respectively. This is given by the constant B, a radius error in Eq. (b) and its associated drift in Eq. (a). The constant C gives an oscillation of the satellite in its orbital plane. This is caused by a residual eccentricity in the orbit. As illustrated in the top view of Fig. 1 the x-y motion always has the direction indicated by the arrows. At perigee the satellite is moving faster than average so it moves ahead of the geostationary point; and at apogee it lags behind. Similarly the constant E gives an oscillating movement in declination, which means that the orbit has a small residual inclination. Finally, the constants D and F determine the phase of the oscillating movements and represent right ascention of the node and the argument of perigee, as shown on page 10 where these orbital elements are defined.

The following subsections separately discuss the unperturbed (Subsec. A-1) and perturbed (A-2) parts of Eq. (A-3) and show that dec-rate tracking will make an important contribution to each.

A-1 Residual Orbit Inclination

The primary purpose here concerns the precision determination of the constants A-F. Since a positive increment in y represents radial

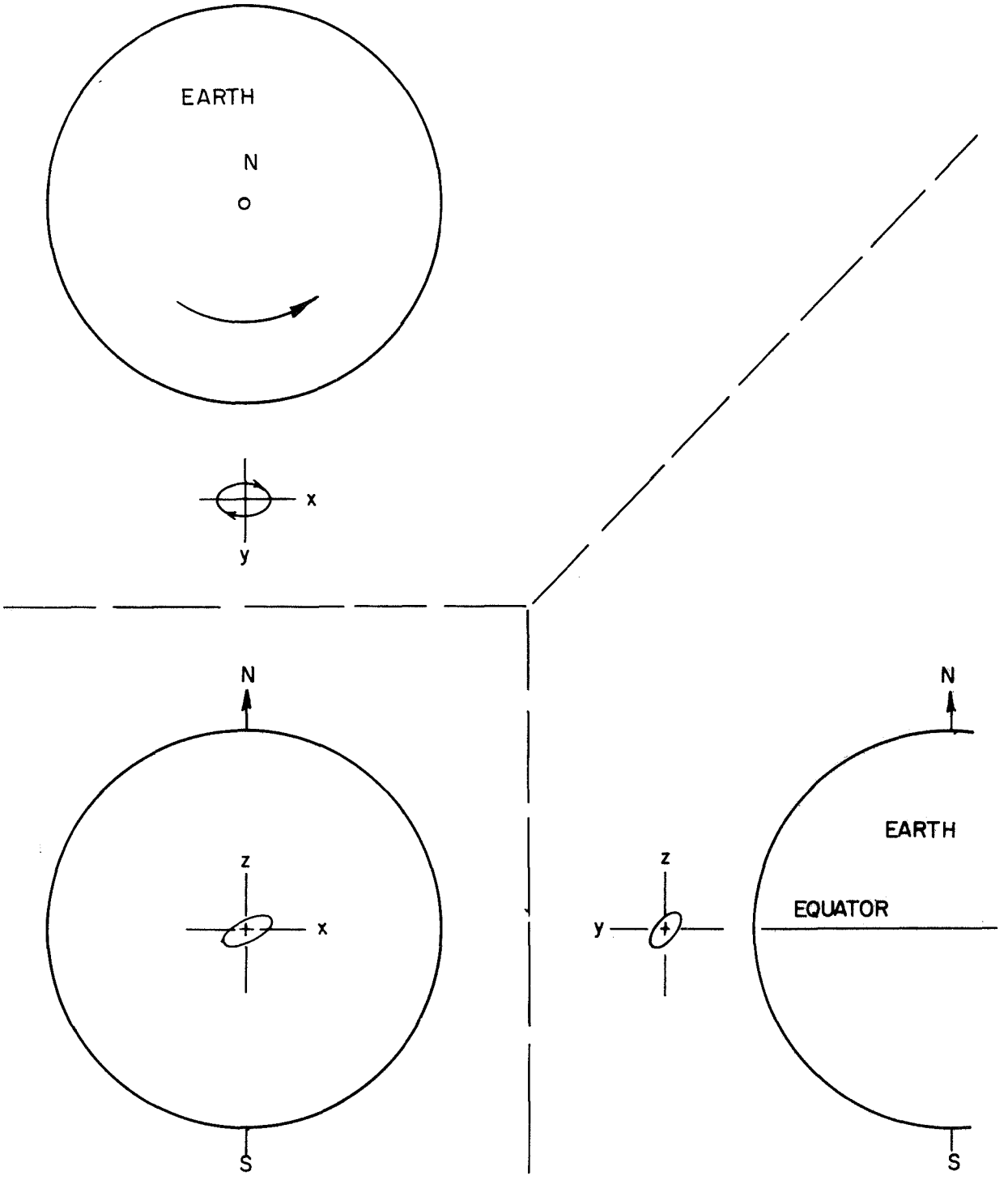

Figure 1 Small displacement from geosynchronous orbit as seen in an earth-fixed coordinate system with its origin at the geostationary orbit point. Residual eccentricity causes x-y ellipse, and residual inclination produces the z displacement.

movement away from the earth, it follows that range and range rate tracking will be very sensitive to changes in y. Therefore the constants B, C, and D which appear in Eq. (b), will be accurately determined by range and range rate tracking. Our concern here is with the fact that the constants A, E, and F do not appear in the equation for $\dot{y}$. In fact E and F, which give the amount (amplitude) and direction (phase) of residual orbit inclination, appear only in Eq. (c) for z, and Fig. 2 shows that the observed range rate will be very insensitive to movements in the z direction. The sensitivity is down to only 10% if the tracking station is situated at high latitude, and the sensitivity decreases with latitude until it vanishes if the tracking station were located at the equator. Even though the projection of z movements along the line-of-sight is small, it would be easy to disentangle this small projection if only it had a different frequency from the oscillations in x and y. However, such is not the case for the three sinusoids in Eq. (2) all have frequency n. Moreover their phase relations are given by two constants F and D which cannot be disentangled without multiple range-rate tracking from stations different latitudes. The precise determination of constants E and F is a strong argument for declination tracking, because z movement, which is determined in part by the constants E and F, is a linear displacement in the out-of-plane direction which corresponds to the declination angle [Eq. (A-1 (c)]; i.e., the measurement of oscillations in integrated dec-rate provides a direct measure of the constants E and F.

When a satellite orbit has appreciable inclination, the degeneracy is lifted, and constants E and F may be determined from range rate. Figure A-3 shows an inclined circular geosynchronous orbit. A second harmonic component of motion in the x direction results in a figure 8 pattern. The satellite moves ahead of the earth at high latitudes because the surface velocity of the earth is slower there where the surface is closer to the earth's axis. Depending on the longitude of a tracking station, the second harmonic will have a small projection along the line-of-sight and will appear in the range rate data, where it is readily

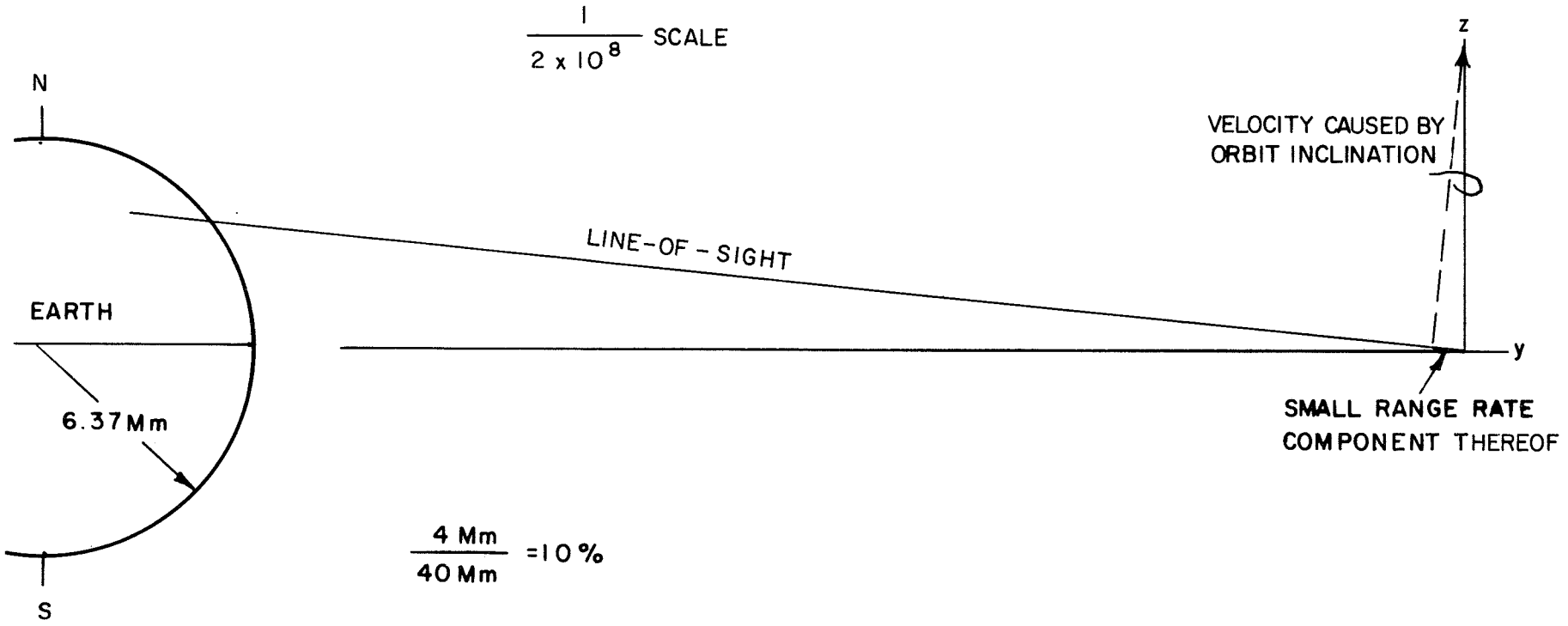

Figure 2 Illustration of the small effect that residual orbit inclination has on range rate. Depending on station latitude only about 10% of the motion in the z (dec) direction projects on the range rate direction (line-of-sight).

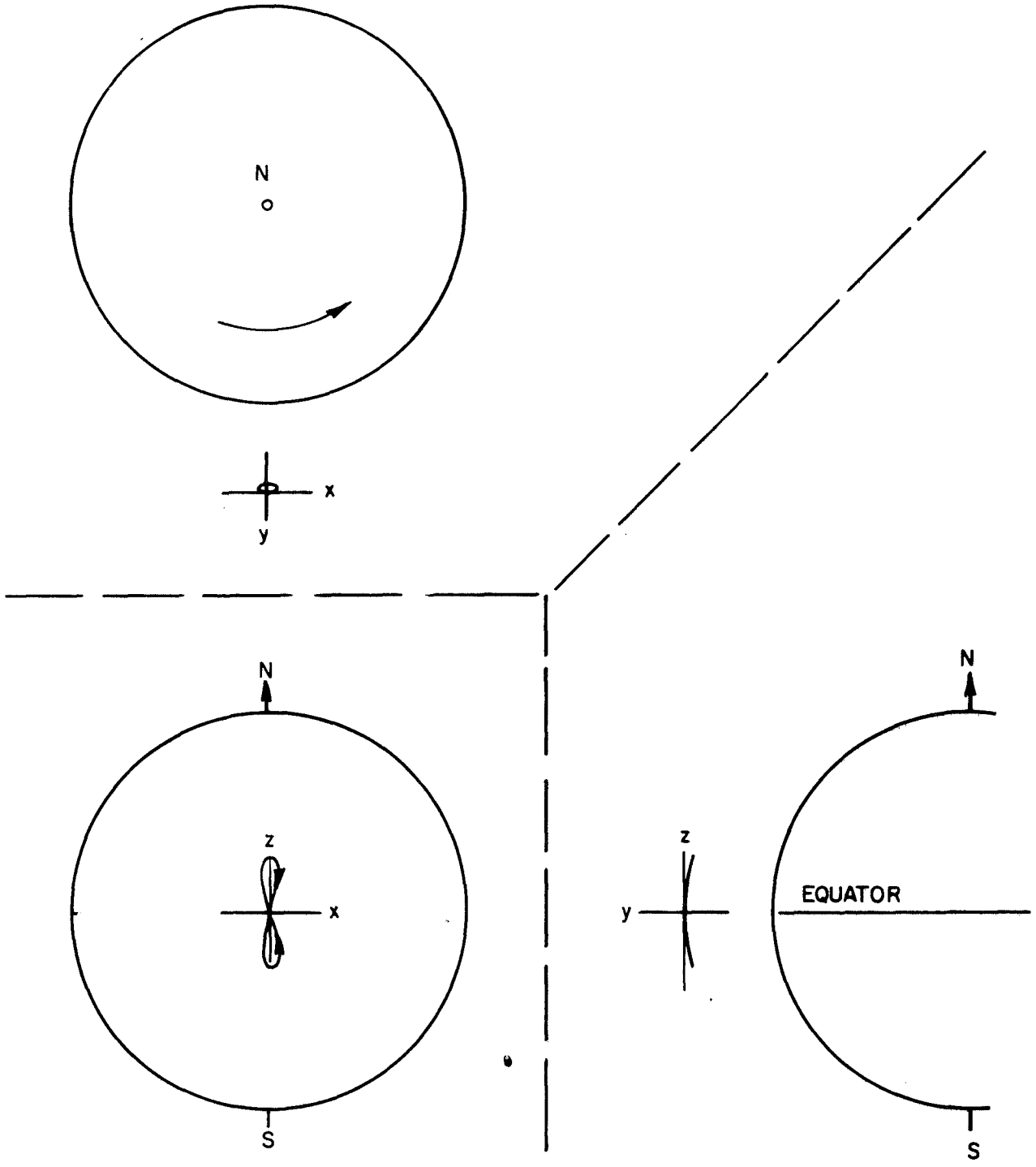

Figure 3 Inclined circular 24-hour orbit. The x-displacement is a second order effect that is noticeable with sufficient inclination.

identified by the second harmonic signature. The equation for the second harmonic can then enter the orbit determination program to strengthen the solution. However, for the ATS-F satellite the orbit is supposed to be geostationary as well as geosynchronous, and the residual inclination is supposed to be less than 1^{o}. The harmonic component discussed above is proportional to 1-cos of the inclination, which for the small values expected will be less than 0.00015.

A-2 Tidal Forces

The constant A in Eq. (A-3 (a)) tells the position on the equator over which the satellite hovers initially ($t = 0$) and B gives the drift in hover position. Obviously A and B (and other parameters as well) can be determined through their effect on the phase of the tidal accelerations by the sun and moon. In this subsection we show that tidal forces have their largest effect on a geostationary satellite in its declination movement, i.e., z as opposed to x or y.

The tidal acceleration acting on the satellite is the vector difference between the acceleration of the satellite and the acceleration of the earth as caused by a third body. Figure 4 is a set of vector diagrams showing the acceleration on a satellite in two views, a polar view at the top of the page, and a view from within the equatorial plane at the bottom of the page. In this figure we have arbitrarily chosen the moon as the third body; a similar diagram applies to the sun. The tidal acceleration vectors are given for 8 positions of the moon at 45^{o} intervals, which covers a complete circle with this interval. The tidal acceleration vector was estimated for each position in the manner shown in the sample vector diagram for position 2 which is inset in the middle of the page. The moon is shown in a southerly direction, i.e., a negative declination.

For our purposes the most important feature of the diagram is the rate at which the x, y, and z components of the tidal acceleration oscillate,

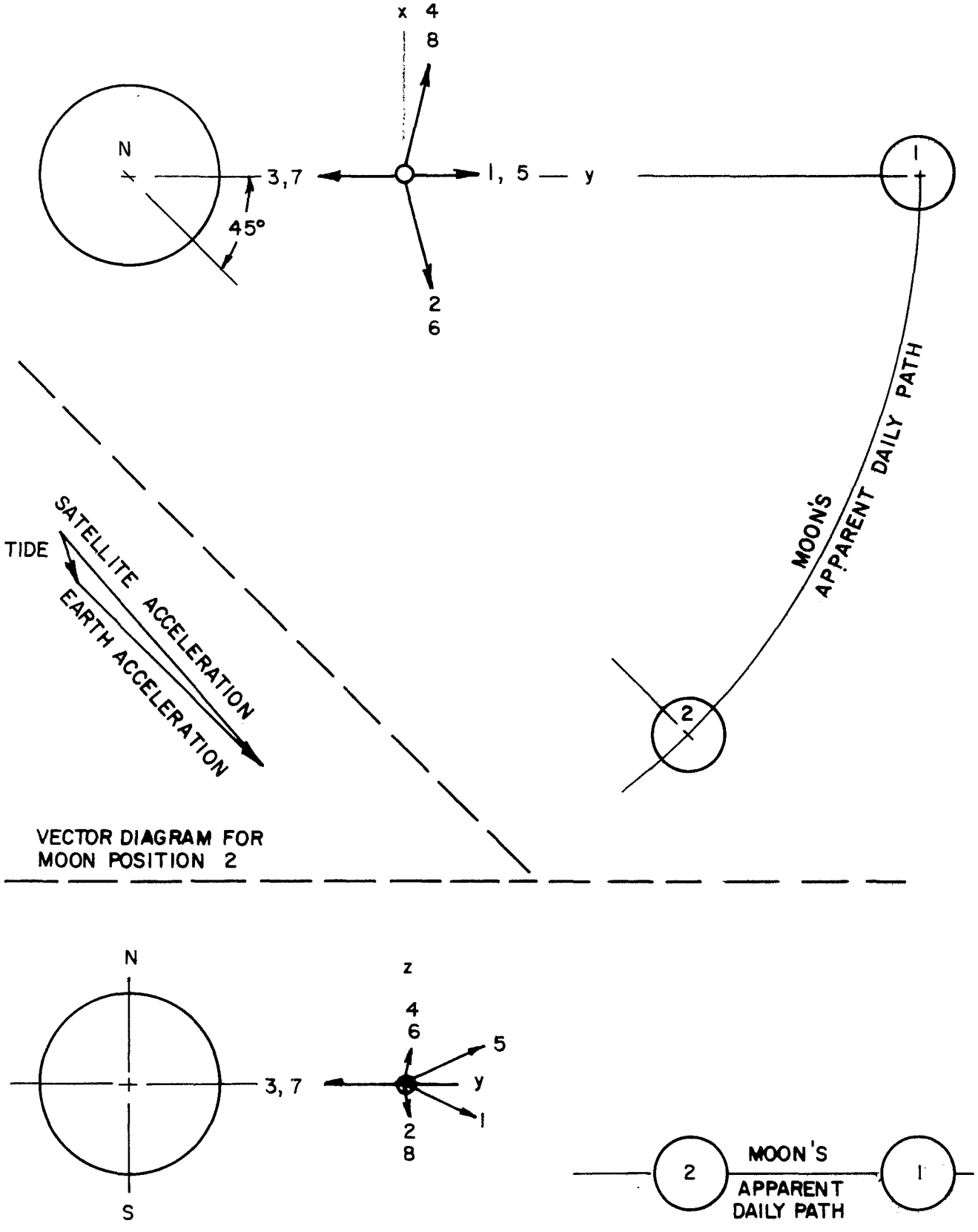
x
4
8
N
3,7
1, 5 — y
45°
2
6
1
MOON'S APPARENT DAILY PATH
2
TIDE
SATELLITE ACCELERATION
EARTH ACCELERATION
VECTOR DIAGRAM FOR
MOON POSITION 2
N
z
4
6
5
3, 7
y
1
2
8
S
2
MOON'S
APPARENT
DAILY PATH
1

Figure 4

In the x and y directions the tidal acceleration vectors encircle the satellite twice per lunar day,* while the z component of acceleration oscillates once per lunar day. Note that a lunar day is slightly longer than a solar day, about 25 hours. Recall that the frequency n that appears in Eqs. (A-2) and (A-3) corresponds to one sidereal day. This means that the z component of tidal acceleration represents a nearly resonant driving force, while the other components are nearly second harmonic. In other words, the effects of z acceleration will accumulate day after day, while the effects of x and y acceleration will average to nearly zero at the end of each lunar day. The effects of resonance versus non-resonance are inversely proportional to the square of the frequency discrepancy, i.e.,

$$\text{amplitude} \sim (f - n)^{-2} ,$$

where f is the frequency of the driving force in question. Thus, the lunar perturbation is about $(28)^2$ times stronger in dec, and the solar perturbation is $(365)^2$ stronger. These factors more than compensate (by far) for the fact that the z component of tidal force is the small component. However, twice a month (year) when the moon (sun) crosses the equatorial plane, i.e., 0 declination, the z component of tidal acceleration will vanish.

In this subsection we have shown that the most sensitive measurement of lunar and solar perturbations, and accordingly the most sensitive way of referring the satellite position to the angular position of these bodies, is by tracking the variations in satellite declination.

* "Lunar day" here refers to the period of the moon crossing any earthly meridian, not to sunrise and sunset as observed on the moon.

APPENDIX B

MICROTHERMAL MEASUREMENTS

At X-band and optical wavelengths, the principal errors in the refractive index are caused by temperature fluctuations in the troposphere. Except for the VLBI systems, the baseline is not long enough to support appreciable pressure differences. At sea level the thermal expansion coefficient for optical phase path is 10^{-6} per degree Centigrade.

We are interested only in the differences in temperature between two simulated lines-of-sight averaged along the line-of-sight and averaged for several minutes of time. The effects of rapid fluctuations can be removed by data smoothing techniques, and equal temperature changes at the two stations have no effect on interferometric data. Most of the published literature on air temperature fails to meet one of the following criteria:

* Differences must be available over distances on the order of one kilometer.
* The slow variations must be recorded (no high pass filter in the system).
* The data must include mountainous or desert areas that are suitable as observatory sites.

For these reasons we were compelled to make our own measurements. We chose Mt. Palomar as a typical site, merely because suitable towers were available, and because it is difficult to make electrical measurements on Mt. Wilson where commercial television transmitters cause severe RFI.

Two field trips were made. On the first we recorded data from 1400 PDT 9 May 1969 until 1400 10 May. On the second we recorded from 1300 PDT 8 July 1969 to 1800 9 July. The results were fairly consistent. They indicate that the worst temperature differences are about 3°C independent of the length of baseline. This difference has a scale height of about 20 meters which implies that the error in the difference between two interferometric propagation paths is about

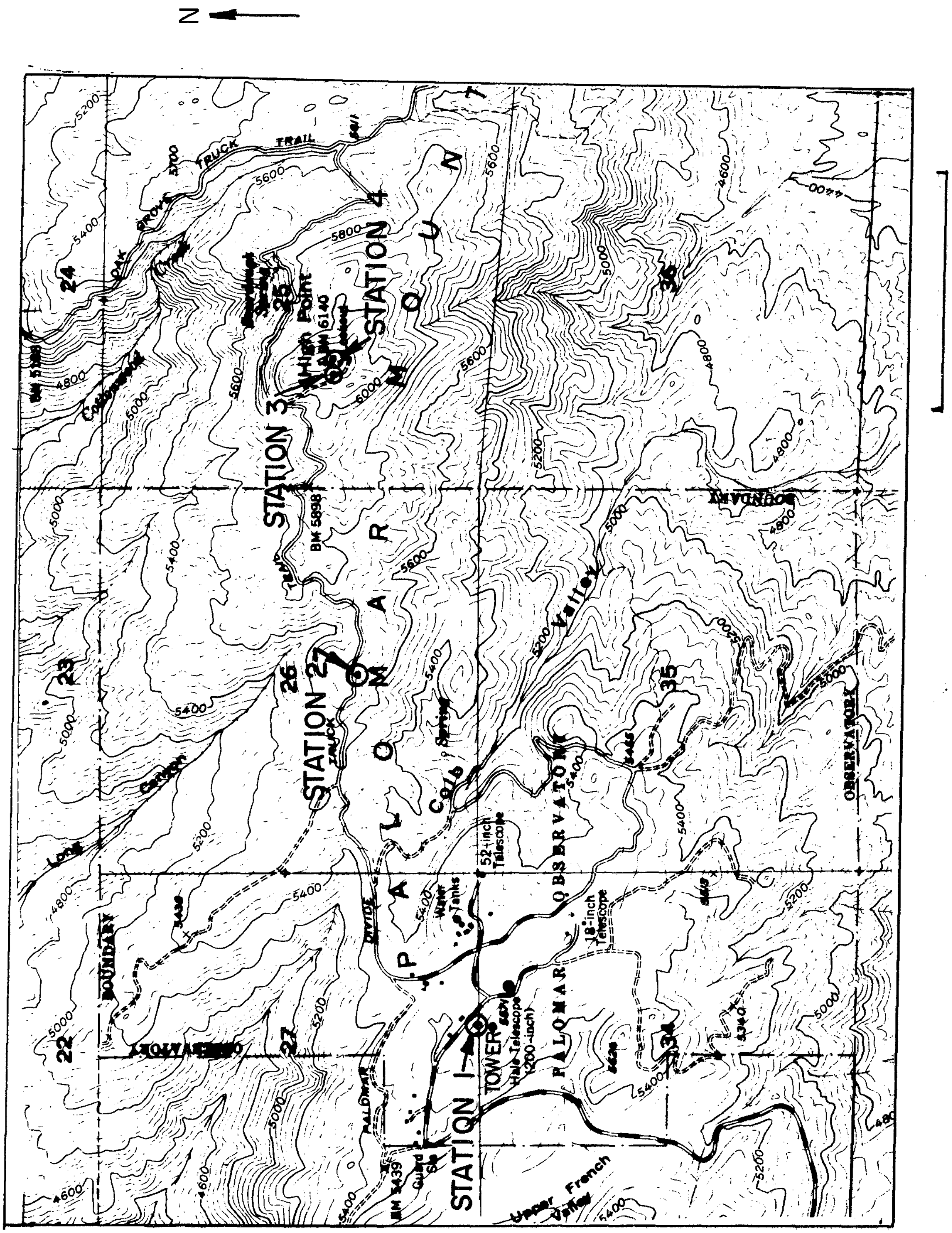
N
1 km
STATION 1
TOWER
Hale Telescope (200-inch)
STATION 2
STATION 3
STATION 4
High Point
BM 5898
52-inch Telescope
18-inch Telescope
PALOMAR OBSERVATORY
OBSERVATORY
BOUNDARY
Valley
Upper French Valley
TRUCK TRAIL
Spring
Water Tanks

$$3 \text{ deg} \times 10^{-6} \text{deg}^{-1} \times 20 \text{ m} = 60 \text{ microns},$$

when the system looks at the zenith. As a typical error we have chosen 100μ, which corresponds to an elevation angle of 37° instead of 90°. Often, especially at night, the error will be only a third as much, i.e., 33μ. Details of the two trips follow.

B-1 Mt. Palomar on 9 and 10 May 1969

Temperature data were taken at two points on Mt. Palomar, approximately three kilometers distant to simulate an interferometric baseline. These points are shown as stations 1 and 4 on the map of p.109. The stations are a microthermal tower slightly northwest of the 200 inch telescope and the ranger lookout tower on High Point to the east. At each tower we had a long tungsten resistance thermometer suspended from the top, which averaged the temperature all the way from the top to the bottom, simulating the desired average of the temperature along the line-of-sight of a telescope. Hall [Ref. 28] has shown that the wire average has the appropriate temperature dependence to substitute for refractive index. Each resistance thermometer consists of approximately 200 feet of thin tungsten wire folded back on itself to make a 100 foot sensor to go in one arm of the Wheatstone bridge. The resistance of each sensor is approximately 10,000 ohms. Each is insulated and covered with aluminum foil to reflect infrared radiation from the environment and thereby give a true measure of air temperature when it is not in direct sunlight. The effect of direct sunlight was small enough that one can learn to make corrections with appropriate study.

On the microthermal tower, station #1, we had two point temperature sensors, thermocouples, one 45 feet and one 80 feet off the ground, with which we hoped to learn something about the proper way to extrapolate the temperature readings to greater height. The point sensors were iron-constantan thermocouples with a sensitivity of 52μ volts/deg C.

The measurements began about 1400 PDT, May 9, and ended about 1400, May 10. The weather was pleasantly cool, winds variable in direction averaging about 15 knots. However, during the middle of the night the air was still at the microthermal tower but blowing 15 knots at High Point. Seeing at the observatory was unusually good that night, the astronomer on duty reporting one second of arc and sometimes better. The data taken at night were excellent, but during the day direct sunshine on the sensors had a significant effect. However, we were able to salvage two good daytime points, one on each day when passing clouds happened to shade the towers sufficiently. The night was clear, but both days had scattered clouds. The two day points are not plotted with the night and twilight data. On 9 May, between 1500 and 1515, the temperature at High Point was 0.9° cooler than the microthermal tower. The cloud pass on 10 May is not quite as valid because the microthermal tower was shaded approximately 40 minutes earlier than the High Point tower, but for what it is worth, the High Point tower was warmer by 2.3°C. The reduced data for twilight and nighttime are shown on the three graphs on the following pages. In these graphs the words "upper" and "lower" refer to the two thermocouples located on the microthermal tower. All temperature readings are degrees centigrade relative to an unknown origin. Note that for all of the points that are known to be valid, either day or night, the difference in temperature between the two stations did not exceed 1°C, except during the twilight cooling off and heating up periods. The third graph shows the temperature difference between the Ranger Tower and the microthermal tower plotted on the same sheet as the temperature difference between the two thermocouples on the microthermal tower. The purpose of this plot is to see if a considerable portion of the temperature difference between the two towers can be explained solely as a result of their altitude difference. As shown on the map, High Point is at 6140 feet, while the microthermal tower is at 5550 feet, a difference of 590 feet elevation. The graph does show the temperature differences due to elevation correlating with the temperature differences of the two towers; however, this correlation is not reliable without further atmospheric information as shown by the

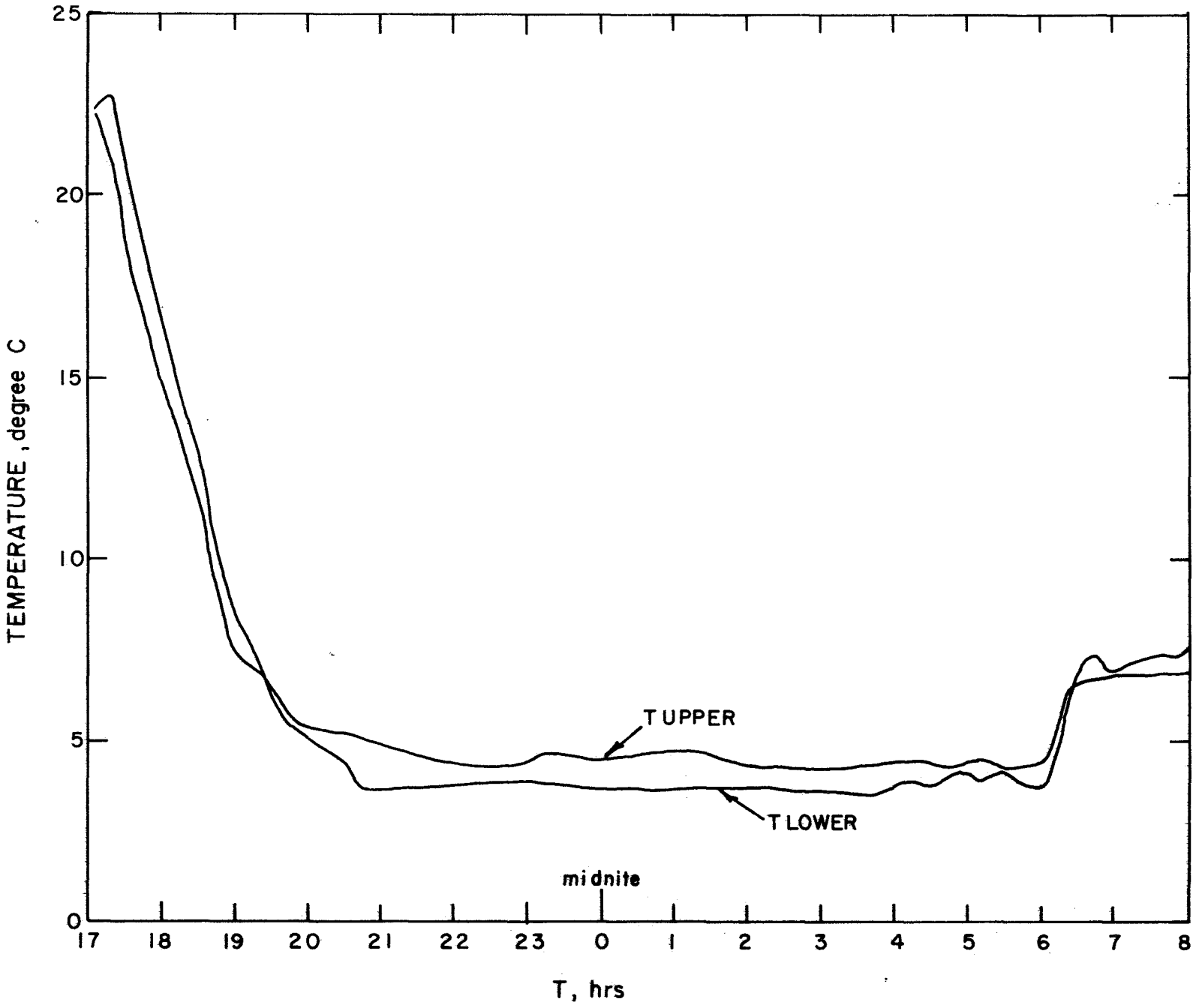
25
20
15
10
5
0
TEMPERATURE, degree C
T UPPER
T LOWER
midnite
17
18
19
20
21
22
23
0
1
2
3
4
5
6
7
8
T, hrs

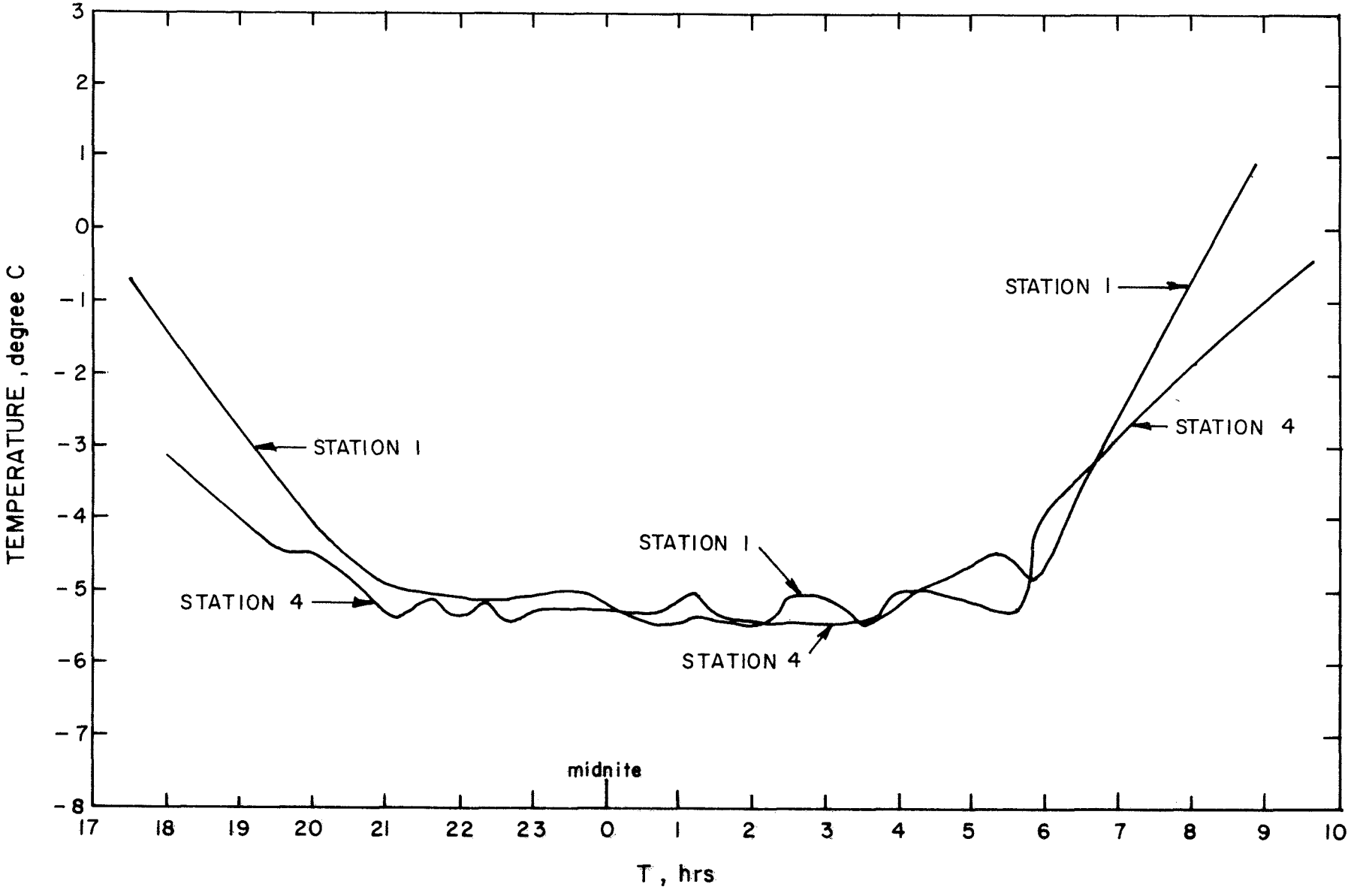
TEMPERATURE , degree C
3
2
1
0
-1
-2
-3
-4
-5
-6
-7
-8
STATION 1
STATION 4
STATION 1
STATION 4
STATION 1
STATION 4
midnite
17
18
19
20
21
22
23
0
1
2
3
4
5
6
7
8
9
10
T , hrs

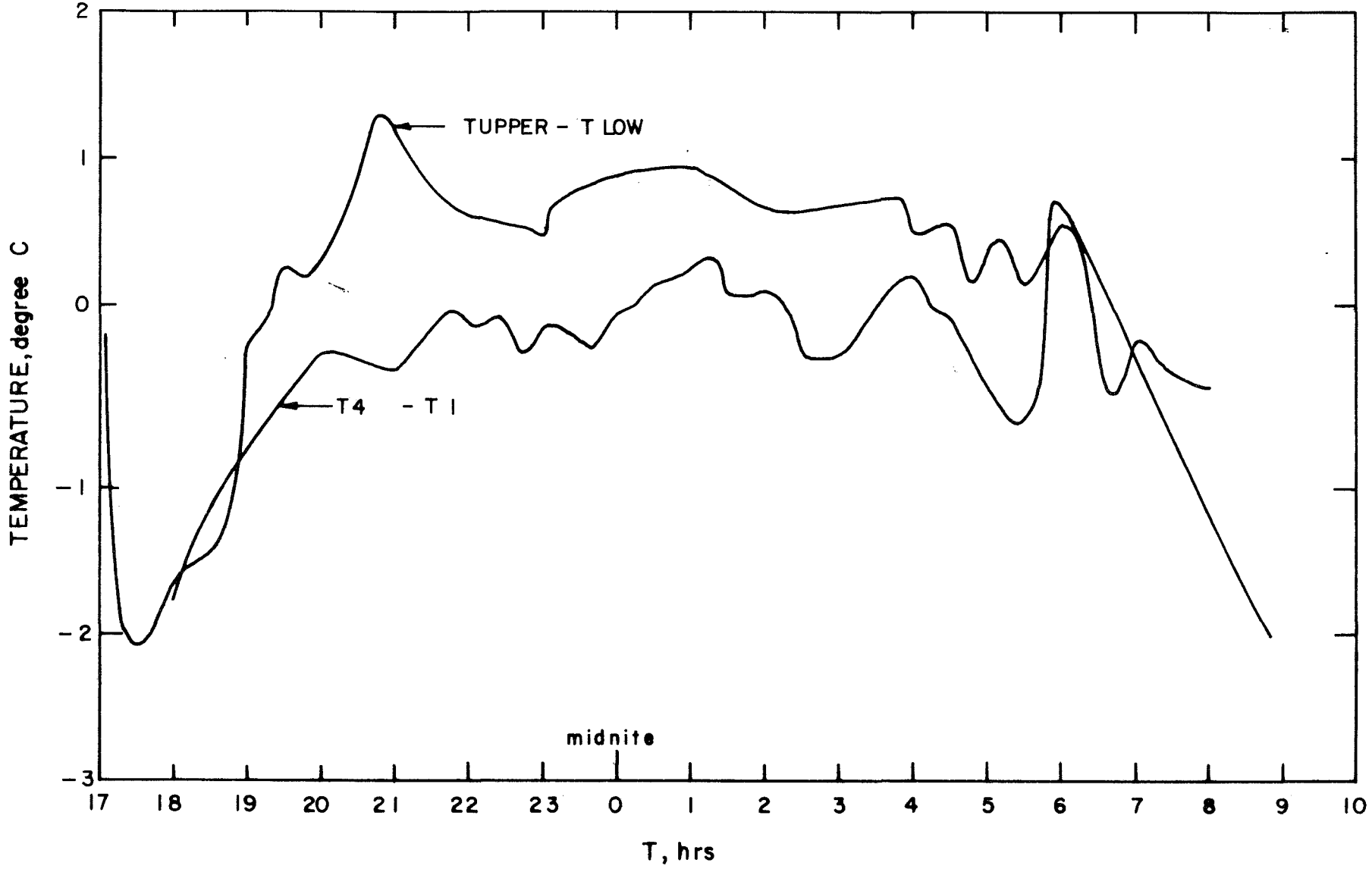
TUPPER - T LOW
T4 - T 1
TEMPERATURE, degree C
2
1
0
-1
-2
-3
midnite
17
18
19
20
21
22
23
0
1
2
3
4
5
6
7
8
9
10
T, hrs

event at time 2100 where the two curves fluctuate in opposite directions. The thermocouple data are not quite as useful as we had hoped, for extrapolating the temperature differences to greater altitude. However, as the first graph shows, the temperature excursions at the top of the tower are somewhat less than those halfway down as one would expect. This lends support to the plausible argument that air is better mixed at higher altitude and that the temperature differences between towers can be expected to decay with some reasonable scale height. The data from the second field trip showed this scale height to be approximately 20 m. A condensed interpretation of the experimental data is that on some nights we can expect temperature differences as small as $1^{o}C$ over 3 kilometers. One degree implies a refractive index difference of 10^{-6}, which, as we have shown, is an encouraging result.

B-2 Mt. Palomar on 8 and 9 July 1969

On this trip the sensors were distributed horizontally as well as vertically to give a rough measure of the optimum length of an interferometric baseline. We used four towers, two permanent 100 foot ones and two short temporary ones. We used a total of nine resistance thermometers; each was wrapped in aluminum foil to reflect ambient radiation, and each was shielded from the sun by a small roof that is painted white on top and covered with shiny aluminum on the bottom.

The map indicates the location of the four towers used for microthermal measurements. Station 1 is the 100 foot microthermal tower near the dome of the 200 inch telescope. Station 4 is the 100 foot Ranger Lookout Tower at High Point. Stations 2 and 3 are portable telescoping towers tied onto small telephone poles. Stations 1, 2 and 3 had two thermistors, one about midway up and the other at the top. Station 4 at High Point was equipped with three thermistors to make a total of 9 resistance thermometers. Station spacing, altitudes, and thermistor spacings are given in Table 1. The wind was so slight and variable on both days that we made no attempt to record it.

Station Number	Elevation, feet	Distance from Station Number 1, km	Thermistor heights off ground, feet
1	5571	0	95 35
2	5720	1.56	50 18
3	6080	5.09	50 18
4	6140	5.17	95 55 15

TABLE 1

Fig. p.118 shows the temperature traces of five of the nine thermistors. The lowest thermistor on each tower was omitted in this figure to reduce clutter. This figure is intended primarily to show horizontal temperature differences, so the readings of the bottom thermistor are shown in subsequent figures. Each trace in this figure represents a different tower with the exception of the two traces labeled "T_4mid" and "T_4top", which represent the middle and top thermistors of the trio at High Point. These two traces stay closer together than the others as expected. There is a large gap in the data from Station 4 owing to the failure of a battery to hold its charge. As expected, the curves all show the diurnal temperature cycle, and they are all considerably smoother at night than they are during the day.

For our study the most significant result to be gained from Fig. p. 118 is the extremely close correlation between the temperatures at Stations 2 and 3, about 1.2 kilometers apart, and the much smaller correlation between the temperatures at Stations 3 and 4, only about 100 meters apart. Clearly the distance of separation, or simulated baseline, is not the major factor in determining how well the temperature of one station tracks that of another, nor does the altitude of the station offer any explanation as Table 1 and the contours on the map show. We suspect that the strong correlation between 2 and 3 and the lack of correlation between 3 and 4 can only be attributed to the characteristics of the particular mountain and the weather pattern of the particular days.

Any conclusions based on a two-day sample of weather and air flow patterns is, of course, very tentative; however the results of Fig. p.118 do indicate that a laser interferometer system should employ the longest possible baseline that mountainous terrain and land acquisition permit, and that a microthermal survey of candidate sites for the stations is advisable if time and funds permit. The reason for long baseline is readily understood by recalling that the angular error in an interferometric measurement is proportional to $\Delta T/b$, where b is the baseline length. The difference

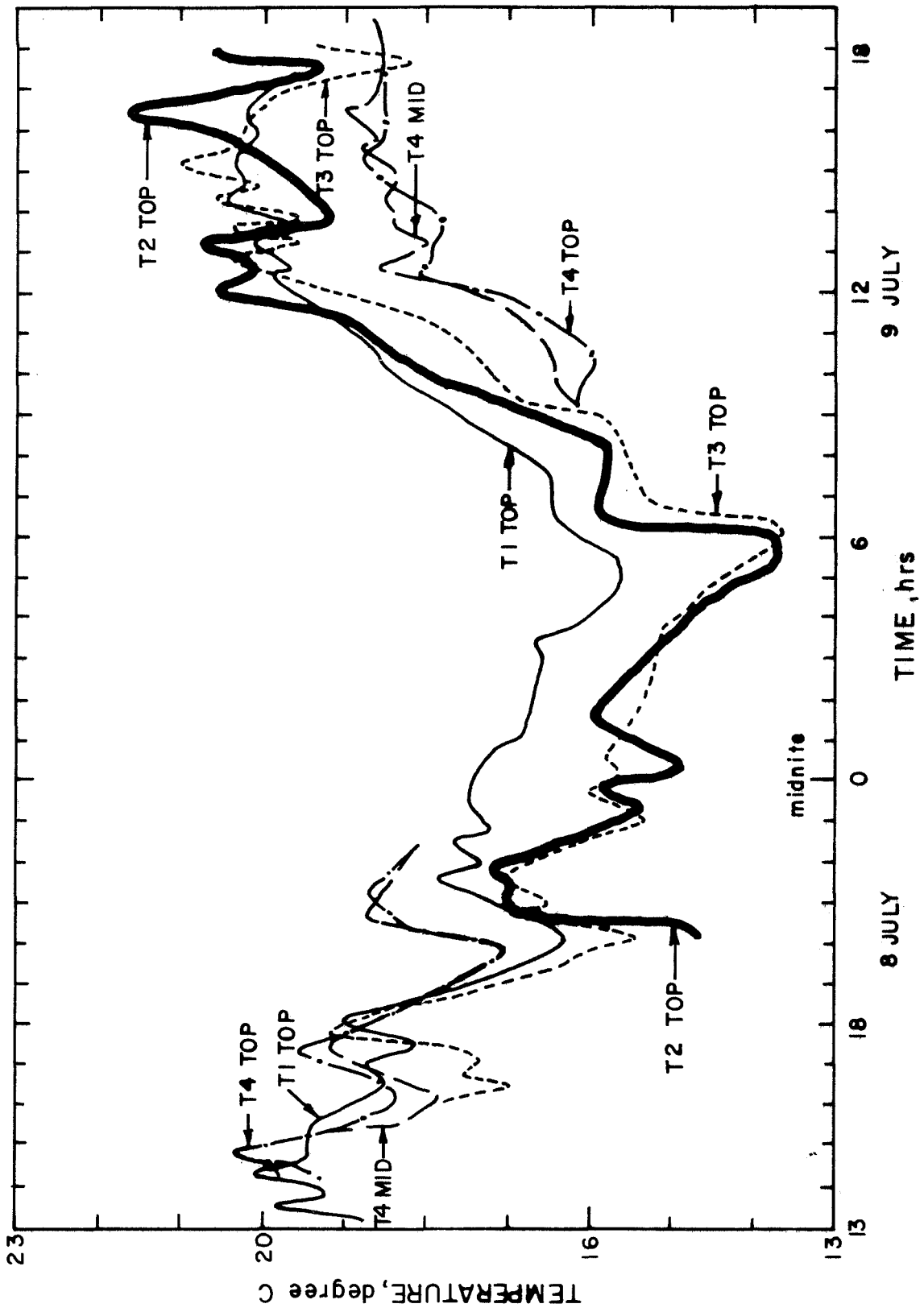

Temperature Fluctuations at all Four Stations

between phase paths along the two lines-of-sight has an error proportional to ΔT, and division of this error by b converts the linear error to an angular error. Now if ΔT is nearly independent of b as our results for 8 and 9 July indicate, then the error is minimized by choosing the maximum possible b.

Vertical variations in temperature are best indicated at Station 4 where we had three thermistors. These data are shown in Fig. p. 120. The tower at High Point was chosen for the main study of vertical distribution, because even the lowest thermistor is at an altitude well above the perturbing effects of trees and other terrain features, since the tower is located on a rocky point. The spacing of the three thermistors at High Point is approximately 40 feet. Fig. p. 120 shows that the temperatures at the middle and top thermistors correlate considerably more closely than the middle and bottom thermistors. We can fit the rms temperature differences to an exponential function and determine an approximate scale height for the temperature fluctuations of interest. This scale height for the decay of vertical temperature gradients turns out to be only 20 meters.* This is a somewhat shorter distance than we had expected and therefore an encouraging result. Moreover, the vertical gradient sometimes reverses sign, so that errors will tend to cancel out in integration along the line-of-sight. For example for a period of about $2\frac{1}{2}$ hours near 1600 o'clock on 8 July note that the middle thermistor at High Point was cooler than either the top or the bottom. Figs. pp. 121 to 123 show the vertical temperature differences on the other towers which are all of comparable magnitude. At all stations the vertical temperature differences more or less follow the normal behavior in which the bottom is warmer during the day but cooler at night.

---

* Recall that this scale height applies to relatively slow frequency components in the fluctuation of temperature and is not to be confused with the heights at which rapid temperature fluctuations cause degradation in astronomical seeing. Also recall that the interest in slow fluctuation derives from the fact that we are planning to count interferometric fringes over a relatively long period of time.

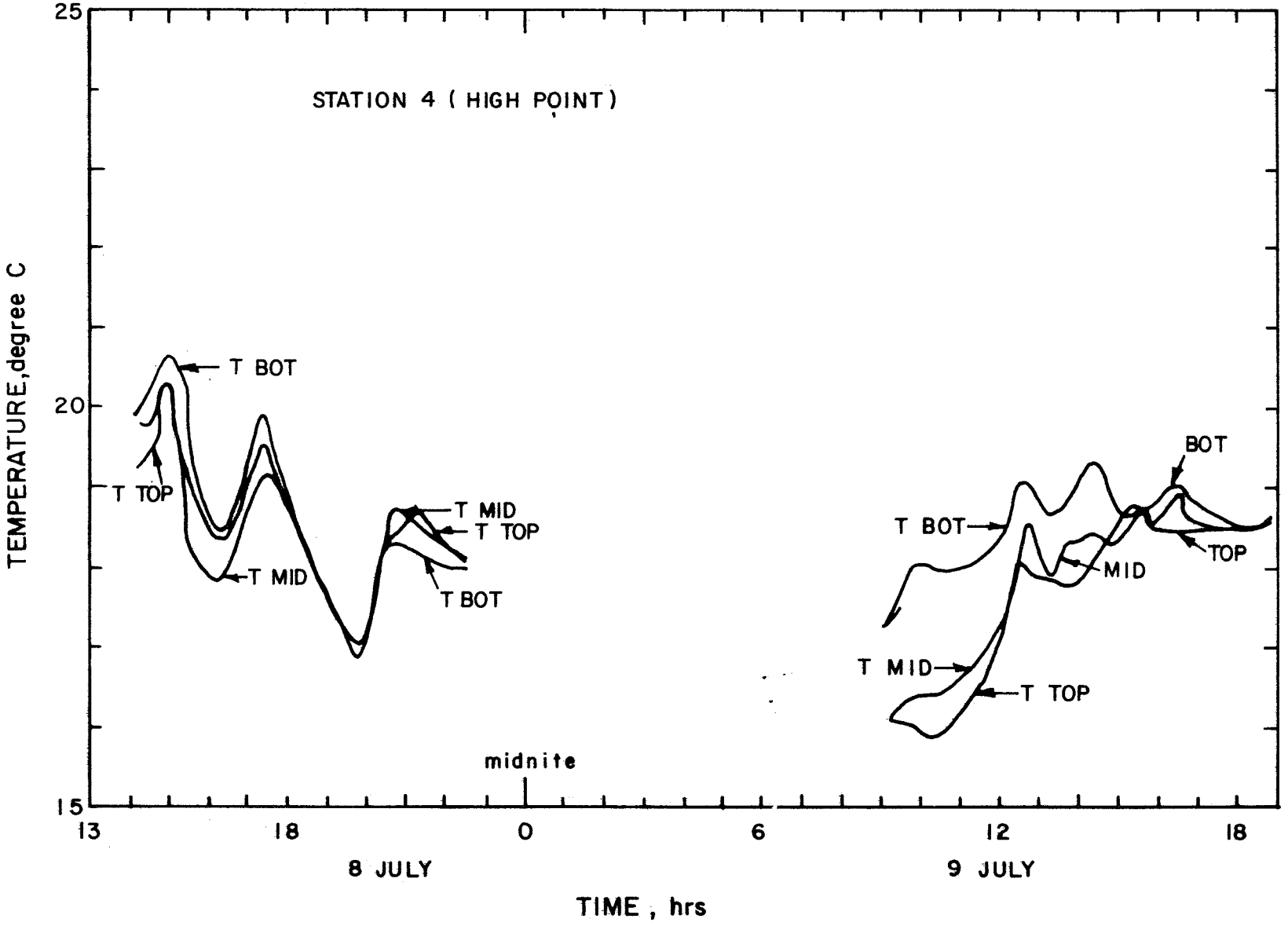

Vertical Temperature Distribution at Station 4, High Point

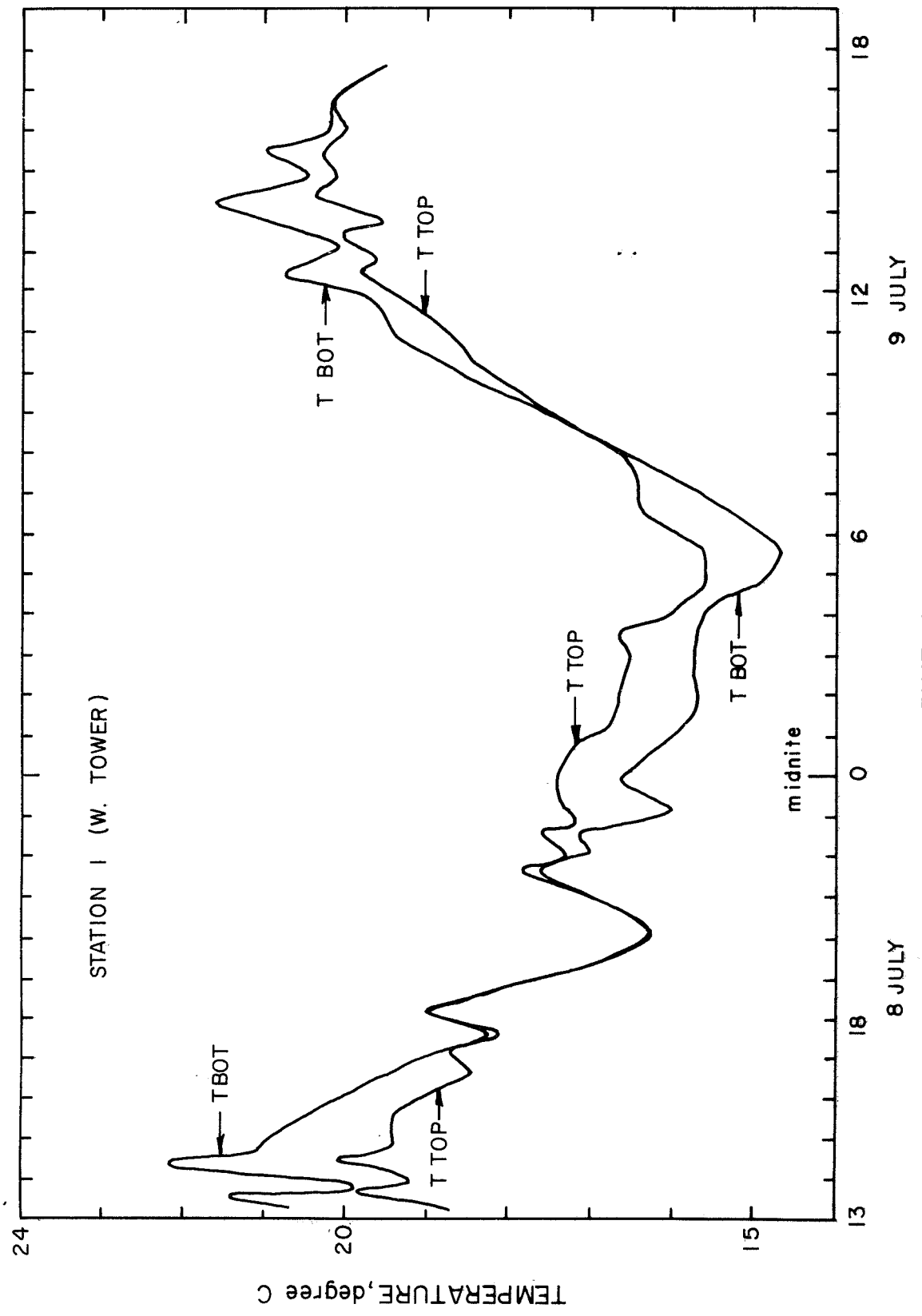

Temperature Fluctuations at Station 1, Microthermal Power

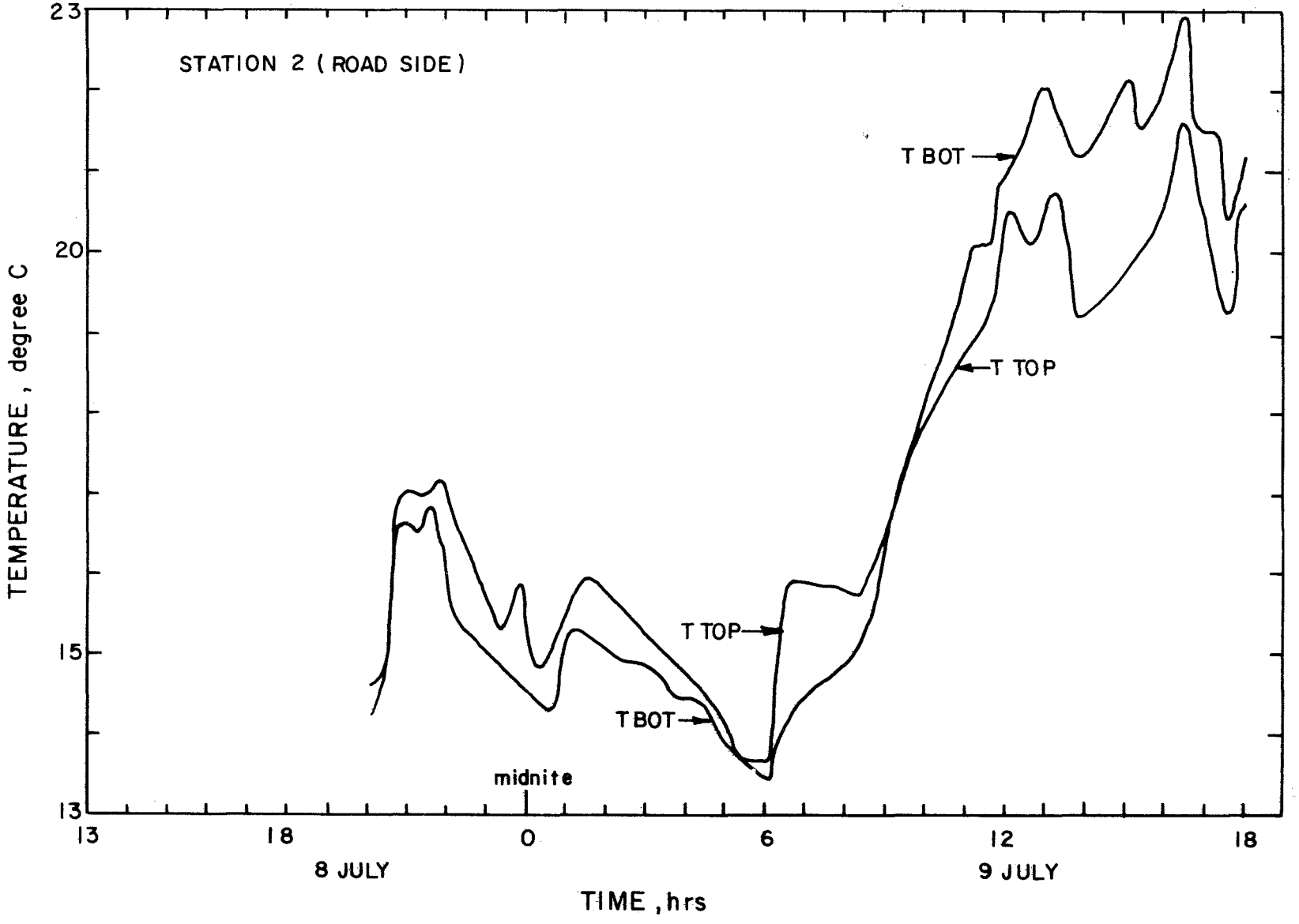
STATION 2 (ROAD SIDE)
T BOT
T TOP
T TOP
T BOT
midnite
TEMPERATURE , degree C
TIME , hrs
8 JULY
9 JULY
23
20
15
13
13
18
0
6
12
18

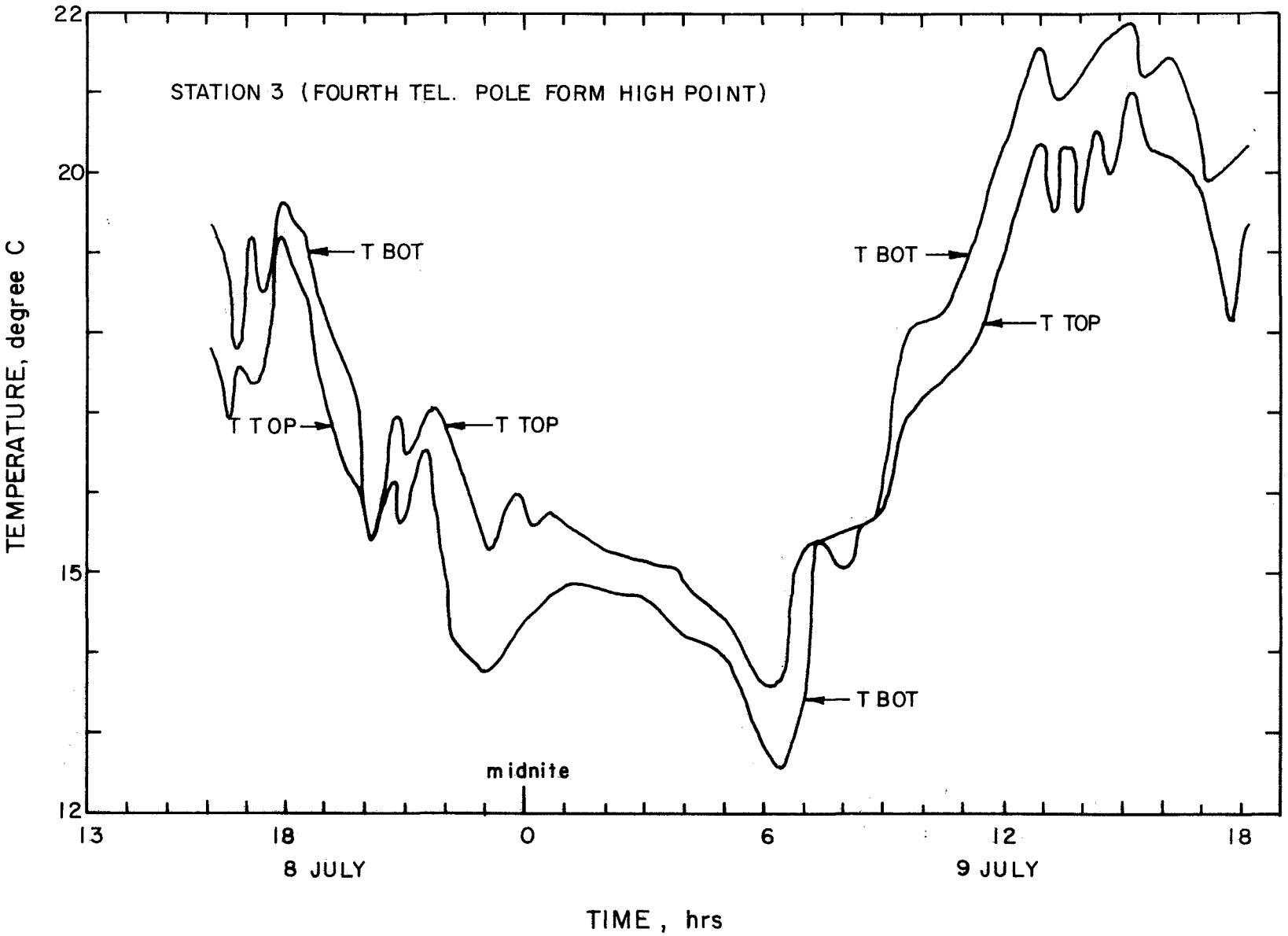
STATION 3 (FOURTH TEL. POLE FORM HIGH POINT)
T BOT
T TOP
T TOP
T BOT
T TOP
T BOT
midnite
22
20
15
12
13
18
0
6
12
18
8 JULY
9 JULY
TEMPERATURE, degree C
TIME , hrs

APPENDIX C

REFRACTION IN THE TROPOSPHERE

The refractivity N of air is usually expressed as parts per million of the refractive index n, i.e.

$$N = 10^6(n-1)$$

For our optical estimates we used the constants given by Allen [Ref. 12]:

$$N_o(\lambda) = 64.328 + \frac{29,498}{146 - \lambda^{-2}} + \frac{255.4}{41 - \lambda^{-2}},$$

for $t = 15^oC$, $p = 760$ torr, in dry air, and λ = wavelength in microns. For other values of p, t, f (humidity)

$$N(p,t,f,\lambda) = \frac{1}{1+.003,661\,t}\left\{\frac{N_o(\lambda)p}{720.883}\left[1+(1.049-.0157t)10^{-6}p\right]\right.$$

$$\left. -(0.0624 - .000,680\lambda^{-2})f\right\},$$

where f and p are in torr, t in deg C. Evaluation of the partial derivatives of the principal terms shows that temperature is responsible for most of the troublesome fluctuations. For Mt. Hopkins conditions

$$\left.\frac{\partial N}{\partial t}\right|_{\substack{t = 15^o \\ p = 569 \text{ torr} \\ f = 10 \text{ torr}}} = -0.706 \text{ per deg C.}$$

For microwaves

$$N(p,t,f) = \theta^{-1}(0.3787p + 0.33f) + 6.70\,f\theta^{-2}$$

where

$$\theta = 1 + 0.003661\, t$$

Two partial derivitives indicate that fluctuations in both temperature and humidity are troublesome

$$\left.\frac{\partial N}{\partial f}\right|_{15^{\circ}} = 6.33 \text{ per torr}$$

$$\left.\frac{\partial N}{\partial t}\right|_{\substack{t = 15^{\circ} \\ p = 569 \text{ torr} \\ f = 10 \text{ torr}}} = -1.138 \text{ per deg.}$$

Thus tropospheric disturbances are somewhat more severe in the microwave bands.

As we noted, existing literature on air temperature was not used for our numerical estimates, because it failed to give data for the particular statistic that affects interferometry. However, some data from the literature is at least related. Dodd et al [Ref. 48] have correlated refraction in air at close points. Thayer [Ref. 49] has used multiple radio and optical frequencies to remove refractive effects by extrapolation. Aircraft and balloon measurements have extended the measured altitude, but do not cover a significant simulated baseline. [Ref. 50] Other tables and empirical formulae for refractivity are available [Refs. 51, 52].

APPENDIX D

SATELLITE RANGE EQUATIONS

In this appendix we derive the various quantities and formulas needed to solve the radar and lidar range equations. This is done in three steps. First, the various ways of specifying satellite reflectors are converted to a single figure-of-merit for reflectors called Q. Next the orbits of existing satellites of interest are taken into account to give a Q_{sat} for each of the satellites. Finally, Q_{sat} is incorporated into a range equation from which the transmitter power requirements may be derived. The range equation takes various forms depending upon whether the system is continuous wave, pulsed, microwave, or optical.

D. 1 Figure-of-Merit for Satellite Reflectors

A convenient quantity for describing the return of radiant energy from satellite reflectors is the ratio

$$Q \equiv \frac{\text{Photons per sterradian - returned along line-of-sight}}{\text{Photons per square meter - incident on the satellite}} = \frac{\sigma}{4\pi}, \quad \text{(D-1a)}$$

where σ is the radar cross-section.

For the panel of quartz retroreflectors on the moon, this quantity is estimated to be $Q = 5 \times 10^7$ m^2/ster, for light at 6943 A^o [Ref. 47] from favorable directions during the lunar night. Since we have considered using this panel only at 1.06μ (the neodymium laser wavelength), we must apply a correction factor. The angular spread of reflected light is almost as small as the diffraction limit of the individual reflectors, so the angle is proportional to the wavelength λ and the solid angle to λ^2. Therefore, the correction factor is $(0.6943/1.06)^2 = 0.429$, which gives

$$\text{Moon: } Q = 2.1 \times 10^7 \text{ m}^2/\text{ster}, \quad \text{or} \quad \sigma = 270 \text{ km}^2 .$$

Properties of other satellite retroreflectors are published in a different form by the Smithsonian Astrophysical Observatory (SAO). Lehr [Ref. 2]

lists the effective area A and divergence θ of the return beam. These can readily be combined to give Q; letting ω be the solid angle of the return beam,

$$\text{photon return per sterradian} = \frac{\text{photons returned}}{\omega} \quad , \text{ and}$$

$$\text{photons returned} = A \times \text{photon flux} \quad , \text{ giving}$$

$$Q \equiv \frac{\text{return/ster}}{\text{flux}} = \frac{A}{\omega} \quad . \tag{D-1b}$$

In the retroreflector case, $\omega = \frac{\pi}{4}\left(\theta \times \frac{4.85 \times 10^{-6}\,\text{rad}}{\text{arc sec}}\right)^2$ which gives

$$Q = 0.54 \times 10^{11} A/\theta^2 \tag{D-2a}$$

where A is in m^2 and θ in arc sec. When the correction is made for 1.06μ, the result is

$$Q\,(1.06\mu) = 2.32 \times 10^{10} A/\theta^2\,(0.69\mu) \tag{D-2b}$$

When the retroreflector is diffraction limited, its gain is determined only by its effective area A_e, and

$$Q = \eta_{ref} \frac{A_e}{4\pi} G \quad , \qquad G = \frac{4\pi A_e}{\lambda^2} \quad .$$

where η_{ref} is the efficiency of reflection. Hence

$$Q = \eta_{ref} (A_e/\lambda)^2 \tag{D-2c}$$

This completes the specification for retroreflectors, and the next step is to derive Q for balloon satellites. In this case, Q will be independent of λ since $\lambda <<$ the balloon radius, and geometric optics applies in all cases considered herein. There are two conditions of the balloon to

consider: One case is a taut sphere and, one the other is wrinkled with age and meteor impacts. We give formulas for both cases, but we assume that the specific satellites considered here are not yet wrinkled, as Echo 1 and 2 were in their old age.

We assume that wrinkles give a lambertian reflection in which case $\omega = \pi$ and $A = \pi r^2$, and Eq. (D-1) gives

$$Q(\text{wrinkled}) = r^2 = (d_b/2)^2 \tag{D-3}$$

where d_b is the balloon diameter. The return from a taut balloon will occur at one small highlight where a line-of-sight to the center of the balloon intercepts the specular surface. Consider a small circle of radius ϵ which surrounds the highlight on the balloon as shown in Fig. p.129. The signal that impinges on the circle re-radiates from a virtual focus at the distance $r/2$ behind the circle, filling a cone of half angle $\epsilon/(r/2) = 2\epsilon/r$ and solid angle $\omega = \pi(2\epsilon/r)^2$. Substituting this into Eq. (D-1) along with $A = \pi\epsilon^2$ gives

$$Q(\text{taut}) = (r/2)^2 = (d_b/4)^2 \tag{D-4}$$

Equations (D-3) and (D-4) show that a lambertian sphere gives four times as much return as a specular sphere, but the lambertian sphere is nevertheless undesirable in most cases, since the observer will see strong scintillations that result from random interference of the radiation from the various wrinkles.

D.2 Range Equations

The task of this subsection is to fit the Q factors defined above into a general range equation. Let us define

$R \equiv$ range to the satellite

$d_e \equiv$ effective telescope aperture diameter

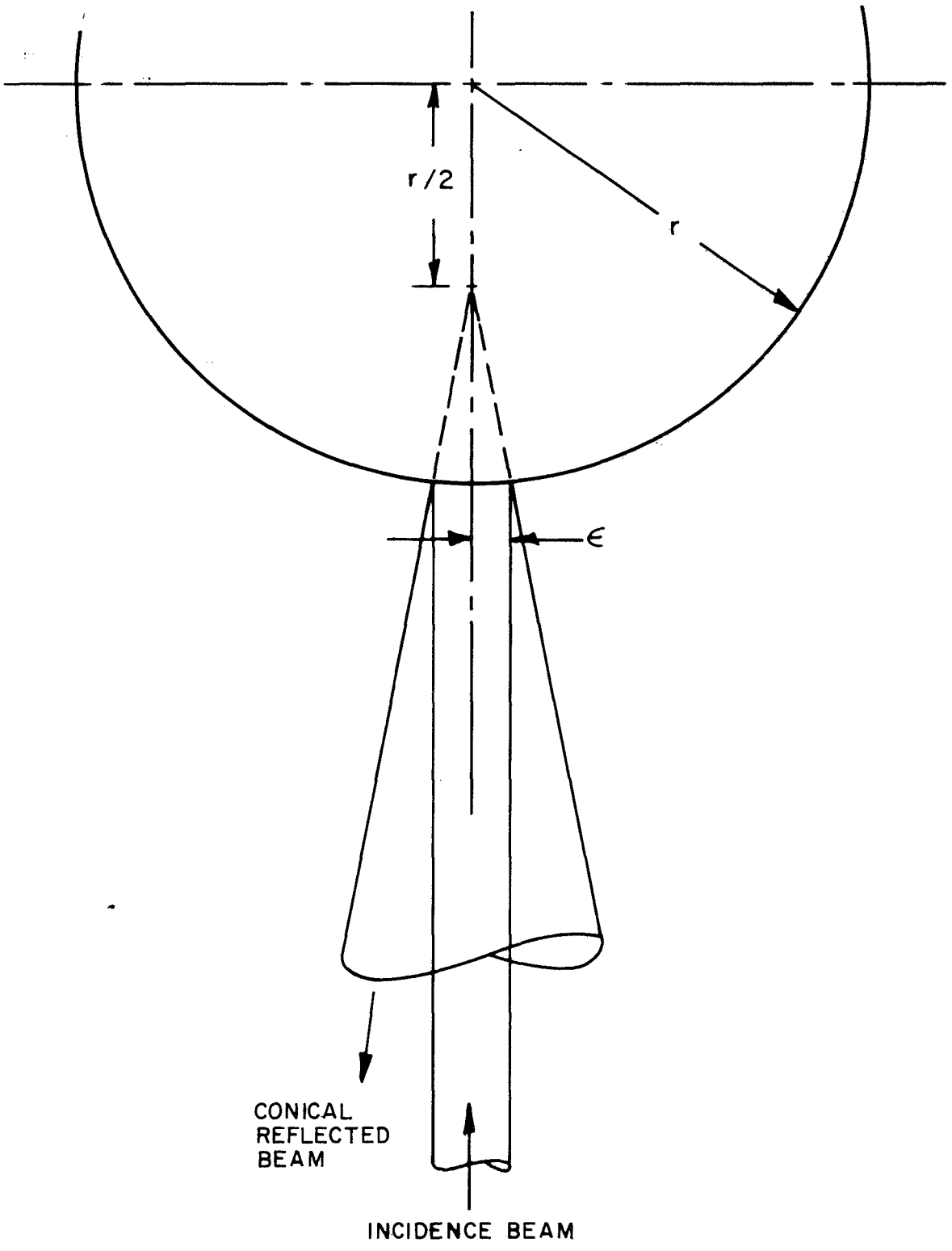

Geometry of Reflection From Specular Sphere

θ_{up} ≡ divergence angle of the upgoing beam

θ_{dn} ≡ seeing angle, i.e., the minimum divergence angle of a beam through the atmosphere (dn = down)

η ≡ one-way efficiency factors (that are squared for two-way propagation) and are not included elsewhere, e.g., transparency of the atmosphere and aperture efficiency of the telescope.

Note that $\theta_{up} \geq \theta_{dn}$. In laser tracking, θ_{up} is often 1 mrad, which is greater than θ_{dn} to assure that the beam intercepts the satellite. This is necessary because the satellite ephemeris predictions and telescope pointing errors do not currently permit blind pointing to accuracy better than 1 milliradian. The reason why d_e is an effective value and therefore sometimes different from the real aperture, will be discussed later.

From the definition of Q, the power or energy received is

$$(E_R \text{ or } P_R) = \eta Q \times \left[\begin{array}{c}\text{flux at the} \\ \text{satellite}\end{array}\right] \times \left[\begin{array}{c}\text{solid angle of the} \\ \text{telescope as seen} \\ \text{from the satellite}\end{array}\right],$$

where energy E applies to pulse cases and power P to CW cases. The quantities in square brackets are readily evaluated:

$$[1st] = \frac{\eta(P_T \text{ or } E_T)}{(\pi/4)(\theta_{up}R)^2} \quad ; \quad [2nd] = \frac{(\pi/4)d_e^2}{R^2}$$

Substitution gives the propagation loss factor:

$$L \equiv \frac{P_R}{P_T} \text{ or } \frac{E_R}{E_T} = \left(\frac{\eta d_e}{\theta_{up} R^2}\right)^2 Q \qquad \text{(D-5)}$$

Finally, we express θ in $\widehat{\text{sec}}$, E_T in joules of energy, and E_R in photons (i.e., 1 $\widehat{\text{sec}}$ = 4.85 μrad, and 1 photon energy = hc/λ). The resulting loss factor is

$$L = 2.14 \times 10^{29} \ \frac{\text{photons-}\widehat{\text{sec}}^2}{\text{J-micron}} \left(\frac{\eta d_e}{\theta_{up}} \right)^2 Q_{sat} \lambda \qquad \text{(D-6)}$$

where

$$Q_{sat} \equiv \frac{Q}{R^4} \qquad \text{(D-7)}$$

The advantage of combining R^{-4} and Q is that all the pertinent properties of the satellite and its orbit are collected into the Q_{sat} factor, which is tabulated in Appendix E for some satellites of interest.

D.3 Variations of the Range Equation

Unlike the existing laser satellite tracking systems, the optical ones studied herein employ coherent optical receivers which in contrast to photon counters preserve the phase of the optical wave. Two types have been built: optical heterodyne and laser amplifier*; both are included in the studies described in the main text. These receivers differ from cooled photon counters in that the signal-to-noise ratio is not determined by the total received power (or energy per pulse or photons per pulse), but rather by the power density per unit solid angle per unit area of the incoming beam. In systems where the solid angle (proportional to image area) is set by atmospheric seeing conditions, there is little to be gained by increasing the aperture area. The receiver collects more signal and

---

*The term "laser amplifier" is redundant because a in laser means amplification. However, since we are accustomed to lasers having feedback mirrors to convert the amplifier into an oscillator or optical power source, we need to distinguish the "pure" amplifier. A proper term would be "traveling-wave laser" as opposed to "standing wave laser."

more noise while the ratio remains constant. However, if the aperture diameter is less than

$$d_0 = \frac{4}{\pi} \frac{\lambda}{\theta_{dn}} \quad , \tag{D-8}$$

then the solid angle is determined by diffraction and is inversely proportional to aperture area. In this diffraction-limited case the signal-to-noise ratio is proportional to aperture area. To cover both cases (atmosphere and diffraction solid angle) we define

$$d_e = \begin{cases} d, & d < d_0 \\ d_0, & \text{otherwise} \end{cases}$$

where

d is actual diameter,

d_e is effective diameter, and

d_0 is given by Eq. (D-8) .

In reality, d_e does not saturate quite so sharply at d_0, but such details are beyond the scope of this study.

D.3.1 Pulsed Nd Laser System

This system has $\lambda = 1.06\mu$, so short that the aperture in all practical cases is larger than the diffraction limit, and seeing determines the solid angle and noise level. Putting $d \geq d_0$ and substituting Eq. (D-8) into Eq. (D-6) gives

$$\text{Nd:} \quad L = 1.47 \times 10^{28} \frac{\widehat{\sec}^4 m^2 \text{photons}}{\text{J-micron}^3} \left(\frac{\eta}{\theta_{up} \theta_{dn}} \right)^2 Q_{sat} \lambda^3 \tag{D-9}$$

D. 3. 2 Garbon Dixoxide Laser System - General

This system uses continuous waves instead of pulses, so we wish to know the power to receive some required signal-to-noise ratio instead of some number of photons. Oliver [Ref. 26] has shown that the equivalent noise power at the input to the receiver corresponds to B/η_q photons per second, where η_q is the quantum efficiency (probability of a detection event per photon) of the infrared detector. Signal-to-noise ratios have been demonstrated to correspond to this formula with $\eta_q \approx 50\%$. Hence, the required photon input rate at the receiver is $(S/N)(B/\eta_r)$, where S/N is the power signal-to-noise ratio, and η_q has changed to η_r to include any other efficiency factors that are peculiar to the receiver. Recall that the other efficiency η is squared because it applies to the antenna, atmosphere, and anything else involved in both up and down propagation. The product $(S/N)B$ is closely related to the information rate in communication theory, so let us give it the symbol:

$$r \equiv (\text{power } S/N) \times B$$

In this form, the required transmitter power is $r/\eta_r L$, or

$$CO_2 \text{ general:} \quad P_T = 4.7 \times 10^{-30} \frac{w - \mu}{\text{Hz-sec}^2} \frac{r}{\eta_r \lambda Q_{sat}} \left(\frac{\theta_{up}}{\eta d_r}\right)^2 \qquad \text{(D-10)}$$

where Eq. (D-6) was used for L, and the subscript e was dropped from d, because the effective aperture of the telescope is the real aperture, since the diameter will be limited by cost in this case rather than by seeing. Also photons per joule was changed to watts per hertz (both of which have the dimension of energy) in Eq. (D-10), as is appropriate with continuous wave reception.

D. 3. 3 Carbon Dioxide Laser System - High Gain

Equation (D-10) allows for the possibility of a defocused upgoing beam to acquire a satellite despite an appreciable ephemeris error. However, the CO_2 laser system is most suited for use with synchronous satellites or retroreflectors on the moon. In these cases target angles are known and a diffraction limited θ_{up} is used, the same as θ_{dn} in Eq. (D-8). Expressing Eq. (D-10) in terms of d_{up} and d_{dn} gives

$$CO_2 \text{ high gain: } P_T = 3.2 \times 10^{-31} \frac{m^2\text{-w}}{\text{Hz-}\mu} \frac{r\lambda}{(\eta d_{up} d_{dn})^2 \eta_r Q_{sat}} \qquad \text{(D-11)}$$

D. 3. 4 Microwave System

One more modification of the range equation will conclude this section. This is the one applicable to microwave reflection from the balloon satellites. Microwave antennas are usually specified by the gain G, which tells the power gain in the forward direction relative to isotropic radiation of the same power. G includes the efficiency factor η; i. e.,

$$\frac{4\pi}{G} = \left[\begin{matrix}\text{effective} \\ \text{solid angle}\end{matrix}\right] = \frac{\pi}{4}\theta^2 \eta$$

We could convert Eq. (D-9) to the microwave case using this equation to intorduce G and replacing photon energy with kT, the unit of thermal noise energy (k ≡ Boltzmann's constant), where T is the effective noise temperature of the receiving system. However, it is probably easier to start over from first principles. The power received is

$$P_R = \left(\frac{P_T G}{4\pi R^2}\right) \times Q \times \left(\frac{A_e}{R^2}\right) \times \left(\frac{G\lambda^2}{4\pi A_e}\right)$$

where the various factors are interpreted as

(1st) = flux at the satellite

Q = return per sterradian

(2nd) = amount intercepted by effective receiving area

(3rd) = 1, but in a form that converts equivalent area A_e to G

However, P_R = (S/N) x B x (spectral density of thermal noise), or $P_R = rkT$. Collecting terms and solving for P_T gives

$$\text{Microwave: } P_T = 2.2 \times 10^{-21} \frac{\text{watt}}{\text{Hz-deg}} \frac{rT}{Q_{sat}(\lambda G)^2} \qquad \text{(D-12)}$$

APPENDIX E
SPECIFIC SATELLITES AND THEIR ORBITS

The table on p.137 gives data for ten objects of special interest and Figs. p.138 through 141 show some representative orbits. Three objects are the largest balloon satellites and seven are satellites (including the moon) that have retroreflector panels. As noted in Sec. 1.2 the orbits of balloon satellites are not predictable enough for geodetic or similar studies, since random forces such as variable earth albedo act on the balloon. However, the balloons are listed anyway as convenient test bodies, or perhaps for study of the random forces.

Factors for the range equations of Appendix D appear in columns 9, 10, and 11 of the table. The lidar (optical radar) cross-section is $\sigma = 4\pi Q$, column 10. This quantity and various forms of the range equation are fully discussed in Appendix D. For the balloons, Q is valid for radar as well as lidar. For lidar, Q should be quadrupled when a balloon becomes wrinkled (but not collapsed) in its old age (i. e. a diffuse reflector). $Q_{sat} = Q/R^4$ was evaluated only at the range in column 9, which is nearly the longest range at which the satellite will appear at a suitable elevation for tracking from any point on earth. These long range values were selected partly to keep our estimates on the conservative side, but mainly because there is much more tracking time near apogee than there is near perigee, as is shown in column 8.

The representative orbit figures show the arcs over which tracking time was estimated and the 45° lines-of-sight near apogee for which radar (lidar) range was measured.

ORBITAL AND REFLECTION PARAMETERS FOR TEN EARTH SATELLITES

Orbits are valid for April 1969

1 Satellite	2 Reflector	3 Apogee, Mm.	4 Perigee, Mm.	5 Inclination, deg.	Period min.	Visual Magnitude	8 Tracking Time Min. (a)	9 Radar Range Mm. (b)	10 Q (c), m^2/ster.	11 -10 log Q_{sat} $ster^{-1}m^{-2}$ (d)	12 Satellite
Pageos A (1966 56A)	135 ft balloon	5.92	2.43	84	180	0	ap 43 per 15	6.74	106	253	Pageos A
Explorer XIX (1063 53A)	12 ft balloon	1.85	0.85	79	113	4	ap 13 per 5	2.34	0.68 (e)	256	Explorer XIX
Explorer XXXIX (1968 66A)	12 ft balloon	2.39	0.73	81	117	4	ap 16 per 5	2.98	0.68 (e)	261	Explorer XXXIX
BE-B (1964 64A)	quartz retroref.	1.09	0.89	80	105	8	ap 8 per 6	1.46	1.29×10^6	185	BE-B
BE-C (1965 32A)	quartz retroref.	1.32	0.94	41	108	8	ap 9 per 6	1.70	1.29×10^6	188	BE-C
Geos 1 (1965 89A)	quartz retroref.	2.27	1.12	59	120	8	ap 15 per 7	2.83	5.5×10^6	191	Geos 1
D1-C (1967 11A)	quartz retroref.	1.35	0.53	40	104	8	ap 9 per 4	1.75	0.91×10^6	190	D1-C
D1-D (1967 14A)	quartz retroref.	1.85	0.58	39	110	8	ap 13 per 4	2.34	0.91×10^6	195	D1-D
Geos 2 (1968 2A)	quartz retroref.	1.61	1.08	74	112	8	ap 11 per 7	2.08	6.4×10^6	185	Geos 2
Moon	quartz retroref.	400	378	5	28 days	--	8 hrs.	401	2.1×10^7	271	Moon

NOTES:

a. Calculated as time between zenith distances of 60° during a pass in which apogee or perigee occurs at zenith.

b. Calculated for apogee at 45° zenith distance.

c. Equals lidar cross-section of the retroreflector at 1.06μ divided by 4π. Valid for radar in the case of balloon satellites. Balloons were assumed specular, in which case $Q = (\text{radius}/2)^2$. For diffuse balloon $Q = (\text{radius}/4)^2$. Retroreflector values are experimentally determined and corrected to 1.06μ.

d. $Q_{sat} = Q/(\text{radar range})^4$.

e. Reduced 19% for white dots painted on the surface.

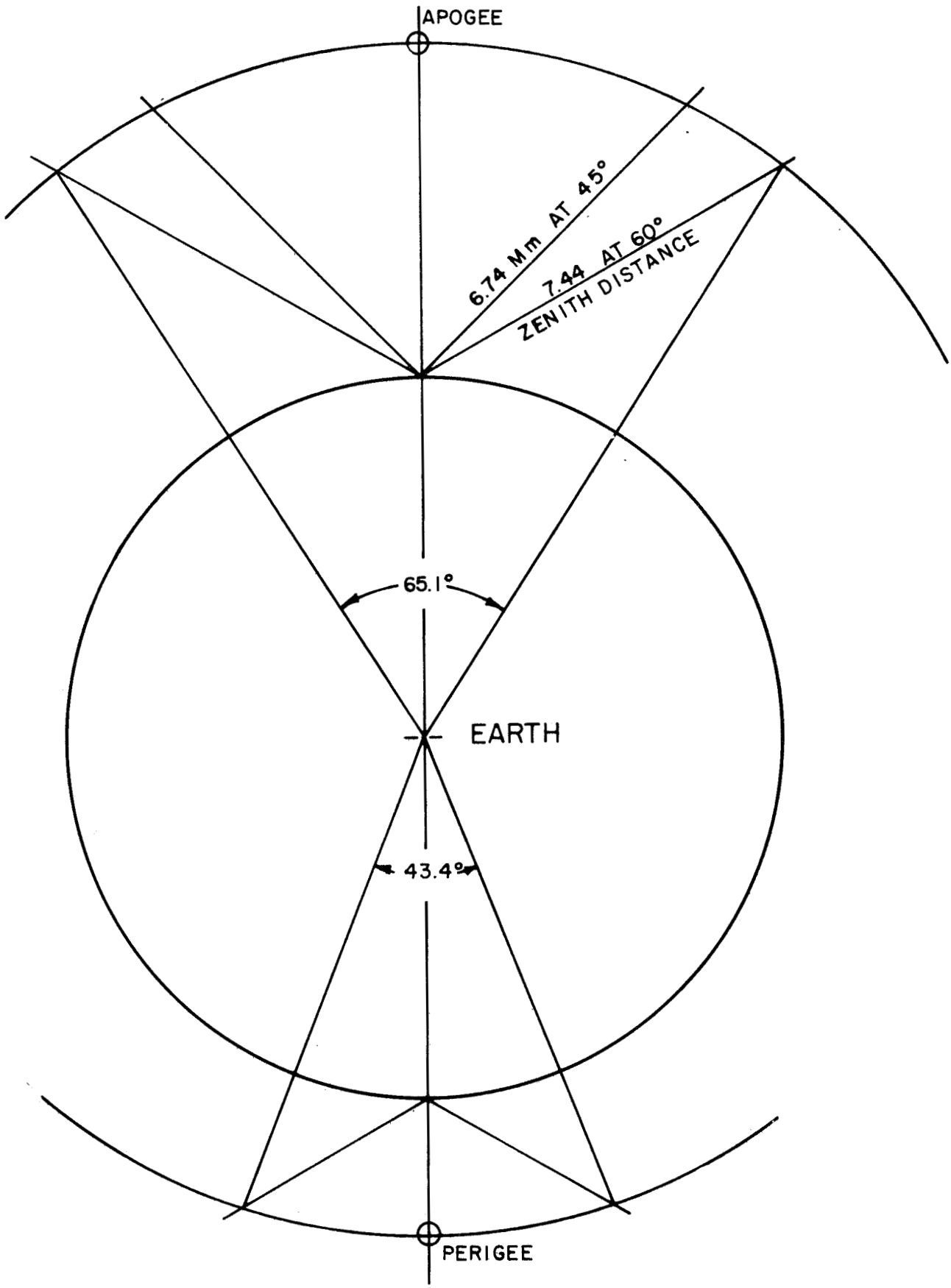

Orbit of Pageos A (1966 56A)

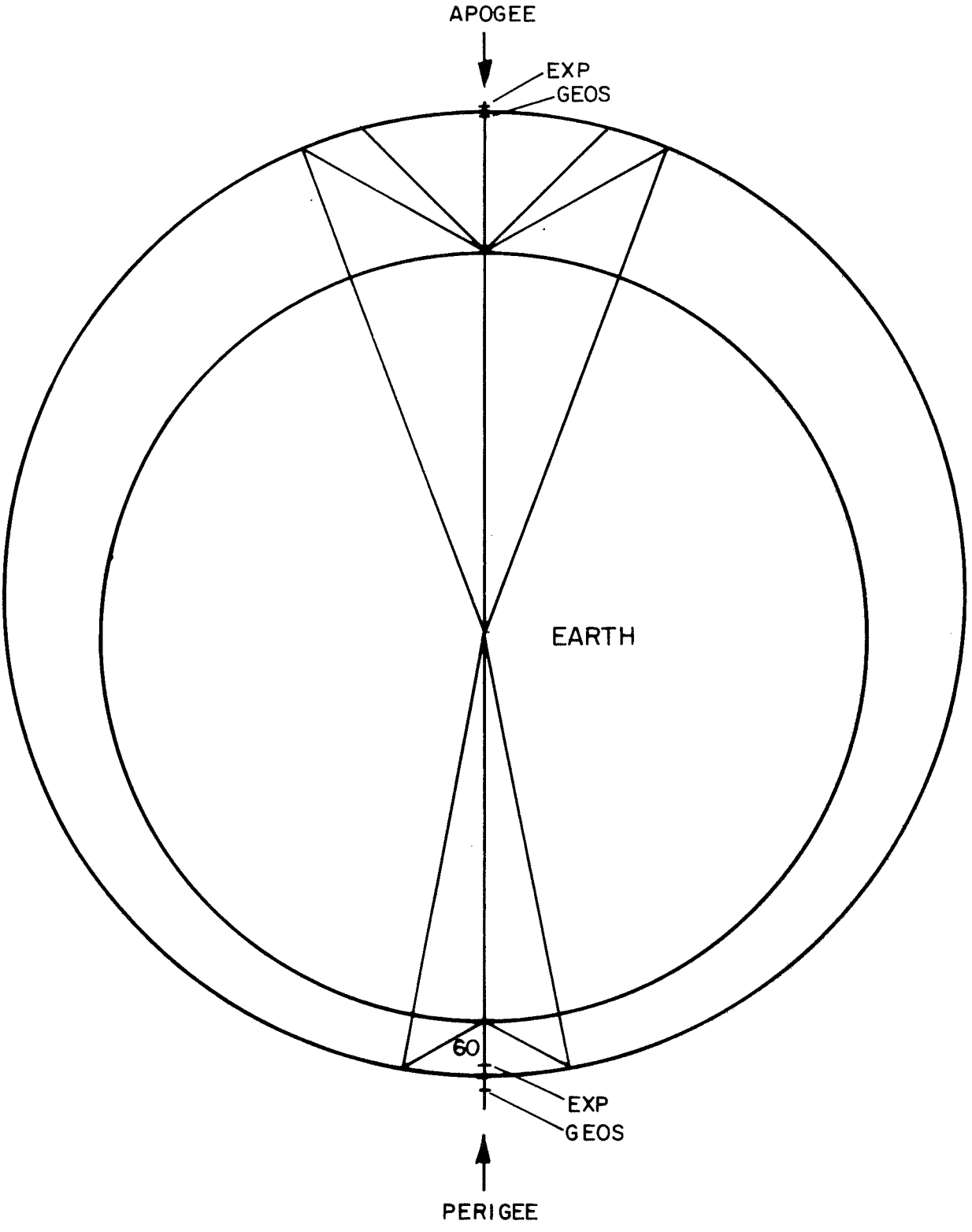

Orbit that represents average of Explorer XXXIX and Geos. 1

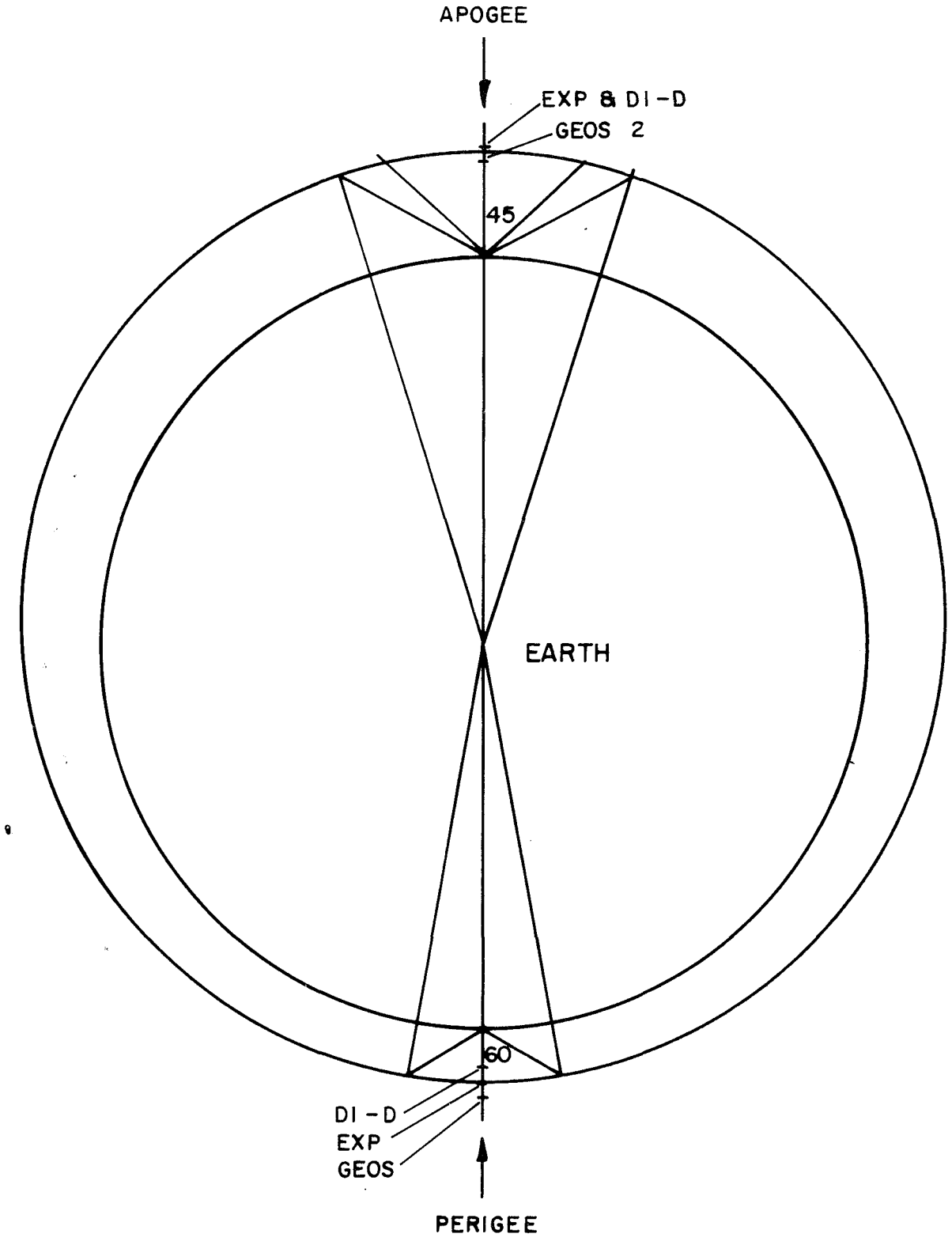

Orbit that represents average of Explorer XIX, D1-D, and Geos. 2

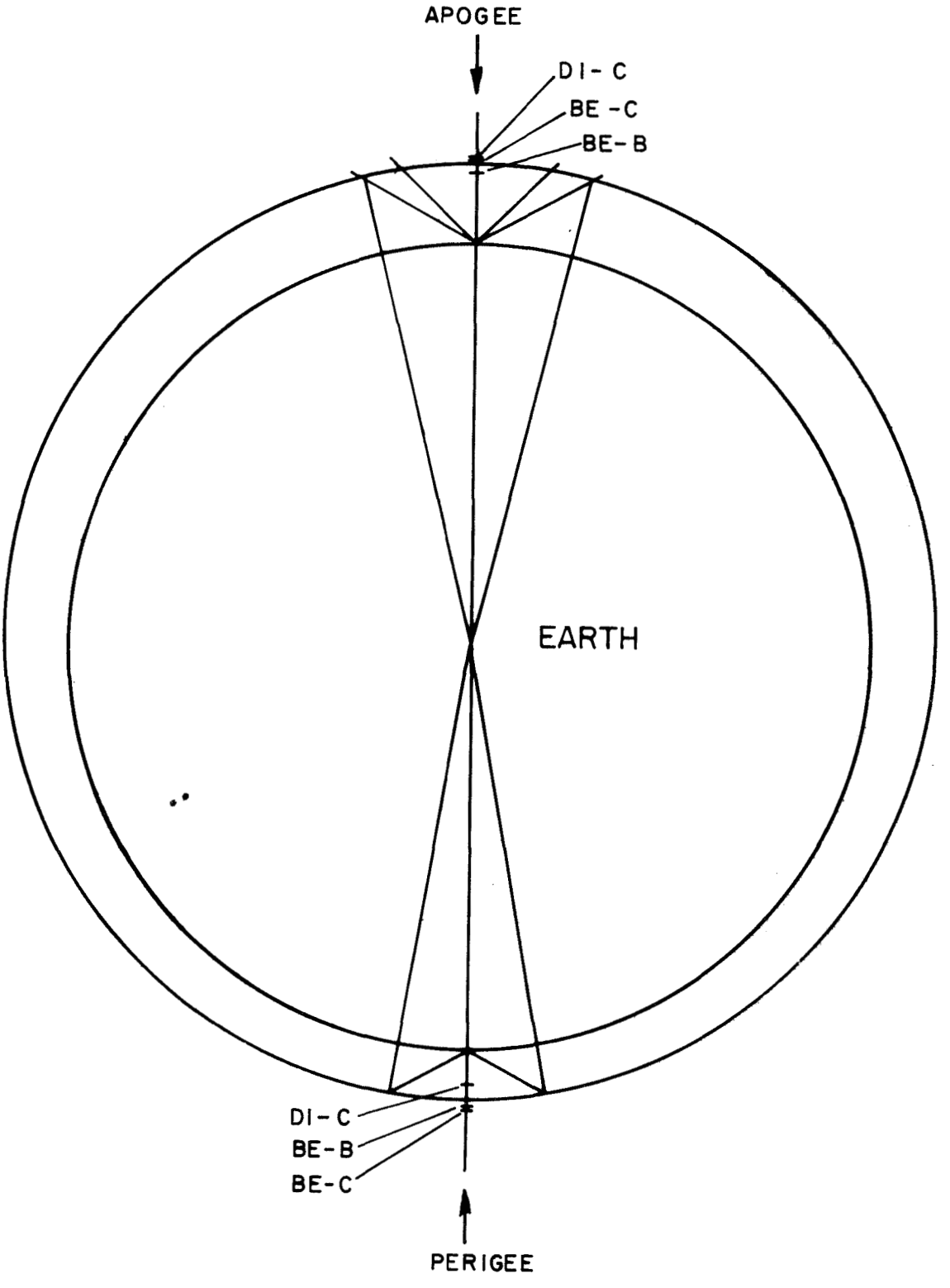

Orbit that represents average of D1-C, BE-B, and BE-C

APPENDIX F

ORBIT PERTURBATIONS DUE TO FLUCTUATING EARTH ALBEDO

Residual orbit perturbations due to random fluctuations in earth albedo will set the lower limit to orbit predictability. The following order-of-magnitude estimate of this effect is based on the simplifying assumption of a circular orbit, deviations from which are denoted by x (measured in the forward orbit direction), y (along radius from earth) and z (normal to orbit plane). Let ω denote orbital angular velocity $2\pi/T$, and let $\vec{a}$ be the instantaneous inertial perturbing acceleration. The (linearized) coordinate equations of motion for small displacements are

$$\ddot{x} + 2\omega\dot{y} = a_x \tag{1}$$

$$\ddot{y} - 2\omega\dot{x} - 3\omega^2 y = a_y \tag{2}$$

$$\ddot{z} + \omega^2 z = a_z \tag{3}$$

Equations (1) to (3) possess three independent solutions for the homogeneous case ($\vec{a} = 0$):

(1) $\quad x = x_o + v_o t, \qquad y = -2v_o/3\omega ,$

(2) $\quad x = 2A \sin(\omega t + \varphi_o) , \qquad y = -A \cos(\omega t + \varphi_o) ,$

(3) $\quad z = B \sin(\omega t + \psi_o) ,$

the first two describing coupled x, y motion as "drifting two-by-one ellipses" and the last describing independent simple harmonic z motions. These motions represent the appearance of a nearby orbit slightly differing in semimajor axis (1), eccentricity (2), and orbit plane tilt (3).

Because of the geometry of albedo forces (See Fig. p. 103) the major component of the fluctuating part will be radial (a_y). In general, the response of the displacement coordinates to an arbitrary acceleration $\vec{a}$ can be written

$$\vec{r} = \begin{Bmatrix} x \\ y \\ z \end{Bmatrix} = \int^{t} dt' \left[\vec{G}_x(t-t')\, a_x(t') + \vec{G}_y(t-t')\, a_y(t') + \vec{G}_z(t-t')\, a_z(t') \right] \tag{4}$$

where $\vec{G}_x(t)$ represents the response to a unit impulse in the x direction at $t = 0$; it is a linear combination of the above homogeneous solutions (1-2) vanishing continuously at $t = 0$ and satisfying

$$\frac{d}{dt} \vec{G}_x(t) \Big|_{-\epsilon}^{\epsilon} = \hat{x} ,$$

$\hat{x}$ being the unit x-vector; and so on.

It can be verified that the response to a radial impulse is

$$\vec{G}_y(t) = \frac{2}{\omega}(\cos \omega t - 1)\hat{x} + \frac{1}{\omega}(\sin \omega t)\hat{y}, \; t \geq 0, \quad 0, \; t \leq 0 \tag{5}$$

the cumulative x and y displacements produced by a_y acting for $0 \leq t \leq T$ are therefore

$$D_x = \frac{2}{\omega} \int_0^T (\cos \omega t - 1)\, a_y(T-t)\, dt , \tag{6}$$

$$D_y = \frac{1}{\omega} \int_0^T \sin \omega t \; a_y(T-t)\, dt \tag{7}$$

For convenience let $\theta = \omega t$ be the angle between the earth-sun line and the earth-satellite line; a_y is naturally characterized as a function of θ:

$$D_x = \frac{2}{\omega^2} \int_0^{\theta_o} (\cos\theta - 1)\, a_y(\theta_o - \theta)\, d\theta \tag{8}$$

$$D_y = \frac{1}{\omega^2} \int_0^{\theta_o} \sin\theta\, a_y(\theta_o - \theta)\, d\theta \tag{9}$$

Fluctuations in reflected earthlight striking a spacecraft are due to variations in cloud cover over the portion of sunlit surface visible from the spacecraft. Let us adopt the following model for random cloud cover: a surface composed of many distinct areas of equal size occupied at random by cloud cover so that each area is independently subject to cloud cover (albedo ρ_c) with probability p or free of cover (albedo ρ_f) with probability $q = 1-p$. The mean albedo is

$$\overline{\rho} = p\rho_c + q\rho_f \tag{10}$$

and the mean square albedo variation,

$$\overline{\Delta\rho^2} = pq(\rho_c - \rho_f)^2 \tag{11}$$

Let θ (in orbit plane) and ϕ (perpendicular) be the angular coordinates of a given surface area element S whose albedo is $\rho = \overline{\rho} + \Delta\rho$. It receives an incident radiation

$$I = I_s \cos\theta \cos\phi \tag{12}$$

and reflects an amount

$$I' = IS\rho\cos(\theta' - \theta)\cos\phi \tag{13}$$

in the direction of a distant satellite at θ'. The total mean reflected radiation in the direction $\theta = 0$ is

$$I_o = I_s \bar{\rho} \int \cos^2\theta \cos^2\phi \, d(\sin\phi)\, d\theta, \quad |\phi| \le \pi/2, \quad |\theta| \le \pi/2 \tag{14}$$

(an element of surface area being $S = \Delta(\cos\phi)\Delta\theta$ in units such that earth's radius = 1) or

$$I_o = I_s \bar{\rho} \left(\frac{2\pi}{3}\right) . \tag{15}$$

The value of this quantity, known from existing satellite measurements, will be used as a constant in subsequent formulae.

Let α be the appropriate constant to convert directed radiation to light-pressure acceleration. It incorporates the factors of satellite altitude, area, reflectivity and mass. The perturbing acceleration $a_y(\theta')$ due to the area element S at θ, ϕ is

$$a_y(\theta') = \alpha I_s \Delta\rho S \cos\theta \cos(\theta' - \theta) \cos^2\phi \tag{16}$$

The displacements produced over a full orbit period will then be (See Eqs. (8) and (9))

$$D_x(2\pi) = \frac{2}{\omega^2} \alpha I_s \Delta\rho S \cos^2\phi \int_{\theta-\pi/2}^{\theta+\pi/2} (\cos\theta' - 1) \cos(\theta' - \theta)\, d\theta'$$

$$= \frac{1}{\omega^2} \alpha I_s \Delta\rho S \cos^2\phi (\pi \cos\theta - 4) \tag{17}$$

$$D_y(2\pi) = \frac{1}{\omega^2} \alpha I_s \Delta\rho S \cos^2\phi \int_{\theta-\pi/2}^{\theta+\pi/2} \sin\theta' \cos(\theta' - \theta)\, d\theta'$$

$$= \frac{1}{\omega^2} \alpha I_s \Delta\rho S \cos^2\phi \cdot \frac{\pi}{2} \sin\theta \tag{18}$$

Area elements at various locations θ, ϕ produce perturbations that add linearly; since the amplitudes are respectively proportional to the independently random albedo fluctuations $\Delta\rho$, the net mean-square displacements are given by

$$\sigma^2_{x,\,y}(2\pi) = \sum_S \left[D^{(S)}_{x,\,y}(2\pi) \right]^2_{\text{avg.}} \tag{19}$$

and for calculation,

$$\sum_S \to \int \frac{d\theta\, d(\sin\phi)}{S} \ .$$

The geometric integrals in the resulting expressions are

$$(x)\ , \quad \int_{|\theta|,\ |\phi| \le \pi/2} \cos^4\phi(\pi\cos\theta - 4)^2\, d\theta\, d(\sin\phi) = \frac{8\pi^3}{15}\ ;$$

$$(y)\ , \quad \int \cos^4\phi(\pi/2\ \sin\theta)^2\, d\theta\, d(\sin\phi) = \frac{2\pi^3}{15}$$

hence

$$\sigma_x = \frac{2\sqrt{S}}{\omega^2}\,\alpha I_s \Delta\rho \sqrt{\frac{2\pi^3}{15}} \ , \tag{20}$$

$$\sigma_y = \frac{1}{2}\sigma_x \ , \tag{21}$$

or, from Eq. (15),

$$\sigma_x = \sqrt{\frac{6\pi}{5}} \left(\ell \frac{\Delta\rho}{\bar{\rho}} \right) \frac{\alpha I_o}{\omega^2} \ , \quad \sigma_y = \frac{1}{2}\sigma_x \ . \tag{22}$$

Here, $\ell = \sqrt{S}$ is the scale size of the cloud-cover albedo variations, and $\Delta\rho$ is the statistical rms value,

$$\Delta\rho = \sqrt{pq}\ |\rho_c - \rho_f| \ .$$

Numbers.

We assume the following values:

$$\left.\begin{aligned} \alpha I_o &= 0.95 \times 10^{-3}\ \text{cm/sec}^2 \\ 1/\omega^2 &= 3.0 \times 10^6\ \text{sec}^2 \end{aligned}\right\} \text{Satellite Pageos}$$

$$p = q = 0.5$$

$$\rho_c = 0.5, \quad \rho_f = 0.1$$

$$\ell \cong 1000\ \text{mi} \simeq 0.12\ \text{earth radii}$$

We then have $\ell\,\Delta\rho/\bar{\rho} = 0.8 \times 10^{-1}$, $\sqrt{6\pi/5} = 1.95$

$$\begin{aligned} \sigma_x &= (0.8 \times 10^{-1})(1.95)(0.95 \times 10^{-3})(3.0 \times 10^6) \\ &= 4.5 \times 10^2\ \text{cm} \\ &= 4.5\ \text{meters}\ , \end{aligned}$$

$$\sigma_y = 2.2\ \text{meters}$$

REFERENCES

1. "Useful Applications of Earth Oriented Satellites," prepared by Panel 13 of the Summer Study on Space Applications, Division of Engineering, National Research Council for the National Aeronautics and Space Administration, published by National Academy of Sciences, Washington, D. C. (1969).

2. Lehr, Carlton G., "Geodetic and Geophysical Applications of Laser Satellite Ranging," Smithsonian Institution Astrophysical Observatory, Cambridge, Mass., Report #904-79 (April, 1969).

3. Cohen, M. H.; Jauncey, D. L.; Kellermann, K. I., and Clark, B. G., "Radio Interferometry at One-Thousandth Second of Arc," Science, 162, pp. 88-94 (October 4, 1968).

4. Michelson, A. A., Astrophys. J., 51, 257 (1920).

5. Lundquist, Charles A., "Satellite Altimetry and Orbit Determination," Research and Space Sciences, SAO Special Report #248, Smithsonian Institution Astrophysical Observatory, Cambridge, Massachusetts 02138 (August 18, 1967).

6. Gordon, Gary P., "Satellite-Star Occultations for Geodetic Determinations," The Use of Artificial Satellites for Geodesy, G. Veis ed., North Holland Publishing Co., p. 293 (1963).

7. Kolaczek, Barbara, "Photoelectric Observation of Satellite-Star Occultations," Smithsonian Institution Astrophysical Observatory, Cambridge, Mass. 02138, Report #807-128

8. Prior, Edwin J., "Earth Albedo Effects on the Orbital Variations of Echo I and Pageos I," presented at the Twelfth Plenary Meeting of COSPAR and Tenth International Space Science Symposium, Prague (May, 1969).

9. Arking, Albert, and Levine, Joel S., "Earth Albedo Measurements: July, 1963 to June, 1964," J. Atmos. Sci., 24, 721 (November, 1967)

10. Keating, Gerald M., et al, "Determination of Mean Atmospheric Densities from the Explorer IX Satellite," NASA Langley, Technical Note D-2895 (July, 1965).

11. Hodara, H.; Wells, W., and Marquedant, R., Final Report NAS1-9167, publication pending, Tetra Tech, Incorporated, 630 North Rosemead Boulevard, Pasadena, California 91107 (December, 1969).

12. Allen, C. W., Astrophysical Quantities, University of London, The Athlone Press, 2nd edition (1962).

13. Snitzer, E., "Glass Lasers," Proc. IEEE, 54, No. 10 (October, 1966).

14. Heynau, H. A., and Foster, M. C., "Single-Subnanosecond Laser Pulse Generation and Amplification: The Second Generation of Q-Switched Lasers," Laser Focus (August, 1968).

15. DeMaria, A. J.; Glenn, W. H.; Brienza, M. J., and Mack, M. E., Proc. IEEE, 57, 2 (January 1, 1969).

16. Miller, R. H., Science, 153, 581 (August 5, 1966).

17. Herriott, D. R., and Schulte, H. J., "Folded Optical Delay Lines," Appl. Optics, 4, 883 (August, 1965).

18. Young, C. G., and Kantorski, J. W., "Saturation Operation and Gain Coefficient of a Neodymium-Glass Amplifier," Appl. Opt., 4, 1675 (December, 1965).

19. Kachen, G.; Steinmetz, L., and Kysilka, J., Appl. Phys. Ltrs., 13, 229 (October 1, 1968).

20. Johnson, L. F., and Kahug, D., "Piezoelectric Optical-Maser Modulator," J. Appl. Phys., 33, 3440 (1962).

21. Kulcke, W., et al, "Digital Light Deflectors," Proc. IEEE, 54, 1419 (October, 1966).

22. Fowler, V. J., and Schlafer, J., "A Survey of Laser Beam Deflection Techniques," Proc. IEEE, 54, 1437 (October, 1966).

23. Giordmaine, J. A.; Rentzpis, P. M.; Shapiro, S. L., and Wecht, K. W., Appl. Phys. Ltrs., 11, 216 (October 1, 1967).

24. Michelson, A. A., and Pease, F. G., Astrophys. J., 53, 249 (1921).

25. Born, Max, and Wolf, Emil, Principles of Optics, Pergamon Press, New York, 3rd edition (1965).

26. Oliver, B. M., Proc. IRE (Correspondence), 49, 1960 (December, 1961).

27. Freed, Charles, "Design and Short-Term Stability of Single-Frequency CO_2 Lasers," IEEE - J. of QE, 4, 404 (June, 1968).

28. Hall, D. N. B., "The Measurement of Optical Seeing by a Resistance Analog," Appl. Opt., 6, 1992 (November, 1967).

29. Mocker, Hans W., "A 10.6μ Optical Heterodyne Communication System," Final Report, Contract NAS8-20645, available as CFSTI CSCL17B also #N69-24088 (September, 1968).

30. Goodwin, Frank E., and Nusemeier, T. A., "Optical Heterodyne Communications Experiments at 10.6μ," J. of QE, 4, 612 (October, 1968)

31. Patel, C. K. N., "Continuous Wave Laser Action on Vibrational-Rotational Transitions of CO_2," Phys. Review, 136, A1187 (November 30, 1964).

32. Stephenson, J. C.; Hazeltine, William A., and Moore, C. Bradley, Appl. Phys. Ltrs., 11, 164 (September 1, 1967) paper corrected Appl. Phys. Ltrs., 9, 399 (December 15, 1967).

33. McCurdy, J., and Wieder, I., Phys. Rev. Ltrs., 16, 565 (March, 1966).

34. Carbone, R. J., J. of QE, 5, 48 (January, 1969).

35. Eisner, R. L., Reversible Photoelectric Finge Counting," The Review of Scientific Instruments, 29, No. 6 (June, 1958).

36. Siegman, A. E., J. of QE, 3, 337 (July, 1967).

37. Borde, C., and Henry, L., J. of QE, 4, 874 (November, 1968).

38. Waksberg, A. L., J of QE, 4, 532 (September, 1968).

39. Mocker, Hans W., "Pressure in Current Dependent Shifts in the Frequency of Oscillation of the CO_2 Laser," Appl. Phys. Ltrs., 12, 20 (January 1, 1968).

40. Fein, Michael E.; Verdeyen, J. T., and Cherrington, V. E., "A Thermally Pumped CO_2 Laser," Appl. Phys. Ltrs., 14, 337 (June 1, 1969).

41. Hocker, L. O., et al, Appl. Phys. Ltrs., 10, 147 (March 1, 1967).

42. Frenkel, L., et al, Appl. Phys. Ltrs., 11, 334 (December 1, 1967).

43. Wade, C. M.; Clark, B. G., and Hogg, D. E., "Accurate Radio Source Position Measurements with the NRAO Interferometer," Astrophys. J., 142, 406 (July 1, 1965).

44. Read, R. B., "Accurate Measurement of the Declinations of Radio Sources," Observations of the Owens Valley Radio Observatory, California Institute of Technology, Pasadena, AD 403 983 (1963).

45. Gubbay, J. S., and Robertson, D. S., "Nine Million Wavelength Baseline Interferometer Measurements of 3C 273B," Nature, 215, 1157 (September 9, 1967).

46. Kellermann, K. I., et al, "High Resolution Interferometry of Small Radio Sources Using Intercontinental Baselines," Astrophys. J., 153, L209 (September, 1968).

47. "Opportunities for Participation in Space Flight Investigations," Change 18 to NHB 8030.1A

48. Dodd, J. L.; Straiton, A. W., and Deam, A. P., "A Study of Some Characteristics of Atmospheric Refractive Index Differences," University of Texas, Report #P-15 (May 15, 1967).

49. Thayer, G. D., "Atmospheric Effects on Multiple-Frequency Range Measurements," ESSA Report #IER 56-ITSA 53, Boulder Colorado (October, 1967).

50. Gossard, Earl E., "Power Spectra of Temperature, Humidity and Refractive Index from Aircraft and Tethered Balloon Measurements," IRE Trans. on Antennas and Propagation (March, 1960).

51. Penndorf, Rudolf, "Tables of the Refractive Index for Standard Air and the Rayleigh Scattering Coefficient for the Spectral Region between 0.2 and 20.0μ and Their Application to Atmospheric Optics," J. of the Optical Soc. of America, 47, No. 2 (February, 1957).

52. Owens, James C., "Optical Refractive Index of Air: Dependence on Pressure, Temperature and Composition," Appl. Opt., 6, No. 1 (January, 1967).